Analytical Framework for Field Positioning and Work Planning for a Backhoe Excavator

by

Md Monjurul Hasan

A thesis submitted in partial fulfillment of the requirements for the degree of

Master of Science

in

Construction Engineering and Management

Department of Civil and Environmental Engineering
University of Alberta

Abstract

The accomplishment of a successful construction project depends on proper planning, progress monitoring and adaptation to the continually changing complex situations in the field. Efficient remote tracking of multiple disparate resources and establishing the collaboration and coordination between them in field operations are indispensable in an efficient construction management system. With the advances in the sensor technology, real-time process monitoring, and site survey capabilities are available and affordable to construction applications. This also presents challenges to advancing work planning methods in order to account for equipment operations in sufficient details. Work planning demands a significant level of expertise and human interaction in applying adaptive decision making by monitoring the ongoing work progress.

This thesis research explains the necessity and advantage of using the construction machinery itself as the automatic data collection device to sense the field it is working on. The research introduces the sensor equipped backhoe excavator which is capable of tracking its bucket tip with respect to its base and functions as the mobile survey robot. The sensor-augmented equipment would thus be instrumental in eliminating human errors but also be effective in avoiding productivity losses, while at the same time making the job site safe. It is the common practice when any underground utility line is confirmed in the midst of excavation operation, manual excavation proceeds in lieu of the mechanical excavator. Precaution is mandatory because even an expert operator of a mechanical excavator may occasionally fail to perceive the safe depth of the operation. The introduction of a bucket tip tracker with sufficient accuracy can make the work safer and faster and also can eliminate the need for manual excavation thus saving time and

cost. The new approach for precise position tracking of the excavator's bucket tip can be used to plan the operation trajectory of the excavator's arm to minimize the movement and cycle time based on the excavating capacity in a single cycle of operation (mainly depends on the bucket capacity). At the same time, the technique discussed above can act as automatic record keeper when integrated with the time domain. These records can be vital to perform the work progress measurement (as needed in productivity study).

A technique to aid in the selection process of sensors (precision level) for tracking the excavator (pose and position) considering the tradeoff between the level of precision required in field operation on a specific task and the cost of sensors, is also elaborated. Besides presenting the analytical methodology of tracking the excavator's pose, this study explains the detailed analytics for positioning the backhoe excavator by three-point reference system without the help of external remote sensing survey devices (such as Global Positioning System, robotic total station, etc.). This thesis shows how the latest self-tracking machinery can be adopted in the field in a more efficient way to confirm the project progress as per engineering design (design grade). Thus, the needs for extra specialized survey equipment, staffing, and remote monitoring would be eliminated all at a time. The operation algorithm developed for such excavator is not limited to only such an excavator retrofitted with sensors but can also be readily adapted for a complete autonomous model in the future. Several civil construction applications are addressed, and potential field applications of this proposed methodology are illustrated.

Acknowledgement

All praise goes to ALLAH, most beneficial, most merciful for providing enough energy and patience to work for completing this thesis successfully.

The author wishes to express sincere appreciation and gratitude to Dr. Ming Lu, Professor, Department of Civil and Environmental Engineering, University of Alberta, Canada for his continuous guidance, invaluable suggestions and affectionate encouragement at all stages of this work. Without his prudential advice and inspiring support, this research work could never be materialized. The author's debt to him is immense.

The author would like to thank his parents for their undying love and encouragement and support at all stages of life. The achievement of this goal would have been impossible without their blessings.

Table of Contents

List of Tables

List of Figures

Chapter 1

Introduction

1.1 General

Compared with other industries (e.g., manufacturing, power, heavy chemical, and mining); construction industry has made the highest amount of investment in machinery. The objective is to deliver higher productivity, saving cost and at the same time ensuring the safety of the operations personnel in the field (Yoon et al., 2014). Backhoe excavators (Fig. 1.1) are the most versatile construction equipment, commonly employed in excavation, grading, pipeline installation, loading dump trucks, etc. An autonomous machine would eliminate many human errors and avoid productivity losses (Rowe, 1999), while proper planning makes a job site safe from machine-related accidents (Talmaki and Kamat, 2014). Autonomous machines can also be deployed to access the areas which are hazardous, toxic to humans. Besides making the workspace safe, lower operational costs can be materialized by reducing the number of guiding staff on site (e.g., spotters). In recent years, the concept of autonomous earth-moving machines has invoked intense interest among manufacturers and contractors in light of the substantial productivity improvement that technological advances would bring about in the construction, mining, and quarrying industries.

1.2 Background and Scope

Earthmoving governs the most common and heavy machine intensive operations among civil engineering projects. Work procedure involves some basic actions, e.g., surveying, excavating, loading, hauling, dumping, grading. All essential steps require the involvement of heavy machinery and show the path of immense opportunities for automation (Navon et al. 2004) since automated earth-moving performed by robotic machinery can increase both safety and efficiency in the construction site. In recent past, a substantial amount of research efforts has been devoted to investigating the feasibility of the automation of the excavation process (Singh 1997; Stentz et al. 1999; Tatum et al.

2006). Automation of excavators offers a promise for increasing productivity of digging. Therefore, numerous recent research efforts are seen on accurate measurement and control of hydraulic machines position and pose using real-time sensor data (Bernold 1993) to provide a straightforward solution through visualization of equipment operations (Kamat and Martinez 2005; Winck et al. 2014). The goal is intended to enhance the operator's productivity and confidence while also making operations safe. Different types of sensors like global positioning system (GPS), gyroscopes, accelerometers, laser beam, have been used so far to track the position and pose of the excavator (Vaha et al. 2013; Vahdatikhaki et al. 2015). Various computer vision based techniques for excavator's pose and position detection have turned out to cost-effective and efficient in many proof-of-concept case studies (Yuan et al. 2016).

Figure 1.1 CAT 325F L (2017) Excavator (cat.com, 2017).

While taking advantage of the sensors for tracking the pose or position of the excavator, every single measurement can be affected by the unavoidable residual error inherent in the sensor (Mao et al., 2015b). Regardless of the graphical aid which is built to assist the

human operator in completing the job with confidence, the significance of visualization based on interpreting sensor data can be jeopardized due to the random noise present in the sensor data (Cho et al., 2004, Li et al., 2015). Considering this fact, identification of the error boundary for sensors' data is crucial and needs to integrate with (1) solutions developed for excavator tracking and (2) real-time visualization mechanisms.

On the other hand, most of the researchers as mentioned above have made significant contributions to solving the problem regarding automation techniques and the guidance system of the robotic excavator. Even though many excavator manufacturers have released some smarter versions of the excavator with operation control technologies but has yet to cater for application needs in construction field (forconstructionpros.com, 2015). A prominent research gap is still evident in between proof of concept and application. A formal methodology for making the step by step working plan of a smart excavator has not been appropriately developed. Again, in most of the demonstration cases the above-discussed technology is expensive in certain terms and requires a specialist to handle. All of the abovementioned facts point towards the substantial research need to formalize a methodology which is capable of turning a regular ordinary excavator into a smart one capable of enhancing operation efficiency, thus to ensuring project economy and safety. Alongside, such excavator can itself act as a survey robot, ultimately eliminating the need for the presence of the survey crew on site during construction.

1.3 Research Objective

The objectives of the research are as follows:

a) To explain the excavator kinematics to accommodate error propagation theory for quantifying the position uncertainty while tracking the bucket tip using integrated sensors.
b) To aid in the selection process of sensors (precision level) for tracking the excavator (pose and position) considering the tradeoff between the level of precision required in field operation on a specific task and the cost of sensors.

c) Developing a feasible (three-point) positioning mechanism for excavator equipped only with the simple angle measuring sensors.
d) Proposing a framework for planning self-guided semi-autonomous excavator operations to eliminate the need for the onsite survey crew and presents a structured process of completing the entire excavation process on the cell of a site grid. Ultimately, improving the productivity and automating the earthmoving operations.

1.4 Research Significance

This research explains an analytical model along with a visualizing mechanism, based on the error propagation theory to quantify and envision the uncertainty present in the position and pose of the excavator obtained from sensor-based measurements regardless of the type of sensors used. A technique is also presented to aid in the selection process of sensors (precision level) for tracking the excavator (pose and position) considering the tradeoff between the level of precision required in field operation on a specific task and the cost of sensors. The basic aim is to turn an ordinary excavator into smart construction equipment by integrating sensors where the user has the freedom of choosing the sensors according to the job-specific need.

Besides, this study focuses on structuring the operation sequence of a sensor-equipped smart excavator. The excavator is termed as the self-guided one because of its capability of fixing its positioning by itself regarding a particular reference system. A three-reference point based positioning system for such excavator is also discussed in detail. Although the proposed methodology is built on top of the working procedure of an excavator equipped with tilt and angle measuring sensors, a similar framework can be adapted for other autonomous excavator operation cases. The purpose of the framework is to plan self-guided semi-autonomous excavator operations. This not only shows the potential to eliminate the need of onsite standby survey crew but also lessen the amount of rework, while at the same time presents a structured process of completing the entire excavation process on the grading cell in the site grid; thus, improving the productivity of the earthmoving operation.

1.5 Organization of the Thesis

The thesis has been divided into six chapters as follows:

Chapter 1 describes the problem background and research scope. Then it introduces the research objective and significance of this research.

Chapter 2 summarizes the review of the literature.

Chapter 3 explains the excavator kinematics and uncertainty visualization techniques for excavator bucket tip through error propagation.

Chapter 4 presents the three-reference positioning technique for the backhoe excavator which is only equipped with angle measuring sensors. It explains how the excavator can efficiently be used as a survey robot in some potential applications.

Chapter 5 explains a framework for planning self-guided semi-autonomous excavator operations on an excavation site.

Chapter 6 recapitulates the contributions of this research and concludes the study with recommendations for future research.

Chapter 2

Literature Review

2.1 General

Construction is considered as one of the world's largest engineering industries besides agriculture and manufacturing. Still, it is also the most primitive concerning methods when compared to others and reveals a disappointing diminishing trend in terms of productivity improvement (Rojas and Aramvareekul 2003; Tiecholz 2013). Luis and Dunston (2017) pointed out three P's: place, process, and product as the critical factors among many which are behind of this less satisfactory state of affair. Construction operations subject to be dynamic in nature. It principally evolves in the outdoor condition and can be influenced by many variables. This characteristic of place dramatically increases the inherent uncertainty in planning construction operations and is not amenable to the artificial environment control which is possible in manufacturing operation setting. On the other side, a typical construction site demands the remote collaboration and coordination between multiple incongruent resources, where industrial assembly line like a linear movement of materials is rare. Besides, every product in the construction process is unique (Vrijhoef and Koskela 2005). Even, whenever a construction team is building a same type of structure over again, it is very natural to face an entirely different set of conditions (e.g., weather condition, materials quality, availability of labor, supply schedule of construction materials, price, etc.). Such challenging nature of the construction site always stresses construction managers to retain a continuous oversight of the operations, measure progress, and check performance to ensure that the work is performed according to plan.

Although, above mentioned traits of this industry impede its flourishment like other industries, at the same time opens a challenge to the researchers to shape the unstructured problems and improve the construction performance matrix (Vereen et al. 2016). Hence, to go beyond the current limit of conventional construction methodology, researchers are

putting their effort to make construction monitoring and decision-making process soothing with the adaptation of advanced sensors technology (Zhang et al. 2017) and at the same time implementation of autonomous machinery for increasing crew efficiency (Alderton 2015; Bock 2015).

2.2 Sensor Technology for Construction Monitoring

The importance of construction monitoring to project success has been noted by several researchers (Bosché 2010; Navon and Sacks 2007). Unfortunately, this process requires a high level of manual involvement to collect, synthesize and analyze the data which not only is time-consuming and labor-intensive but also can cost delay and price. Using the vision of digital cameras to monitor the operation progress (Golparvar-Fard et al. 2015), the laser scanning technique for quality control of the built environment (Bosché 2010); the radio-frequency identification (RFIDs) and global positioning system (GPS) sensors to track the movement of crews and materials (Soleimanifar et al. 2014; Su et al. 2014) are some of the technological means through which recent research efforts have sought to remedy this situation. Hence, several commercial vendors and original equipment manufacturers are also stepping forward to offer integrated data collection mechanism with construction machinery (e.g., Earthwave Technologies 2017; Caterpillar 2017).

Technologies as mentioned earlier meant to provide construction managers with timely and accurate access to updated status information of crews and materials and at the same instance helps to ensure site safety. But the fact is, the nature of the technologies mentioned above still does not picture the full potential to lend real-time operation-centric information applicable to a variety of construction processes. For instance, vision-based sensing can be disturbed by the impact of surrounding environment, such as lighting condition and background color (Zhang et al. 2017). Laser scanners can be very beneficial in construction data collection for construction quality control, condition assessment, health monitoring, and component tracking but still involve the limitations like discontinuity of spatial information, the mixed-pixel phenomenon, the need for regular sensor calibrations, and slow warm-up time (Golparvar-Fard et al. 2015). Both RFID and GPS sensors are susceptible to the signal obstruction and large margin of error (Razavi and Moselhi 2012). There are some other sensors (e.g., temperature, angle/tilt,

pressure, displacement, etc.) which are frequently applied in construction domain but possess the typical limitations of accurate reading (Zhang et al. 2017). This phenomenon exhibits the need to prepare error models for sensors data depending on job-specific need. Besides, many experts agreed upon the fact that a project-specific suitable integrated framework for decision making, process planning by analyzing the sensors data is also a subject area for construction research (Luis and Dunston 2017).

2.3 Automation and Robotics in Construction

Construction automation research in the field of robotics has two major distinct divisions concerning its applications. One is civil infrastructure, and another one is the house building (Balaguer and Abderrahim 2008). Automation of road, tunnel, and bridge construction, earthwork, etc. are some typical civil infrastructure applications. Structural health monitoring devices, automated concrete compactor, interior finisher, building skeleton erection and assembly robot, etc. are some typical examples in the field of house construction.

Over the past few years, autonomous machinery for road construction has been introduced time to time (Momin et al. 2015). First successful project with new generation automatic road paver and asphalt was reported by Peyret et al. (2000). GPS based tracking technologies are an integral part of these mobile machines (robots) for navigation (Li et al. 1996; Sukkarieh et al. 1999). Instant quality control and field management of compacted material (asphalt) is another crucial aspect of applying robotic technology (Oloufa 2002) in road construction. Therefore, carrying so much attention nowadays (Ardiny et al. 2015). Vision-enabled teleoperated pavement crack sealer (Lee et al. 2006), and automatic road strip removers (Ham et al. 2006) are some other examples.

Tunnel construction is another pioneer in the advancement and application of automation technology is prominently visible (Ford 2009). Tunnel boring machine (TBM) is a widely used tunneling device, which has gained tremendous popularity over conventional tunneling technologies because of its higher advancement rates and better safety performance (Delisio and Zhao 2014). Latest technologies have enabled to turn the entire

construction process into a total automated one (pmsolid.com, 2017). Automatic high-pressure concrete liner, tunnel formwork distributor, TBM integrated conveying mechanism for dirt removal, etc. are some of the examples. This area is still under the research interest of numerous scholars. Research efforts have been seen to the development of the automated and cost-effective solution to guide the advance of a tunnel-boring machine construction researchers (Linag and Lu 2010; Shen e al. 2011; Mao et al. 2015).

The automatic or semiautomatic construction of bridges, dams, offshore platforms, and other prominent civil infrastructures is a vital research and development field in construction automation. The development of the 15-m range auto-conveying concrete system based on the SCARA robot concept for dam construction in Japan or the development of a column-field-welding robot for bridge construction (Gambao and Balaguer 2002) using laser-based high-precision feedback for verticality control are some of the significant, initial development examples. Several projects are ongoing which is related to this field of application that deal with the architectonic design oriented to the automatic movement of civil infrastructures like roofs and bridges (Mirjan et al. 2016).

Automation technology has advanced a lot in the sector of periodic inspection and maintenance of bridges (Myung et al. 2011). Besides regular building structures, a large number of brides around the world need periodic examination every year (Oh et al. 2009). Monitoring capacity and mobility of the sensor mounted device are two critical aspects of research in this field (Mascarenas et al. 2009). In the year 2000, North Carolina State University successfully demonstrated a smart inspection system based on a four degree of freedom robot for the first time (Lorenc et al. 2000). At the very same time, University of Carlos III of Madrid successfully tested an autonomous climbing robot (Balaguer et al. 2000) in a complex three-dimensional environment which is capable of transmitting onboard sensor data (image, laser, X-ray, etc.). Since then technology has evolved a lot but still facing many challenges (Liu et al. 2008), which keep it under the curiosity of researchers onwards.

Residential construction, mainly high-rise buildings, promise to be one of the most significant scopes of adapting autonomous technologies. In last decade, innovative

systems were developed by several companies (Yoo et al. 2012). The SMART system, developed in 1992-1994, was the pioneer of a computer integrated automated construction system (Maeda and Miyatake 1997). It was used for the construction of more than 30 stories automates a wide range of major construction procedures like erecting and welding of steel frames, installation of exterior and interior wall panels, laying of concrete floor planks and some finishing activities (Maeda 1994). Several research efforts are significant in steel frame fabrication process automation (Cho et al. 2007). Besides, the adaptation of 3D printing technology in construction is another hot topic for researchers, as well as practitioners (Hager et al. 2016; Sakin and Kiroglu 2017).

Earthwork research activities focused towards the introduction of new control techniques to existing civil machinery: excavators, graders, etc. are big filed for construction automation research. Dynamics and kinematics control together with the force/torque feedback in the excavator bucket are important issues towards autonomous robotic excavation (Bernold 1993; Hwang and Liu 2007). Operators appreciate teleoperation of backhoe excavators, remotely operated using visual and force feedback (Feng et al. 2015). Detail discussion on the advancement and scopes of autonomous technologies focusing earth-moving excavators is presented in the following section of this chapter.

2.4 Automation in Earthmoving Operations

Earthmoving is one of the rudimentary operations for construction and mining industries. Even industries like agriculture, forestry, waste management, etc. need to deal with a large extent of earth/dirt moving (Dadhich et al. 2015). For being one of the dominant parts of any civil project, this operation is under constant pressure to improve productivity (amount of work done), thus to ensure project economy (Sing 1997). Besides, safety is another significant concern nowadays (Chi and Caldas 2012). Compared to other civil construction sectors, earthmoving is one of the early adaptors of robotic machinery. Among many types of earthmoving machines available with different combinations of the vehicle with the attached robotic mechanism, the wheel loaders and excavators are the most popular (Dadhich et al. 2016). It is agreed upon by many researchers of the construction engineering domain that the incorporation of autonomous technology with integrated operation framework with these types of machinery can

promise productivity, efficiency and safety of the earthmoving work in a great extent (Bock 2015). Therefore, this field is gaining much more attention both from manufacturers and researchers.

Autonomous earthmoving implies a fully automated scenario where excavation to dumping kind of works entirely performed by autonomous machines. Despite a bulk number of research on this subject area, fully automated machines which can readily be applied in the field still not yet been demonstrated (Maeda 2013). Therefore, needs more efforts from the researchers as well as manufacturers (Hemami and Hasani 2009). According to Dadhich et al. (2015), it is still not feasible to accurately model the earthmoving process because of difficulty in modeling interaction between the tool and the environment as according to the current state of the art research achievement. Understanding the complexity, current researchers are more focused on small steps in moving towards full automation. Five steps approach from manual operation to fully autonomous operation, is summarized by Dadhich et al. (2015) in a review article. Those are,

I. Manual process: Operation is entirely controlled by the operator sitting inside and guided by the other crew member from outside.
II. In-sight teleoperation: The operator performs by a hand-held remote from the vicinity of the machine. Often does not require any extra helper to guide.
III. Tele-remote operation: The operator performs all the tasks remotely sitting in a control room via audio-video feedback from the machine.
IV. Assisted tele-remote operation: There is no operator. The machine performs many tasks by itself via minimum supervision.
V. Fully autonomous: The machine performs all tasks by itself. The operator is only needed to give high-level commands, take care of emergencies and handle failures.

According to the author's understanding, there is no significant difference between step II and step III. Once it can be controlled locally with the remote control, can be controlled from far from remote access control room. So, these two categories can be marge together. Instead, an important step is missing. It should be "advanced manual control"

(Hasan and Lu 2017) and can be numbered as step II on the above mentioned five steps approach towards automation. The advanced manual control means, the operation will be performed manually but will be guided by work plan included visualization technique and decision support tools (Feng et al. 2015).

2.5 Excavator Research

Research contributions investigating the feasibility of automating excavation are significant. These excavator researches can be separated into two major divisions. The first group is more focused on the teleoperation of the excavator (Kim et al. 2009; Yoon et al. 2010). Besides, the other group focuses on tracking and controlling the maneuvering process of the excavator's arm (Wink et al. 2015; Lundeen 2016). There are a number of topics that can be classified into these two subjects. Hemami and Hassani (2009) summarized those topics as follows,

I. *Modeling of the excavator as a robot manipulator or determining the kinematic relationships between the actuator motion and the bucket motion.*
II. *Determining the force and velocity relationships between the bucket and the actuators.*
III. *Trajectory studies and planning for the bucket motion.*
IV. *Dynamic modeling of the bucket and actuators.*
V. *More specific studies of the hydraulics related to bucket motion (Since almost all the excavators work with hydraulic power).*
VI. *Computer modeling of the heap of soil and dynamics of changes due to excavation.*
VII. *Automatic recognition of the shape of the heap and decision making for the starting point for loading.*
VIII. *Automatic recognition of the environment geometry (Inside a mine, for example)*
IX. *Analysis of the composition of the fragmented rock (size variation) and its effect on loading.*
X. *Analysis of the forces (various force components) of interaction of bucket and medium.*

XI. *Analysis and formulation of the cutting force and the mechanism of material failure when subject to bucket forces.*

XII. *Use of computer vision to estimate the amount of loaded material.*

XIII. *Methods to control the motion (Control strategy).*

XIV. *Computer simulation of the process*

As discussed earlier, construction research effort still immature to move towards fully automated field equipment's, most of the studies are concerned towards solving a small problem at a time to make a path forward towards the fully autonomous solution. Research effort demonstrated in this study fits into the first kind and is focused on excavator's pose estimation in real time and integrating it with the planning.

2.5.1 Excavator's Position Tacking Technology

Excavators are one of most common and versatile construction machine. Most often, excavator's operation is guided by an external crew member to ensure precision, productivity, and most importantly safety. Many scholars agree that the tracking and controlling the excavator's arm in real time can promise to satisfy such agenda (Azar et al. 2015b). Even though excavator's pose estimation mechanisms are commercially available with new generation machinery but still yet to become popular. Most of the companies offer Global Navigation Satellite System (GNSS) based machines pose estimation solution (Lundeen et al. 2016) which are expensive. Besides, GNSS systems are susceptible to signal strength. Most importantly, a large portion of the construction industry is still using the conventional machines which are still well functioning and adopting a new generation of machines will obsolete the old one. Hence, construction practitioners are reluctant to make that sacrifice for the just extra single feature. These needs are still driving the researchers to find some low-cost solution for this problem and which not cost the construction people to lose existing machine. Alternatively, some research literature presents the possibility of using the robotic total station to serve the purpose, but real-time operation monitoring is not viable with using technology. Again, cost of a dedicated robotic total station is also a significant concern in this case (Azar et al. 2015a). Although laser level pose estimation systems can offer an affordable

alternative to the robotic total station for determining the excavator's pose in real time, their potential is hindered by limited functional range (Kashani et al. 2010).

Lundeen et al. (2015) propose a camera marker based pose estimation technique for excavator, which is very cost effective at the same time. This technology owns some shortcomings too. Major limitations of using camera-based methods can be the vulnerability to the luminosity and line of sight. Lately, angular sensor dependent mechanisms are addressed as lightweight and infrastructure independent (Lee et al. 2012). Nevertheless, most of the present solution is suffering from the accuracy of estimation and current research only support the structured methodology to measure the pose with respect to the base of the articulated machines (Lu and Liang 2012). Some investigators tried to use an integrated global pensioning system (GPS) dependent mechanism as a solution of tracking the dynamic machine in a 3D environment, but GPS brings its own challenges (e.g., cost, accuracy, signal interference).

2.6 Summary

Mentioned challenges on the previous sections of this chapters clearly show a need a low-cost solution of pose estimation technique for the earthmoving excavator. This method can be integrated with the existing regular excavator, will cost like buying a new one and will guarantee productivity and safety. The new positioning mechanism needs to be appropriately elaborate to track the movement of the machine in the 3D working environment and should overcome the limitations like signal interference, obstructed line of sight, luminosity, etc. as discussed over the previous sections. At the same time, this technique requires to sufficiently accurate to serve the purpose.

Chapter 3

Uncertainty Quantification and Visualization: Positioning of Backhoe Excavator

3.1 General

Surveying is a prime requirement of any civil engineering project. Accurate analysis is as critical as the observation made in the survey. The most important aspect of surveying is to aid in planning a civil design, monitoring the job progress to check that the work is happening/done according to the design/plan. Trying to identify the position of the object of interest is always a challenging part of surveying. In case of the application on alignment checking during the progress of tunneling (guide the tunnel boring machine), trenching and even for collision avoidance for open-cut like project, accurate and precise measurement is mandatory. Most often devices/sensors are used for the purpose of measurement. All measurements can be affected by errors (except counting) due to the presence of the residual error in the manufacture of the instrument, human observations and environmental conditions and it is imperative to quantify and characterize those errors in both geospatial and time domains. Errors in measurement can be categorized into three types, random errors, systematic errors, and blunders. The objective of a well-designed survey is to eliminate blunders, account for any systematic error within the measurement process and minimize the effect of random errors.

Following sections of this chapter will discuss a unique process to quantify the survey error using error propagation theory and an error visualization technique with the aid of error ellipse to provide decision support to deal with positioning uncertainty. The theoretical contents of this chapter (section 3.2 to 3.4) are compiled from different book chapters or published articles (Montgomery and Runger 2003; Cursi et al. 2015; Spong et al. 2004; Corke 2011; WenzhongShi 2014; Ghanem et al. 2017;) but organized and explained according to the need to explain the solving process of the problem stated in Chapter 1 of this thesis.

3.2 Error Propagation

Measurement is a process subject to variation. Since all the measurements are subject to the discrepancy, what is conceived as the actual value of a measurement is merely an estimate of the true value. Difference between a measured value of a quantity and its true value, is considered as an error. If it is possible to obtain a reasonable estimation of true value, then it can be used to get an estimated value of error which is basically known as the residual. Among different types of error, only blunder can be avoided during the measuring process through verification. Systematic error of any measurement can be obtained if the true nature of the error is known and can be derived accordingly. This is done by functional substitution with truncated Taylor Series which actually behaves like removing the first term.

Taylor series is a representation of a function as an infinite sum of terms calculated from the values of its derivatives at a single point. Eq. 3.1 expresses a function of *x, f(x)* which can be expanded value of $x = x_o$.

$$f(x) = \sum_{n=0}^{\infty} \frac{f^n(x_0)}{n!}(x - x_0)^n \qquad (3.1)$$

Eq. 3.1 can be further expanded as,

$$f(x) = f(x_0) + \frac{f^1(x_0)}{1!}(x - x_0) + \frac{f^2(x_0)}{2!}(x - x_0)^2 + \ \ldots\ldots\ldots \qquad (3.2)$$

As the value of *n* goes up, the higher-order terms become insignificant. Thus, keeping the first two terms of the series Eq. 3.2 can be written as,

$$f(x) = f(x_0) + \frac{f^1(x_0)}{1!}(x - x_0) \qquad (3.3)$$

or,

$$y = y_0 + y'\Delta x$$

or,

$$y - y_0 = y'\Delta x$$

or,

$$\Delta y = y'\Delta x$$

or,

$$dy = \frac{\partial y}{\partial x} dx \qquad (3.4)$$

Now if *y* has *m* number of observations and each of them is dependent on *n* number of independent variables for *x* then the Eq. 3.4 becomes,

$$\begin{bmatrix} dy_1 \\ dy_2 \\ \vdots \\ dy_m \end{bmatrix} = \begin{bmatrix} \frac{\partial y_1}{\partial x_1} & \frac{\partial y_1}{\partial x_2} & \cdots & \frac{\partial y_1}{\partial x_n} \\ \frac{\partial y_2}{\partial x_1} & \frac{\partial y_2}{\partial x_2} & & \frac{\partial y_2}{\partial x_n} \\ \vdots & & \ddots & \vdots \\ \frac{\partial y_m}{\partial x_1} & \frac{\partial y_m}{\partial x_2} & \cdots & \frac{\partial y_m}{\partial x_n} \end{bmatrix} \begin{bmatrix} dx_1 \\ dx_2 \\ \vdots \\ dx_n \end{bmatrix}$$

or,

$$dy = J_{xy} dx \qquad (3.5)$$

Eq. 3.5 is the general form of systematic error propagation where J_{xy} is called the Jacobian (Jacobian matrix) of the equation. This one is the equation for quantifying the systematic error of a measurement.

3.2.1 Concept of Variance and Covariance

Two numbers are often used to summarize a probability distribution for any random variable *(x_i)*. These are the mean and variance of the measurement. The mean is a measure of the concentration of the probability distribution, and the variance is a measure of the dispersion, or variability in the distribution (Montgomery and Runger, 2003). For

any n number of observation of a specific measurement x_i $\{1 \leq i \leq n\}$, follows normal distribution then, the mean or expected value of the discrete random variable x, denoted as μ or $E(x)$ is,

$$\mu_x = E(x) = \frac{1}{n}\sum_{i}^{n} x_i \qquad (3.6)$$

The variance of x, denoted as σ^2 or V_x is,

$$\sigma_x{}^2 = V_x = E(x - \mu_x)^2$$

$$= \frac{1}{n-1}\sum_{i=1}^{n}(x_i - \mu_x)^2 \,; n \text{ is the sample size}^1 \qquad (3.7)$$

Eq. 3.7 can also be written as,

$$\sigma_x{}^2 = V_x = E(x - \mu_x)^2 = E(x^2 - 2x\mu_x + \mu_x{}^2)$$

$$= E(x^2) - 2E(x)\mu_x + \mu_x{}^2$$

$$= \left(\frac{1}{n-1}\sum_{i=1}^{n} x_i{}^2\right) - 2\mu_x\mu_x + \mu_x{}^2$$

$$= \left(\frac{1}{n-1}\sum_{i=1}^{n} x_i{}^2\right) - \mu_x{}^2 \qquad (3.8)$$

On the other hand, covariance is the measure of a relationship between two different random variables. For any n number of random observation of any specific measurement which is a set of two variable x_i and y_i $\{1 \leq i \leq n\}$, then the covariance of x and y denoted as C_{xy}, would be,

$$C_{xy} = E\big[(x - \mu_x)(y - \mu_y)\big]$$

[1] if total sample size is same as the population size then "n" should use instead of "(n-1)"

$$= \frac{1}{n-1}\sum_{i=1}^{n}(x_i - \mu_x)(y_i - \mu_y)\,;\ as\ n\ is\ the\ sample\ size \quad (3.9)$$

Eq. 3.9 can be written as

$$C_{xy} = \left(\frac{1}{n-1}\sum_{i=1}^{n}(x_i)(y_i)\right) - \mu_x\mu_y \qquad (3.10)$$

Value of covariance does not have any direct meaning. A positive value of covariance means the variables are positively related (in a 2D plot values remain on 1st and/or 3rd quadrant), while a negative covariance means the variables are inversely related (in a 2D plot values will remain on 2nd and/or 4th quadrant). If the value is zero that means, there is no relationship exists between the variables. Fig. 3.1 shows examples of pairs of random variables with positive, negative, and zero covariance.

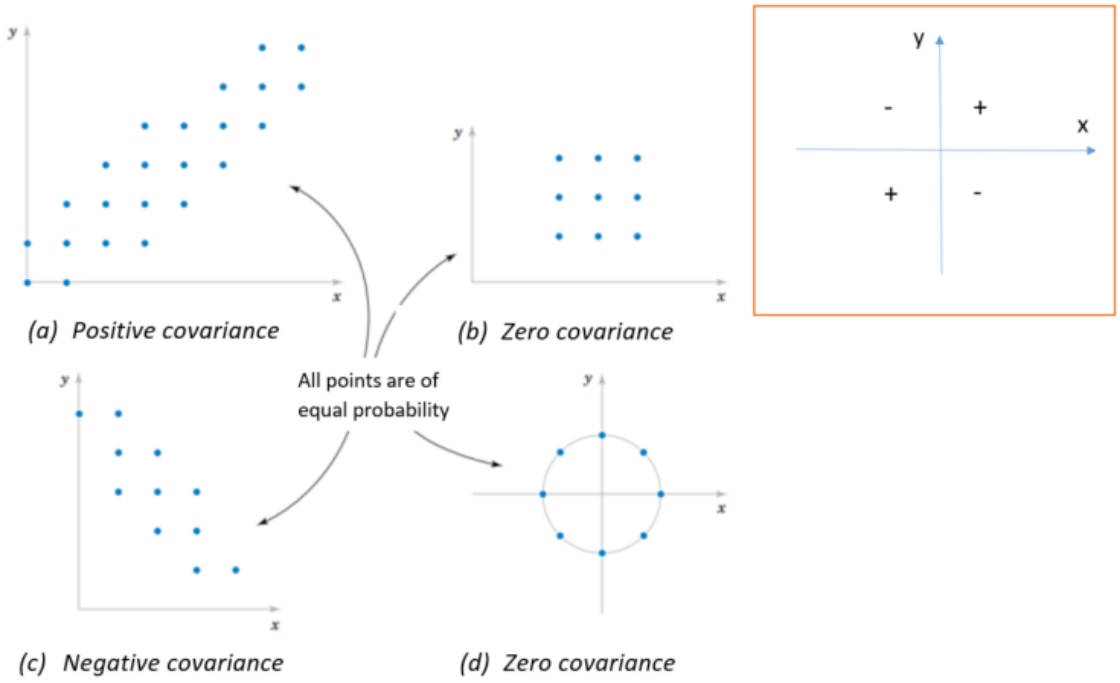

Figure 3.1 The sign of covariance between *x* and *y* (Montgomery and Runger, 2003).

A major application of covariance is to determine the coefficient of correlation (ρ) which mainly represents the scale of correlation between variables. Coefficient of correlation can be determined by the following formula,

$$\rho_{xy} = \frac{C_{xy}}{(\sigma_x)(\sigma_y)} \qquad (3.11)$$

If the correlation coefficient is one, that indicates the variables have a perfect positive correlation. This means that if one variable moves a given amount, the second move proportionally in the same direction. A positive correlation coefficient less than one indicates a less than perfect positive correlation, with the strength of the correlation growing as the number approaches one. If the correlation coefficient is zero, no relationship exists between the variables. If one variable move, you can make no predictions about the movement of the other variable; they are uncorrelated. If the correlation coefficient is –1, the variables are perfectly negatively correlated (or inversely correlated) and move in opposition to each other. If one variable increases, the other variable decreases proportionally. A negative correlation coefficient greater than –1 indicates a less than perfect negative correlation, with the strength of the correlation growing as the number approaches –1.

3.2.2 Propagation of Random Error

It is not perfect using Eq. 3.5 to quantify the random error of any measurement. Values of any particular measurement follow Gaussian distribution due to the presence of the randomness of error. Standard deviation/Variance of any set of measured values is a reasonable estimate of randomness. Thus, propagation of random error follows the law of propagation of variance and covariance (POV) which can be expressed by the following equation,

$$\sum\nolimits_{yy} = J_{xy} \sum\nolimits_{xx} J_{yx}^{T} \qquad (3.12)$$

or,

$$C_y = J_{yx}\, C_x\, J_{yx}^{T} \qquad (3.13)$$

or,

$$\begin{bmatrix} \sigma_{y_1}^2 & \sigma_{y_1y_2} & \cdots & \sigma_{y_1y_m} \\ \sigma_{y_2y_1} & \sigma_{y_2}^2 & & \sigma_{y_1y_m} \\ \vdots & & \ddots & \vdots \\ \sigma_{y_my_1} & \sigma_{y_my_2} & \cdots & \sigma_{y_m}^2 \end{bmatrix}$$

$$= J_{yx} \begin{bmatrix} \sigma_{x_1}^2 & \sigma_{x_1x_2} & \cdots & \sigma_{x_1x_n} \\ \sigma_{x_2x_1} & \sigma_{x_2}^2 & & \sigma_{x_1x_n} \\ \vdots & & \ddots & \vdots \\ \sigma_{x_nx_1} & \sigma_{x_nx_2} & \cdots & \sigma_{x_n}^2 \end{bmatrix} J_{yx}^T \qquad (3.14)$$

Here, $\sum_{yy}$ is the covariance matrix of random output *y* and $\sum_{xx}$ is the covariance matrix of random input *x.*

3.2.3 Explanation for $\boldsymbol{C_y = J_{yx}\, C_x\, J_{yx}^T}$

For a specific measurement, any observation (input) *x* can be mapped onto output *y* which is shown in Fig. 3.2(a). Output *y* basically can be expressed as a function of *x* in 2D space. Now if any error (Δx) exists in input value of *x*, this will propagate onto *y* through *f(x)*. This error can be quantified with the approximation of linearization of *f(x)* at the point *(x,y)* and the slope of the line would be $\frac{dy}{dx}$. Using the same basic principle of Eq. 3.4 the measurement of the error would be,

$$\Delta y = \frac{dy}{dx} \Delta x \qquad (3.15)$$

If now a set of observation (input) of a specific measurement *x*, which is random in nature and follows normal distribution, can be mapped onto a set of random output (normally distributed also) *y* with a relationship function *f(x)*, its shape would be somewhat distorted, and the resulting distribution would be asymmetric, certainly not Gaussian anymore. This phenomenon is shown in the Fig. 3.2(b) where the simple case with one input and one output is illustrated. Suppose that *x* is normally distributed with mean μ_x and standard deviation σ_x. The propagation strategy from *x* to *y* is explained in the following section.

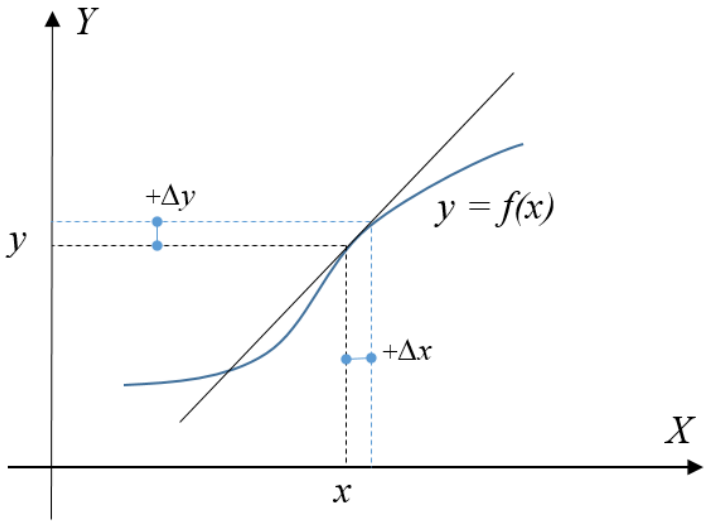

(a)

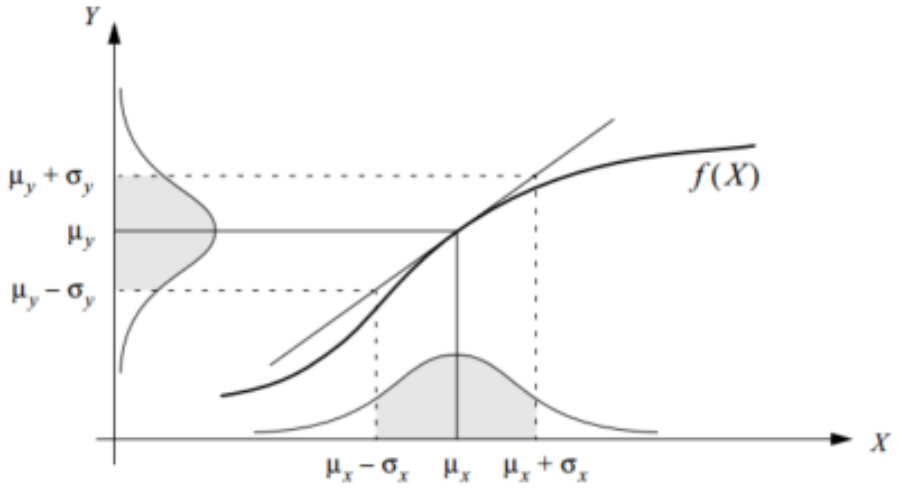

(b)

Figure 3.2 One-dimensional case of a nonlinear random error propagation problem

When approximating *f(x)* by a first-order Taylor series expansion (Eq. 3.3) about the point $x = \mu_x$, the following linear relationship can be obtained,

$$y = f(x) \approx f(\mu_x) + \frac{\partial f(\mu_x)}{\partial x}(x - \mu_x) \qquad (3.16)$$

If $y = f(x_1, x_2, x_3, \ldots \ldots, x_n)$ then the Eq. 3.16 becomes,

$$y \approx f(\mu_1, \mu_2, \dots\dots, \mu_n) + \sum_{i=1}^{n} \left[\frac{\partial f}{\partial x}((\mu_1, \mu_2, \dots\dots, \mu_n)\right](x_i - \mu_i)$$

or,

$$y \approx a_o + \sum_{i=1}^{n} a_i \ (x_i - \mu_i) \qquad (2.17)$$

where, $a_o = f(\mu_1, \mu_2, \dots\dots, \mu_n)$ and $a_i = \frac{\partial f}{\partial x}((\mu_1, \mu_2, \dots\dots, \mu_n)$

Now

$$\mu_y = E[y] = E\left[a_o + \sum_{i=1}^{n} a_i \ (x_i - \mu_i)\right]$$

$$= E\ [a_o] + \sum_{i=1}^{n} E[a_i x_i] - E[a_i \mu_i]$$

$$= a_o + \sum_{i=1}^{n} a_i E[x_i] - a_i E[\mu_i]$$

$$= a_o + \sum_{i=1}^{n} a_i \mu_i - a_i \mu_i$$

$$= a_o + \sum_{i=1}^{n} a_i \mu_i - a_i \ = a_o$$

$$\mu_y = f(\mu_1, \mu_2, \dots\dots, \mu_n) \qquad (3.18)$$

And,

$$\sigma_y^2 = E\left[\left(y - \mu_y\right)^2\right]$$

$$\sigma_y^2 \approx E\left[\left(a_o + \sum_{i=1}^{n} a_i \ (x_i - \mu_i) - a_o\right)^2\right] = E\left[\left(\sum_{i=1}^{n} a_i \ (x_i - \mu_i)\right)^2\right]$$

$$= E\left[\sum_{i=1}^{n} {a_i}^2 \ (x_i - \mu_i)^2\right]$$

$$= \sum_{i=1}^{n} {a_i}^2 E[(x_i - \mu_i)^2]$$

$$= \sum_{i=1}^{n} {a_i}^2 \sigma_i^2$$

$$= \sum_{i=1}^{n} \left(\frac{\partial f}{\partial x_i}\right)^2 \sigma_i^2$$

So, the final equation becomes,

$$\sigma_y^2 = \sum_{i=1}^{n} \left(\frac{\partial f}{\partial x_i}\right)^2 \sigma_i^2 \qquad (3.19)$$

If *y* has *m* number of observation which is dependent on *n* number of variables of *x*, then general matrix form of Eq. 3.19 would be,

$$\begin{bmatrix} \sigma_{y_1}^2 & \sigma_{y_1 y_2} & \cdots & \sigma_{y_1 y_m} \\ \sigma_{y_2 y_1} & \sigma_{y_2}^2 & & \sigma_{y_1 y_m} \\ \vdots & & \ddots & \vdots \\ \sigma_{y_m y_1} & \sigma_{y_m y_2} & \cdots & \sigma_{y_m}^2 \end{bmatrix}$$

$$= \begin{bmatrix} \frac{\partial f_1}{\partial x_1} & \frac{\partial f_1}{\partial x_2} & \cdots & \frac{\partial f_1}{\partial x_n} \\ \frac{\partial f_2}{\partial x_1} & \frac{\partial f_2}{\partial x_2} & & \frac{\partial f_2}{\partial x_n} \\ \vdots & & \ddots & \vdots \\ \frac{\partial f_m}{\partial x_1} & \frac{\partial f_m}{\partial x_2} & \cdots & \frac{\partial f_m}{\partial x_n} \end{bmatrix} \begin{bmatrix} \sigma_{x_1}^2 & \sigma_{x_1 x_2} & \cdots & \sigma_{x_1 x_n} \\ \sigma_{x_2 x_1} & \sigma_{x_2}^2 & & \sigma_{x_1 x_n} \\ \vdots & & \ddots & \vdots \\ \sigma_{x_n x_1} & \sigma_{x_n x_2} & \cdots & \sigma_{x_n}^2 \end{bmatrix} \begin{bmatrix} \frac{\partial f_1}{\partial x_1} & \frac{\partial f_2}{\partial x_1} & \cdots & \frac{\partial f_m}{\partial x_n} \\ \frac{\partial f_1}{\partial x_2} & \frac{\partial f_2}{\partial x_2} & & \frac{\partial f_m}{\partial x_n} \\ \vdots & & \ddots & \vdots \\ \frac{\partial f_1}{\partial x_n} & \frac{\partial f_2}{\partial x_n} & \cdots & \frac{\partial f_m}{\partial x_n} \end{bmatrix}$$

or,

$$C_y = J_{yx}\, C_x\, J_{yx}^T \qquad (3.20)$$

Which cross validates the Eq. 3.14.

3.3 Error Visualization Technique

3.3.1 1D Error Visualization

Plotting the distribution (histogram) of a particular measurement is a very common practice to understand the randomness of the error when the output of measurement is one dimensional (dependent on a single variable x). Fig. 3.3(a) represents random measurements of x, the distribution which is normal in nature. The mean/expected value of x is μ_x, can be found at the center of the distribution. Any value left or right of the mean has error and the value of error increases as the value of observation (x) falls as much apart from the mean (either left or right). Sometimes it is more convenient only to isolate the error from the actual values. To isolate the error from the original value, mean of the distribution has to shift to the origin. Fig 3.3(b) represents only the distribution of the error residing on the measurement.

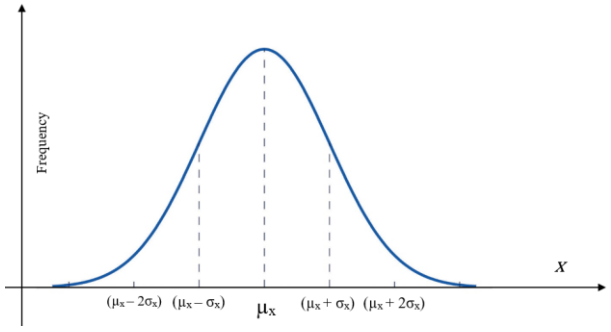

(a)

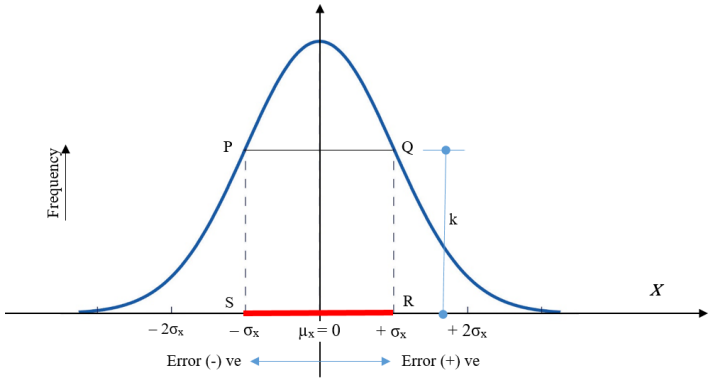

(b)

Figure 3.3 1D error visualization.

Now if a line parallel to the *x axis* cuts the distribution curve at height k from the base (*x axis*) at points *P* and *Q*, the projection of edge *PQ* at *x axis* [*SR; red colored on Fig. 3.3(b)*] represents the one-dimensional (1D) error where points *S* and *R* are the boundary (upper limit and lower limit) of the error. Left to origin at Fig. 3.3(b) represents negative error and right to the origin represents positive error. Depending on different *k* value the spread (length) of *SR* would be different. When the confidence level would be higher, then the spread of *SR* will increase and vice versa.

To summarize, 1D error can be represented by a single line centered at the origin. The spread of the line depends on the confidence level considered.

3.3.2 2D Error Visualization with Error Ellipse

If a specific observation consists two variables *x* and *y,* the joint distribution of two random variables *x* and *y* are shown in the upper part of the Fig. 3.4 and the lower represents the 2D projection of the joint distribution of variables *x* and *y*. Density function *f(x,y)* is a bell shaped surface centered at $x = \mu_x$ and $y = \mu_y$. The individual density function of *x* and *y* can be denoted as *f(x)* and *f(y)* respectively.

The joint density function *f(x,y)* can be expressed with the following equation,

$$f(x,y) = \frac{1}{2\pi\sigma_x\sigma_y\sqrt{1-\rho^2}} exp\left\{\frac{-1}{2(1-\rho^2)}\left[\left(\frac{x-\mu_x}{\sigma_x}\right)^2 - 2\rho\left(\frac{x-\mu_x}{\sigma_x}\right)\left(\frac{y-\mu_y}{\sigma_y}\right) + \left(\frac{y-\mu_y}{\sigma_y}\right)^2\right]\right\} \quad (3.21)$$

Where, μ_x and σ_x = mean and standard deviation of *x;*

μ_y and σ_y = mean and standard deviation of *y*;

$\rho = \frac{\sigma_{xy}}{\sigma_x\sigma_y}$, is the correlation coefficient.

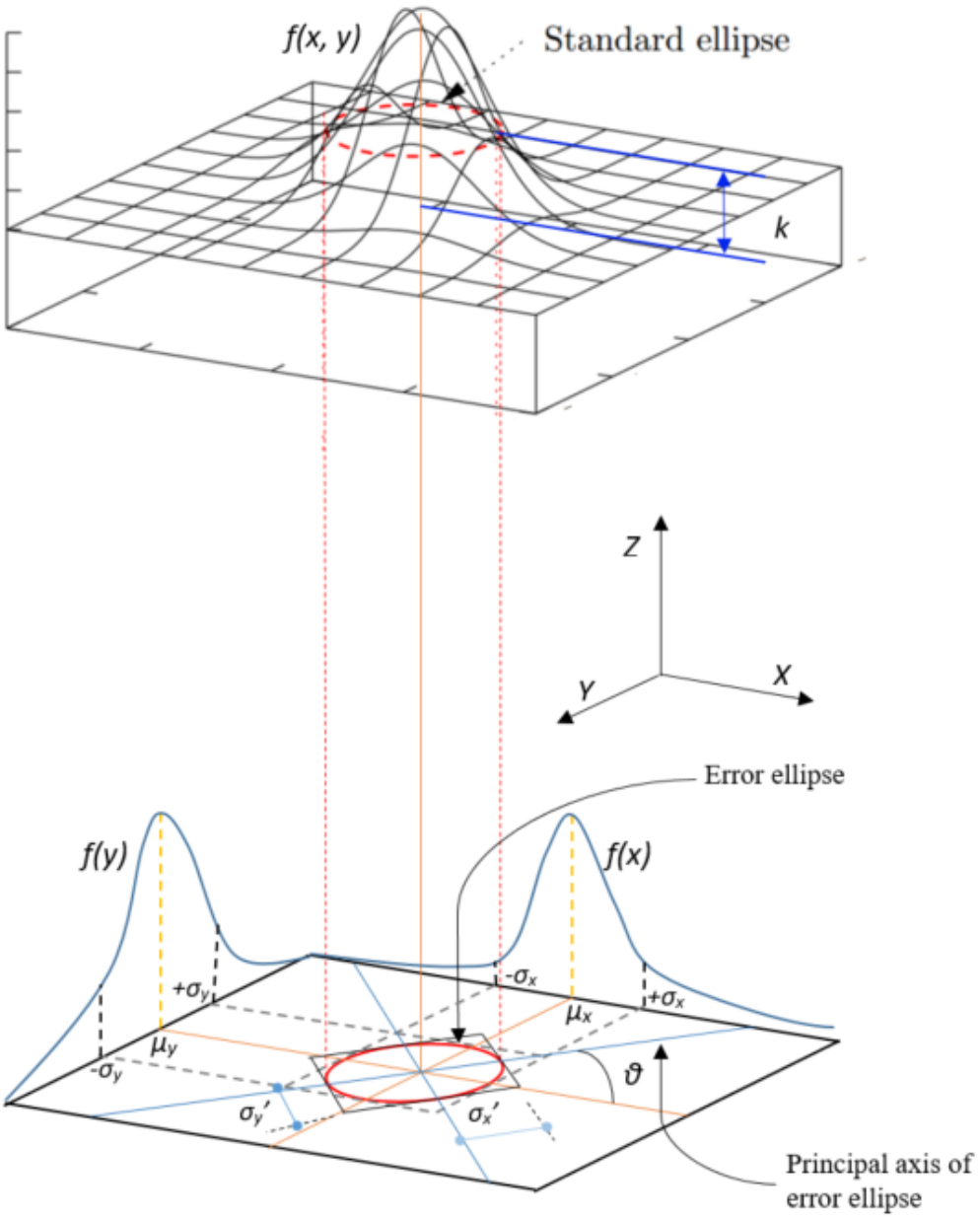

Figure 3.4 Joint distribution of two random variable x and y.

When a parallel to the x-y coordinate plane cuts the bivariate density surface at a height k an ellipse is formed and it is called the **error ellipse** and the equation for the error ellipse would be the following

$$\left(\frac{x-\mu_x}{\sigma_x}\right)^2 - 2\rho\left(\frac{x-\mu_x}{\sigma_x}\right)\left(\frac{y-\mu_y}{\sigma_y}\right) + \left(\frac{y-\mu_y}{\sigma_y}\right)^2 = (1-\rho^2)c^2 \qquad (3.22)$$

Here, $c^2 = ln\left[4\pi^2 k^2 \sigma_x^2 \sigma_y^2 (1-\rho^2)\right]^{-1} = constant$

Bottom figure of Fig. 3.4 shows the 2D projection of joint density function *f(x, y)* where error ellipse can be identified clearly. Centre of the error ellipse is at (μ_x, μ_y). The perimeter of the error ellipse depends on value *k,* represents the dispersion of the error around the mean. Practically it means the true value of observation can be any value restricted by the perimeter of the ellipse. Value of *k* depends on the confidence level of the distribution. As much higher the confidence level expected, *k* value would decrease and thus the spread of the error will increase (perimeter of the error ellipse will increase) and vice versa.

If the bivariate probability distribution is centered at the origin ($\mu_x = \mu_y = 0$), then Eq. 3.22 becomes

$$\left(\frac{x}{\sigma_x}\right)^2 - 2\rho\left(\frac{x}{\sigma_x}\right)\left(\frac{y}{\sigma_y}\right) + \left(\frac{y}{\sigma_y}\right)^2 = (1-\rho^2)c^2 \qquad (3.23)$$

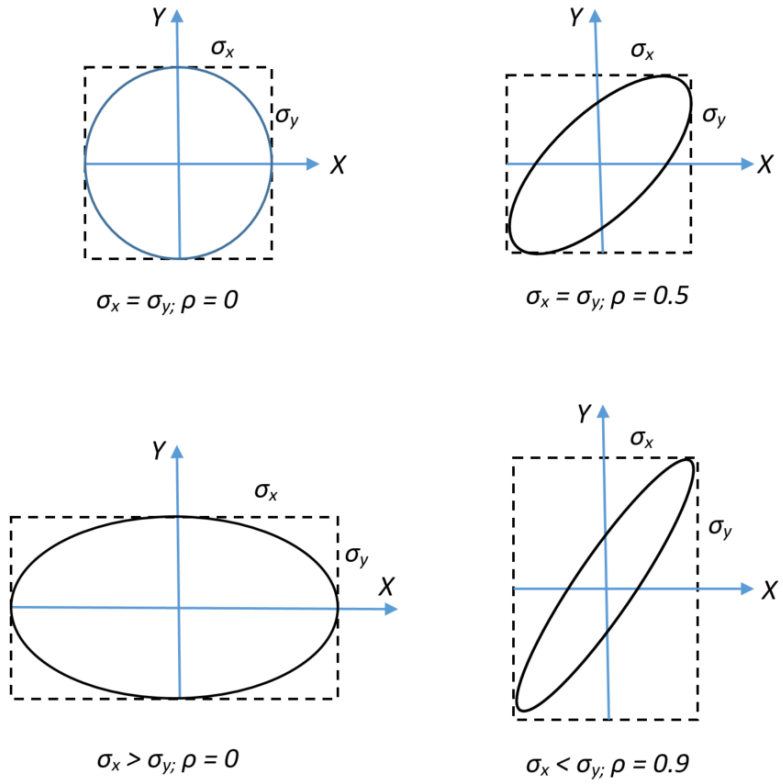

Figure 3.5 Sample variants of standard error ellipse.

When $c = 1$ Eq. 3.23 gives the equation of a standard error ellipse which represents the area of uncertainty for the location of a control point. From the above equation, it is seen that the size shape and the orientation of an error ellipse is governed by the parameters σ_x, σ_y and ρ. Fig 3.5 shows sample variants of standard error ellipse.

In general, the *principle axes X'Y'* does not coincide with the *coordinate axes XY* because principle axes represent the uncorrelated values for *x* and *y*. The uncorrelated major axis *X'* makes an angle θ with respect to the *X* axes (Fig. 3.6).

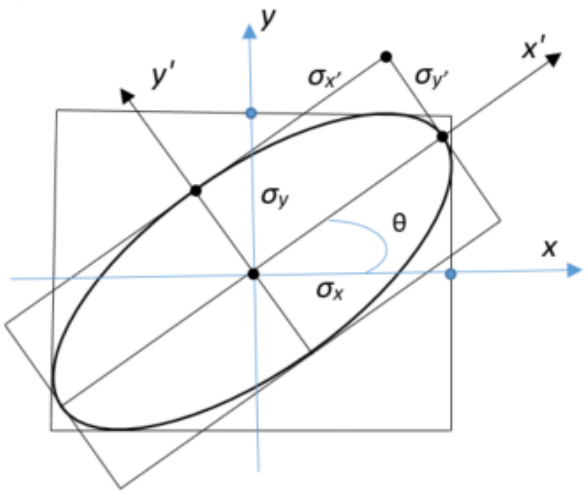

Figure 3.6 Error ellipse's orientation.

Potential errors now can be expressed in the *coordinate axes xy* and transform to *coordinate axes X'Y'*. Two vectors can be correlated by the following transformation matrix

$$\begin{bmatrix} x' \\ y' \end{bmatrix} = \begin{bmatrix} cos\theta & sin\theta \\ -sin\theta & cos\theta \end{bmatrix} \begin{bmatrix} x \\ y \end{bmatrix} \qquad (3.24)$$

or,

$$P_{x'y'} = Q_\theta P_{xy} \qquad (3.25)$$

here, $P_{x'y'} = \begin{bmatrix} x' \\ y' \end{bmatrix}; Q_{xy} = \begin{bmatrix} cos\theta & sin\theta \\ -sin\theta & cos\theta \end{bmatrix}; P_{xy} = \begin{bmatrix} x \\ y \end{bmatrix}$

To draw the error ellipse, it is important to identify the variances for (*x'*, *y')* values. According to the law of propagation of variance/covariance (Eq. 3.12),

$$C_{x'y'} = Q_\theta C_{xy} Q_\theta^T \tag{3.26}$$

or,

$$\begin{bmatrix} \sigma_{x'}^2 & \sigma_{x'y'} \\ \sigma_{x'y'} & \sigma_{y'}^2 \end{bmatrix} = \begin{bmatrix} cos\theta & sin\theta \\ -sin\theta & cos\theta \end{bmatrix} \begin{bmatrix} \sigma_x^2 & \sigma_{xy} \\ \sigma_{xy} & \sigma_y^2 \end{bmatrix} \begin{bmatrix} cos\theta & -sin\theta \\ sin\theta & cos\theta \end{bmatrix} \tag{3.27}$$

As *x'* and *y'* are uncorrelated, $\sigma_{x'y'} = 0$. Then the Eq. 3.2.7 would become

$$\begin{bmatrix} \sigma_{x'}^2 & 0 \\ 0 & \sigma_{y'}^2 \end{bmatrix} = \begin{bmatrix} cos\theta & sin\theta \\ -sin\theta & cos\theta \end{bmatrix} \begin{bmatrix} \sigma_x^2 & \sigma_{xy} \\ \sigma_{xy} & \sigma_y^2 \end{bmatrix} \begin{bmatrix} cos\theta & -sin\theta \\ sin\theta & cos\theta \end{bmatrix} \tag{3.28}$$

Solving the above equation (Eq. 3.28), the following solutions are obtained,

$$\sigma_{x'}^2 = \sigma_x^2 cos^2\theta + 2\sigma_{xy} sin\theta cos\theta + \sigma_y^2 sin^2\theta \tag{3.29}$$

$$\sigma_y^2 = \sigma_y^2 sin^2\theta - 2\sigma_{xy} sin\theta cos\theta + \sigma_y^2 cos^2\theta \tag{3.30}$$

$$0 = (\sigma_y^2 - \sigma_x^2) sin\theta cos\theta + \sigma_{xy}(cos^2\theta - sin^2\theta) \tag{3.31}$$

From Eq. 3.29

$$\sigma_{x'}^2 = \sigma_x^2 \frac{1 + cos2\theta}{2} + \sigma_{xy} sin2\theta + \sigma_y^2 \frac{1 - cos2\theta}{2}$$

or,

$$\sigma_{x'}^2 = \frac{\sigma_x^2 + \sigma_y^2}{2} + \frac{\sigma_x^2 - \sigma_y^2}{2} cos2\theta + \sigma_{xy} sin2\theta$$

or,

$$\sigma_{x'}^2 - \frac{\sigma_x^2 + \sigma_y^2}{2} = \frac{\sigma_x^2 - \sigma_y^2}{2} cos2\theta + \sigma_{xy} sin2\theta \tag{3.32}$$

From Eq. 3.31

$$0 = -\frac{(\sigma_x^2 - \sigma_y^2)}{2} sin2\theta + \sigma_{xy} cos2\theta \tag{3.33}$$

After squaring adding Eq. 3.32 & Eq. 3.33

$$\left(\sigma_{x'}^2 - \frac{\sigma_x^2 + \sigma_y^2}{2}\right)^2 = \left(\frac{\sigma_x^2 - \sigma_y^2}{2}\right)^2 + \sigma_{xy}^2$$

$$\sigma_{x'}^2 = \frac{\sigma_x^2 + \sigma_y^2}{2} + \sqrt{\left(\frac{\sigma_x^2 - \sigma_y^2}{2}\right)^2 + \sigma_{xy}^2} \tag{3.34}$$

Similarly,

$$\sigma_{y'}^2 = \frac{\sigma_x^2 + \sigma_y^2}{2} - \sqrt{\left(\frac{\sigma_x^2 - \sigma_y^2}{2}\right)^2 + \sigma_{xy}^2} \tag{3.35}$$

Adding Eq. 3.34 and Eq. 3.35

$$\sigma_{x'}^2 + \sigma_{y'}^2 = \sigma_x^2 + \sigma_y^2 \tag{3.36}$$

From Eq. 3.33

$$tan2\theta = \frac{2\sigma_{xy}}{\sigma_x^2 - \sigma_y^2} \tag{3.37}$$

Eq. 3.37 can be used to identify the orientation of the principal axis of the error ellipse.

To summarize, the error ellipse visualizes the joint error of two variables *(x, y)*, which is counted from the individual variable error, thus, is addressed in a 2D error visualization system. That means it is necessary to know the randomness (standard deviation, σ; correlation coefficient, ρ) of error for each variable among two in order to visualize the joint error of two variables. These randomness parameters basically decide the shape (σ' *from Eq. 3.34 and Eq. 3.35*) and orientation (θ *from Eq. 3.37*) of the error ellipse (bottom of Fig. 3.4 and orientation is clearly illustrated in Fig. 3.6).

It is to be noted that, in 3D space, where the joint density function will consist of three variables *x, y and z,* [*f(x, y, z)*] then the error ellipse will turn into an ellipsoid, like Fig. 3.7(rugby).

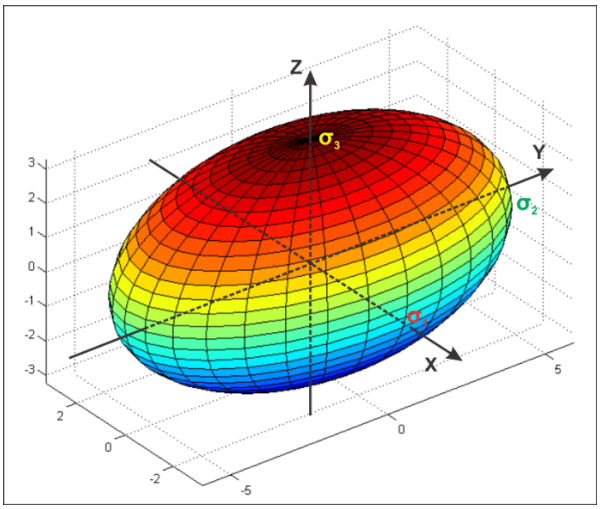

Figure 3.7 Error ellipsoid.

3.3.3 Setting the Limit for the Error Ellipse

For any independent (uncorrelated, $\rho=0$) random errors of *x* and *y* Eq. 3.23 becomes

$$\left(\frac{x}{\sigma_x}\right)^2 + \left(\frac{y}{\sigma_y}\right)^2 = c^2 \qquad (3.38)$$

Eq. 3.38 defines the spread (boundary) of the error. Here the constant c is the parameter regulates the perimeter of the error ellipse. So, for a given point whose position is defined by the random error, the point will lie within the error ellipse if,

$$U = \left(\frac{x}{\sigma_x}\right)^2 + \left(\frac{y}{\sigma_y}\right)^2 \leq c^2 \qquad (3.39)$$

U has randomness and follows a chi-square distribution with two degrees of freedom. Therefore, the probability that the position of *x* and *y* lies on/within the error ellipse is,

$$P[U \leq c^2\ ] = \int_0^{c^2} \frac{1}{2} e^{\frac{-u}{2}} du$$

$$= \left[\frac{1}{2 \times \left(-\frac{1}{2}\right)} e^{\frac{-u}{2}} \right]_0^{c^2}$$

$$= \left[-e^{\frac{-u}{2}} \right]_0^{c^2}$$

$$= \left[-e^{\frac{-c^2}{2}} - (-1) \right]$$

$$= 1 - e^{\frac{-c^2}{2}}$$

So,

$$P[U \leq c^2\ ] = 1 - e^{\frac{-c^2}{2}} \qquad (3.40)$$

3.4 Kinematics of Backhoe Excavator

3.4.1 The Denavit Hartenberg (DH) Convention

The backhoe excavator's arm is composed of links connected together with the revolute joint. Basically, this arm operates with the help of hydraulic actuator which itself is nothing but special kind of prismatic joint. Both revolute and prismatic joints have only single degree of freedom of motion; the angle of rotation in the case of a revolute joint and amount of displacement in the case of a prismatic joint. With this assumption that each joint has single degree of freedom, the action can then be described by the real number.

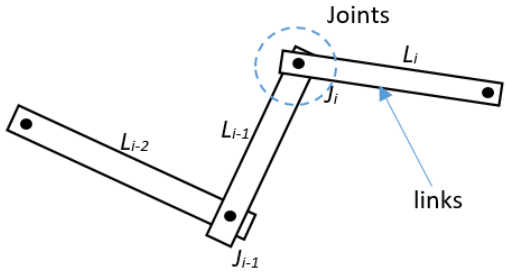

Figure 3.8 Links and joints of a robot manipulator.

A robot manipulator with n joints will have $n+1$ links since each joint can connect two links (Fig. 3.8) and the joints can be numbered from 1 to n ($J_{i=1-n}$) and the number of links will be from 0 to n ($L_{i=0-n}$). By this convention joint J_i connects link L_i to link L_{i-1} and the location of joint J_i is to be fixed with respect to link L_{i-1}. That means when joint J_i is actuated, link L_i moves. Therefore, link 0 (the first link) is fixed, and does not move when the joints are actuated.

With the *i-th* joint, a joint variable can be assigned, denoted by q_i and in the case of a revolute joint, q_i is the angle of rotation θ_i, and in the case of a prismatic joint, q_i is the joint displacement d_i (Eq. 3.41).

$$q_i = \begin{cases} \theta_i \\ d_i \end{cases} \qquad (3.41)$$

To perform the kinematic analysis, it is necessary to attach a coordinate frame to each link. In particular, plane $o_i x_i y_i z_i$ has to attach to link L_i. This means that, whatever motion the robot executes, the coordinates of each point on link L_i are constant when expressed in the *ith* coordinate frame. Furthermore, when joint J_i is actuated, link L_i and its attached frame, $o_i x_i y_i z_i$, experience a resulting motion. The frame $o_0 x_0 y_0 z_0$, which is attached to the robot base, is referred to as the inertial frame.

Now A_i is a homogeneous transformation matrix can be declared to express the position and orientation of $o_i x_i y_i z_i$ with respect to $o_{i-1} x_{i-1}\ y_{i-1}\ z_{i-1}$ and varies as the configuration of the robot is changed. So,

$$A_i = f(q_i) \qquad (3.42)$$

Now the homogeneous transformation matrix that expresses the position and orientation of $o_j x_j y_i z_j$ with respect to $o_i x_i y_i z_i$ is called, by convention, a transformation matrix, and is denoted by T_j^i.

$$T_j^i = \begin{cases} A_{i+1} A_{i+2} \dots\dots A_{j-1} A_j \ ; \ if\ i < j \\ I \qquad\qquad\qquad\qquad\quad ; \ \ if\ i = j \\ \left(T_i^j\right)^{-1} \qquad\qquad\quad ; \ \ if\ j > i \end{cases} \qquad (4.1.3)$$

Denavit Hartenberg, or D-H convention is widely used for the purpose of frames of reference. In this convention, each homogeneous transformation A_i is represented as a product of four basic transformations

$$A_i = Rot_z(\theta_i)Trans_z(d_i)Trans_x(\alpha_i)Rot_x(\alpha_i) \qquad (3.44)$$

Here,

$$Rot_z(\theta_i) = \begin{bmatrix} cos\theta_i & -sin\theta_i & 0 & 0 \\ sin\theta_i & cos\theta_i & 0 & 0 \\ 0 & 0 & 1 & 0 \\ 0 & 0 & 0 & 1 \end{bmatrix}, Trans_z(d_i) = \begin{bmatrix} 1 & 0 & 0 & 0 \\ 0 & 1 & 0 & 0 \\ 0 & 0 & 1 & d_i \\ 0 & 0 & 0 & 1 \end{bmatrix},$$

$$Trans_x(a_i) = \begin{bmatrix} 1 & 0 & 0 & a_i \\ 0 & 1 & 0 & 0 \\ 0 & 0 & 1 & 0 \\ 0 & 0 & 0 & 1 \end{bmatrix}, Rot_x(\alpha_i) = \begin{bmatrix} 1 & 0 & 0 & 0 \\ 0 & cos\alpha_i & -sin\alpha_i & 0 \\ 0 & sin\alpha_i & cos\alpha_i & 0 \\ 0 & 0 & 0 & 1 \end{bmatrix}$$

So,

$$A_i = \begin{bmatrix} cos\theta_i & -sin\theta_i & 0 & 0 \\ sin\theta_i & cos\theta_i & 0 & 0 \\ 0 & 0 & 1 & 0 \\ 0 & 0 & 0 & 1 \end{bmatrix} \begin{bmatrix} 1 & 0 & 0 & 0 \\ 0 & 1 & 0 & 0 \\ 0 & 0 & 1 & d_i \\ 0 & 0 & 0 & 1 \end{bmatrix} \begin{bmatrix} 1 & 0 & 0 & a_i \\ 0 & 1 & 0 & 0 \\ 0 & 0 & 1 & 0 \\ 0 & 0 & 0 & 1 \end{bmatrix} \begin{bmatrix} 1 & 0 & 0 & 0 \\ 0 & cos\alpha_i & -sin\alpha_i & 0 \\ 0 & sin\alpha_i & cos\alpha_i & 0 \\ 0 & 0 & 0 & 1 \end{bmatrix}$$

$$A_i^{i-1} = \begin{bmatrix} cos\theta_i & -sin\theta_i cos\alpha_i & sin\theta_i sin\alpha_i & a_i cos\theta_i \\ sin\theta_i & cos\theta_i cos\alpha_i & -cos\theta_i sin\alpha_i & a_i sin\theta_i \\ 0 & sin\alpha_i & cos\alpha_i & d_i \\ 0 & 0 & 0 & 1 \end{bmatrix} \qquad (3.45)$$

here the four quantities θ_i, a_i, d_i, α_i are parameters associated with link L_i and joint J_i. The four parameters a_i, α_i, d_i, and θ_i in Eq. 3.45 are generally given the names *link length, link twist, link offset*, and *joint angle*, respectively illustrated in Fig. 3.42. Since the matrix A_i is a function of a single variable, it turns out that three of the above four quantities are constant for a given link, while the fourth parameter, θ_i for a revolute joint and d_i for a prismatic joint, is the joint variable.

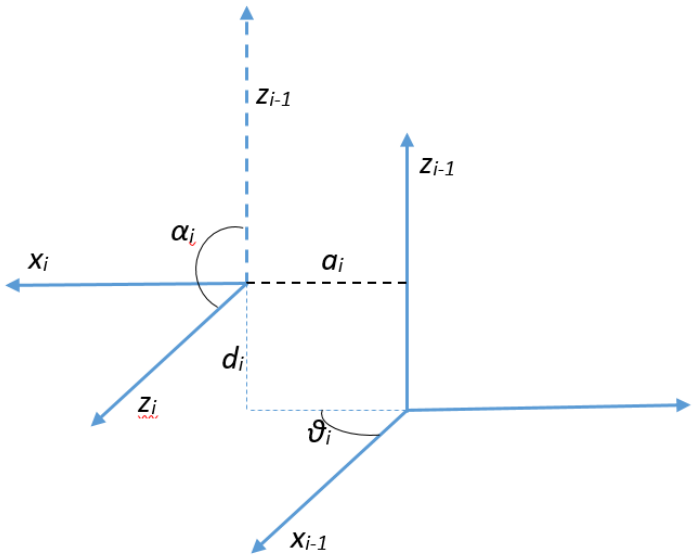

Figure 3.9 D-H parameters.

Some key features need to be followed while assigning the frames. Which are,

- Axis x_i is set so it is perpendicular to axis z_{i-1} (DH rule 1).
- The axis x_i intersects the axis z_{i-1} (DH rule 2).
- z_{i-1} is axis of actuation of joint J_i; axis of revolution of revolute joint and axis of translation of prismatic joint.
- y_i can be derived from x_i and z_i.

Homogeneous coordinates are widely used for coordinate transformations. Each four-dimensional homogeneous coordinate $(x, y, z, s)$is identical to a 3D point $(x/s, y/s, z/s)$ in a Cartesian coordinate system. Thus, each Cartesian coordinate $(\mathrm{x}, \mathrm{y}, \mathrm{z})$ in 3D can be represented as a homogeneous point $(x, y, z, 1)$. Assume the end effector of L_i is j_{i+1} with coordinates $(\mathrm{x}_i, \mathrm{y}_i, \mathrm{z}_i)$ in $o_i x_i y_i z_i$, its homogenous coordinates in $o_{i-1} x_{i-1} y_{i-1} z_{i-1}$ can be derived with Eq. 3.46.

$$\begin{bmatrix} \mathrm{x}_{i-1} \\ \mathrm{y}_{i-1} \\ \mathrm{z}_{i-1} \\ 1 \end{bmatrix} = T_i^{i-1} \begin{bmatrix} \mathrm{x}_i \\ \mathrm{y}_i \\ \mathrm{z}_i \\ 1 \end{bmatrix} \tag{3.46}$$

3.4.2 Forward Kinematics of Excavator

A typical backhoe excavator can be separated into 4 rigid components: platform, boom, stick and bucket. Thus, the full kinematics of a typical backhoe excavator can be modeled with 3 joints representing the components and 4 links indicating the rotation axes as presented in Fig. 3.10.

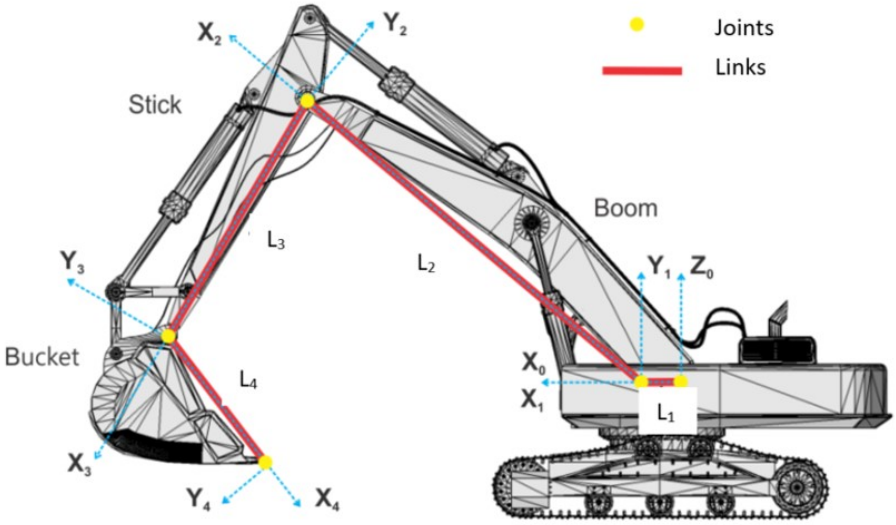

Figure 3.10 Kinematics of backhoe excavators (simplified).

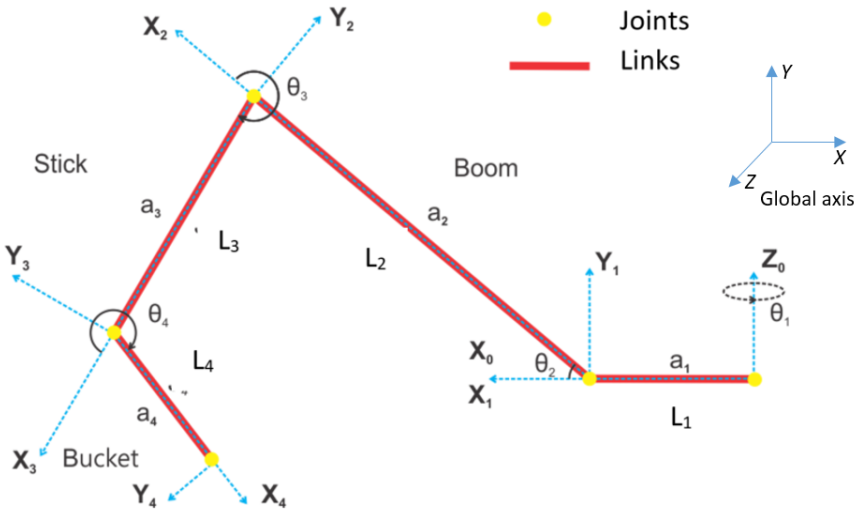

Figure 3.11 D-H convention coordinate frames & parameters for an excavator.

Five coordinate frames are also assigned to each link and a base is defined following the D-H convention. Fig. 3.11 shows the detailed frames assignment and the parameters corresponding to the frames based on D-H convention. In this figure (Fig. 3.11), two axes of each coordinate frame are explicitly presented, the other axis complements the two axes to form a right-hand coordinate frame. The parameters used to transform the coordinates between successive coordinate frames, i.e. from coordinate frame i to frame $i-1$, are listed in Table 3.1. It is noteworthy that a_i, d_i, α_i are constants and only the rotation angle θ_i of each joint is the variable.

Table 3.1. D-H convention parameters

Link	$\boldsymbol{a_i}$	$\boldsymbol{d_i}$	$\boldsymbol{\alpha_i}$	$\boldsymbol{\theta_i^*}$
L1	a_1	0	90°	θ_1
L2	a_2	0	0°	θ_2
L3	a_3	0	0°	θ_3
L4	a_4	0	0°	θ_4

Among the 5 coordinate systems, the coordinate system $ox_0y_0z_0$ (base frame coordinate) is used to depict the horizontal motion of the excavator, and other coordinate frames are applied to describe the vertical motion of the arm of the excavator. As according to the shown link parameters shown in Table 1, the corresponding A and T matrices would be (from Eq. 3.45),

$$A_1 = \begin{bmatrix} cos\theta_1 & 0 & sin\theta_1 & a_1 cos\theta_1 \\ sin\theta_1 & 0 & -cos\theta_1 & a_1 sin\theta_1 \\ 0 & 1 & 0 & 0 \\ 0 & 0 & 0 & 1 \end{bmatrix}$$

$$A_2 = \begin{bmatrix} cos\theta_2 & 0 & sin\theta_2 & a_2 cos\theta_2 \\ sin\theta_2 & 0 & -cos\theta_2 & a_2 sin\theta_2 \\ 0 & 1 & 0 & 0 \\ 0 & 0 & 0 & 1 \end{bmatrix}$$

$$A_3 = \begin{bmatrix} cos\theta_3 & -sin\theta_3 & 0 & a_3cos\theta_3 \\ sin\theta_3 & cos\theta_3 & 0 & a_3sin\theta_3 \\ 0 & 0 & 1 & 0 \\ 0 & 0 & 0 & 1 \end{bmatrix}$$

$$A_4 = \begin{bmatrix} cos\theta_4 & -sin\theta_4 & 0 & a_4cos\theta_4 \\ sin\theta_4 & cos\theta_4 & 0 & a_4sin\theta_4 \\ 0 & 0 & 1 & 0 \\ 0 & 0 & 0 & 1 \end{bmatrix}$$

From Eq. 3.45

$$T_4^0 = A_1A_2A_3A_4$$

$$T_4^0 = \begin{bmatrix} cos\theta_1 & 0 & sin\theta_1 & a_1cos\theta_1 \\ sin\theta_1 & 0 & -cos\theta_1 & a_1sin\theta_1 \\ 0 & 1 & 0 & 0 \\ 0 & 0 & 0 & 1 \end{bmatrix} \begin{bmatrix} cos\theta_2 & 0 & sin\theta_2 & a_2cos\theta_2 \\ sin\theta_2 & 0 & -cos\theta_2 & a_2sin\theta_2 \\ 0 & 1 & 0 & 0 \\ 0 & 0 & 0 & 1 \end{bmatrix}$$

$$\begin{bmatrix} cos\theta_3 & -sin\theta_3 & 0 & a_3cos\theta_3 \\ sin\theta_3 & cos\theta_3 & 0 & a_3sin\theta_3 \\ 0 & 0 & 1 & 0 \\ 0 & 0 & 0 & 1 \end{bmatrix} \begin{bmatrix} cos\theta_4 & -sin\theta_4 & 0 & a_4cos\theta_4 \\ sin\theta_4 & cos\theta_4 & 0 & a_4sin\theta_4 \\ 0 & 0 & 1 & 0 \\ 0 & 0 & 0 & 1 \end{bmatrix} \quad (3.47)$$

So,

$$T_4^0 = t(\theta_1, \theta_1, \theta_1, \theta_1); as\ a_1, a_2, a_3\ and\ a_4\ are\ constant \quad (3.48)$$

Now, position of bucket tip, P4 (x_4, y_4, z_4) can found after substituting values on Eq. 3.46,

$$\begin{bmatrix} x_4 \\ y_4 \\ z_4 \\ 1 \end{bmatrix} = T_4^0 \begin{bmatrix} x_0 \\ y_0 \\ z_0 \\ 1 \end{bmatrix} \quad (3.49)$$

or,

$$P_4 = t(\theta_1, \theta_2, \theta_3, \theta_4)P_0 \quad (3.50)$$

Where, $P_n = \begin{bmatrix} x_n \\ y_n \\ z_n \\ 1 \end{bmatrix}$

3.4.3 Calculation Summary

Total calculation can be summarized in the following steps,

1. Eq. 3.20 is to be used to quantify the propagated random error and identify the variance/covariance matrix for the point of interest.
2. Eq. 3.34 and Eq. 3.35 give the convenience along with the principal axis of the error ellipse and Eq. 3.37 shows the orientation of the principal axis with the major axis for of the error ellipse draw for the position of the point of interest from the variance/covariance matrix obtained from Eq. 3.20.
3. Eq. 3.48 is applicable to fix the location of the point of interest (the bucket tip) which also acts as the center of the ellipse showing the associated uncertainty of the position.

3.4.4 Actuator's Length Based Bucket Tip Positioning

Actuator lengths based methods adopt another indirect approach which uses the length of hydraulic actuators as dynamic measurements. However, to derive the position of the bucket tip, the length of key lines and the angle between the key lines have to be calibrated. For typical backhoe excavator, 8 key nodes besides the joints and 9 key lines except the lines and 3 actuators are identified and illustrated in Fig. 3.12. The length of all of the key lines can be measured through calibration except for the length of the actuators which needs to be tracked in real-time during the movements of the excavator. This means the 3 variables (S_1, S_2, S_3) in this approach will be the lengths of the three actuators driving the boom, stick and the bucket.

The basic idea of actuator length based bucket tip tracking is to relate the actuator lengths to tilt angles (θ_1, θ_2, θ_3 *and* θ_4). To do that basic nodes and links are specified in Fig. 3.12. Some key lines are drawn joining the nodes, where dotted lines mean that the length of the lines are constant but the solid lines (green colored) indicate the actuators which can linearly change its length to move the exactor's arm. The whole *node, link* and *Keyline* scenario are further illustrated in Fig. 3.13 and Fig. 3.14 which is isolated from the body of the excavator. It is worth noting that, all the angles indicated by β_i are constant angles depending only by the particular model of the excavator.

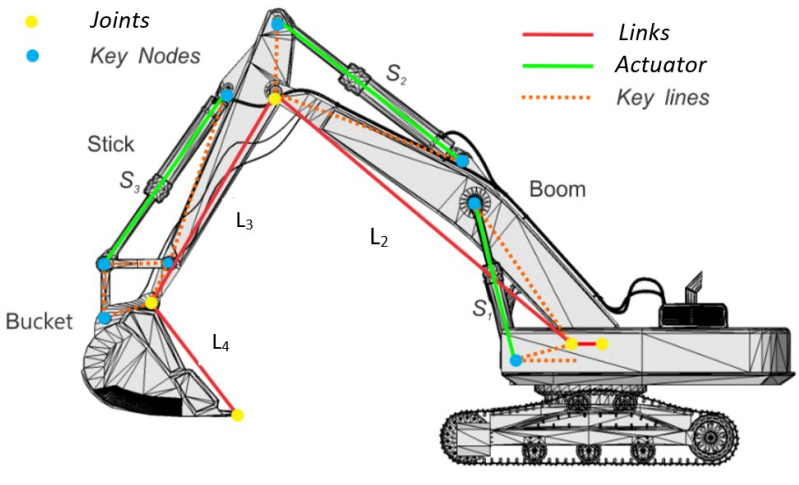

Figure 3.12 Key nodes and key lines for actuator length based bucket tip tracking.

Now, for backhoe, excavator θ_1 angle changes independently. That is why one tilt angle sensor is indispensible besides the length sensor. θ_2 can be deduced with the use of the following equation with use of the illustration Fig. 3.13,

$$\theta_2 = \varphi_1 - \beta_1 - \beta_2 \qquad (3.51)$$

Where φ_1 can be derived from the following equation

$$\varphi_1 = \cos^{-1}\left(\frac{(O_1A_1)^2 + (O_1B_1)^2 - S_1^2}{2(O_1A_1)(O_1B_1)}\right) \qquad (3.52)$$

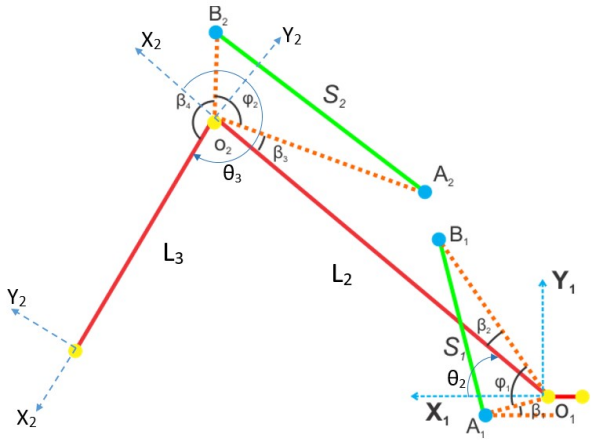

Figure 3.13 Nodes, links and key lines of boom and stick of an excavator.

In the same manner, θ_3 can be deduced with the use of the following equation,

$$\theta_3 = 3\pi - \varphi_2 - \beta_4 - \beta_3 \qquad (3.53)$$

Where,

$$\varphi_2 = \cos^{-1}\left(\frac{(O_2A_2)^2 + (O_2B_2)^2 - S_2^2}{2(O_2A_2)(O_2B_2)}\right) \qquad 3.54)$$

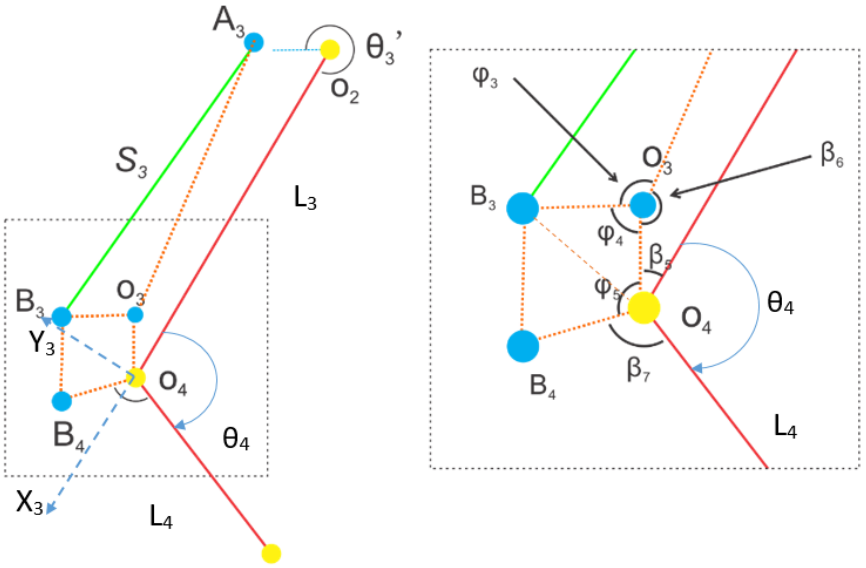

Figure 3.14 Nodes, links and key lines of the bucket of an excavator.

Next step is to track the position of the bucket tip. To do that, the orientation of link L_4 (θ_4) is needed to know. A node, link and Keyline scenario of the link attached to bucket tip are further illustrated in Fig. 3.53. Now, θ_4 can be derived from the following equation,

$$\theta_4 = 2\pi - \varphi_5 - \beta_7 - \beta_5 \qquad (3.55)$$

Where,

$$\varphi_5 = \angle B_4O_4O_3 = \angle B_4O_4B_3 + \angle B_3O_4O_3$$

and,

$$\angle B_4O_4B_3 = \cos^{-1}\left(\frac{(O_4B_4)^2 + (O_4B_3)^2 - (B_4B_3)^2}{2(O_4B_4)(O_4B_3)}\right)$$

$$\angle B_3O_4O_3 = \cos^{-1}\left(\frac{(O_4O_3)^2 + (O_4B_3)^2 - (O_3B_3)^2}{2(O_4O_3)(O_4B_3)}\right)$$

$$\varphi_4 = \cos^{-1}\left(\frac{(O_3O_4)^2 + (O_3B_3)^2 - (O_4B_3)^2}{2(O_3O_4)(O_3B_3)}\right)$$

or,

$$(O_4B_3)^2 = (O_3O_4)^2 + (O_3B_3)^2 - (O_3O_4)(O_3B_3)\cos\varphi_4$$

$$\varphi_4 = 2\pi - \beta_6 - \varphi_3$$

$$\varphi_3 = \cos^{-1}\left(\frac{(O_3A_3)^2 + (O_3B_3)^2 - S_3^2}{2(O_3A_3)(O_3B_3)}\right)$$

Finally, all the tilt angles (θ_2, θ_3 *and* θ_4) can be derived from the variable actuator lengths (S_1, S_2 *and* S_3) which can be used at the actual equation (Eq. 3.49). Now, for actuator's length based bucket tip measurement Eq. 4.50 can be rewritten as,

$$P_4 = t(\theta_1, \theta_2, \theta_3, \theta_4)P_0$$

or,

$$P_4 = l(\theta_1, S_1, S_2, S_3)P_0 \qquad (4.56)$$

3.5 Position Uncertainty Quantification and Visualization

This section will discuss the elaborate methods to quantify the uncertainties of the estimated bucket tip location while tracking using the forward kinematics model and error propagation theory which are elaborately explained in the earlier sections. The role of the error propagation model is quantifying the covariance matrix of the estimated position from the measurements. This covariance matrix can be used to quantify the error ellipse to quantify the position uncertainty of the bucket tip around the derived position

from the kinematic model. Later a practical visual will be presented showing the position of the bucket tip along with uncertainty presented for the different posture of the excavator's arm.

3.5.1 Bucket Tip Uncertainty Quantification

Excavator's bucket tip position vector P_4 can be derived either from $t(\theta_1, \theta_2, \theta_3, \theta_4)$ [for angular based measurement] or from $l(\theta_1, S_1, S_2, S_3)$ [for actuator length based measurement]. To simplify the case, the excavator body rotation angle is considered zero ($\theta_1 = 0$) and it is also assumed the excavator boom is attached at the origin ($x_0 = 0, y_0 = 0$). This assumption helps to visualize the arm movement in 2D space (there will be no z coordinate). So, position vector can be written as,

$$P_4 = \begin{cases} t(\theta_i);\ angular\ based\ measurement \\ l(S_i);\ actuator\ length\ based\ measurement \end{cases} \tag{4.57}$$

Now covariance matrix of the measurement of the position vector P_4 can be obtained using Eq. 2.2.1.6. Here, it is important to keep in mind that the values of individual tilt angle (θ_i) and actuator length (S_i) are independent to each other and thus correlation between them is zero ($\rho_\theta = 0$ *and* $\rho_S = 0$).

Covariance matrix of position P_4, (for tilt angle based measurement)

$$C_{P_4} = \begin{bmatrix} \sigma_{x_4}^2 & \sigma_{x_4y_4} \\ \sigma_{x_4y_4} & \sigma_{y_4}^2 \end{bmatrix} = \begin{bmatrix} \frac{\partial t_1}{\partial \theta_2} & \frac{\partial t_1}{\partial \theta_3} & \frac{\partial t_1}{\partial \theta_4} \\ \frac{\partial t_2}{\partial \theta_2} & \frac{\partial t_2}{\partial \theta_3} & \frac{\partial t_2}{\partial \theta_4} \end{bmatrix} \begin{bmatrix} \sigma_{\theta_2}^2 & 0 & 0 \\ 0 & \sigma_{\theta_3}^2 & 0 \\ 0 & 0 & \sigma_{\theta_4}^2 \end{bmatrix} \begin{bmatrix} \frac{\partial t_1}{\partial \theta_2} & \frac{\partial t_2}{\partial \theta_2} \\ \frac{\partial t_1}{\partial \theta_3} & \frac{\partial t_2}{\partial \theta_3} \\ \frac{\partial t_1}{\partial \theta_4} & \frac{\partial t_2}{\partial \theta_4} \end{bmatrix} \tag{4.58}$$

Similarly, covariance matrix of position P_4, (for actuator length based measurement)

$$C_{P_4} = \begin{bmatrix} \sigma_{x_4}^2 & \sigma_{x_4y_4} \\ \sigma_{x_4y_4} & \sigma_{y_4}^2 \end{bmatrix} = \begin{bmatrix} \frac{\partial l_1}{\partial S_1} & \frac{\partial l_1}{\partial S_2} & \frac{\partial l_1}{\partial S_3} \\ \frac{\partial l_2}{\partial S_1} & \frac{\partial l_2}{\partial S_2} & \frac{\partial l_2}{\partial S_3} \end{bmatrix} \begin{bmatrix} \sigma_{S_1}^2 & 0 & 0 \\ 0 & \sigma_{S_2}^2 & 0 \\ 0 & 0 & \sigma_{S_3}^2 \end{bmatrix} \begin{bmatrix} \frac{\partial l_1}{\partial S_1} & \frac{\partial l_2}{\partial S_1} \\ \frac{\partial l_1}{\partial S_2} & \frac{\partial l_2}{\partial S_2} \\ \frac{\partial l_1}{\partial S_3} & \frac{\partial l_2}{\partial S_3} \end{bmatrix} \tag{4.59}$$

Here, $\begin{bmatrix} \sigma_{\theta_2}^2 & 0 & 0 \\ 0 & \sigma_{\theta_3}^2 & 0 \\ 0 & 0 & \sigma_{\theta_4}^2 \end{bmatrix}$ and $\begin{bmatrix} \sigma_{S_1}^2 & 0 & 0 \\ 0 & \sigma_{S_2}^2 & 0 \\ 0 & 0 & \sigma_{S_3}^2 \end{bmatrix}$ both can be found from the manufactures specifications as a form of standard deviation of the measurement of the sensors. Also, $\sigma_{\theta_2}^2 = \sigma_{\theta_3}^2 = \sigma_{\theta_4}^2$ and $\sigma_{S_1}^2 = \sigma_{S_2}^2 = \sigma_{S_3}^2$ because the same type sensor is generally used.

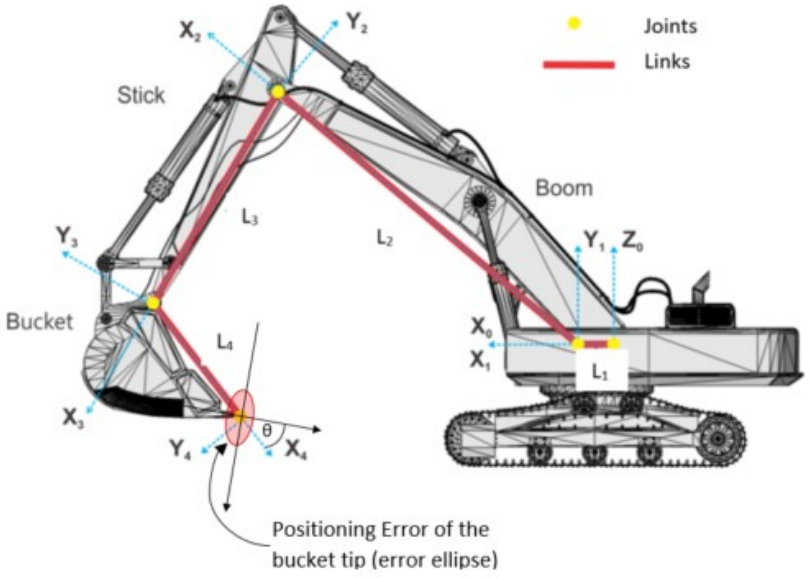

(a)

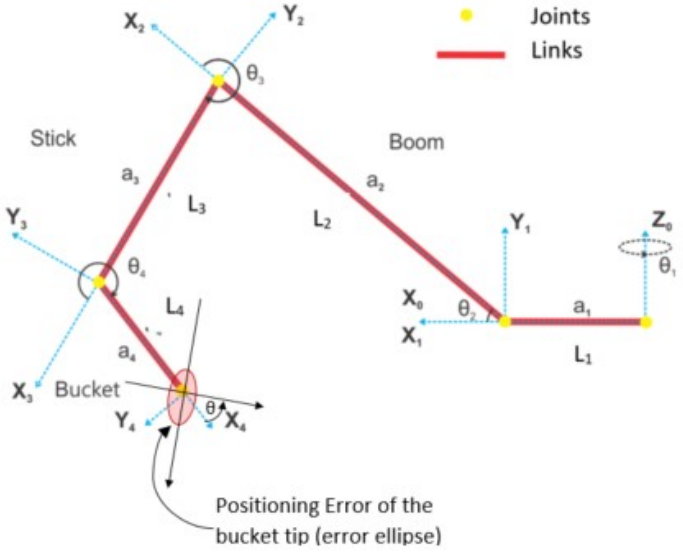

(b)

Figure 3.15 Error visualization with the error ellipse.

3.5.2 Bucket Tip Uncertainty Visualization

As stated above, error ellipse can be used efficiently, to visualize 2D uncertainty. To visualize the bucket tip position uncertainty error ellipse can be drawn to show the most probable position of the tip (inside ellipse). Two parameters are needed to identify the error ellipse shape and orientation. One is the covariance of the measured variables (x and y) which determines the shape and orientation of the error ellipse. Another is the confidence level of the output which defines the spread of the ellipse.

Covariance of the ellipse can be found easily either from Eq. 3.58 or Eq. 3.59. This can be directly used on Eq. 3.34, Eq. 3.35 and Eq. 3.37 to find the orientation and spread of the error ellipse. Where, Eq. 3.40 is also needed to determine the spread of the ellipse.

Fig. 3.15 illustrates the actual theme of visualizing the uncertainty of the tip position. On Fig. 3.15(a) the major links and the tip position is shown, and the links are separately drawn in Fig. 3.15(b) for better understanding.

Actual position uncertainty in 3D space can be visualized with the aid of the equation above (Eq. 3.20). Given the three unknown variables, the visual shape of the uncertain region will be an ellipsoid. Both the maximum spread and the orientation of the ellipsoid can be found by interpreting the eigenvalue and the eigenvector of the covariance matrix C_{P_4}, respectively. The spread of the ellipsoid can be varied with the desired confidence level (three degrees of freedom). A 2D visual of the position uncertainty should be as the same as the figure is shown in Fig. 3.15(b). Here, at the bucket tip, a tiny red-colored ellipse (2D visual of the ellipsoid) is illustrated to represent the uncertainty of the tip position. The red ellipse means: the actual tip position can be anywhere inside the ellipse with a certain level of confidence. This type of visualization can assist the operator to handle the object of interest with ease. For instance, the limit for unrestricted movement can be easily defined along with the caution zone (red ellipse zone) in real time.

A simulation was made based on the trajectory data sourced from existing autonomous excavator research (Rowe, 1999) where the original data set was used in adaptive loading optimization for autonomous excavators based on historical trajectory data of an excavator. The rotation angles θ_i of the deck (swing angle), boom, stick and bucket based

on DH conventions were recorded and synchronized with the time, as presented in Fig. 3.16. The whole loading process can be divided into 6 stages,

i. Raise the boom and close the bucket (A, 1 sec)
ii. Swing to the truck (B, 4sec)
iii. Raise the stick to dumping position (C, 6sec)
iv. Open the bucket and lower down the stick to dump the material (D, 9sec)
v. Swing back to digging position (E, 11sec)
vi. Prepare the boom, stick and bucket in digging position (F, 14 sec)

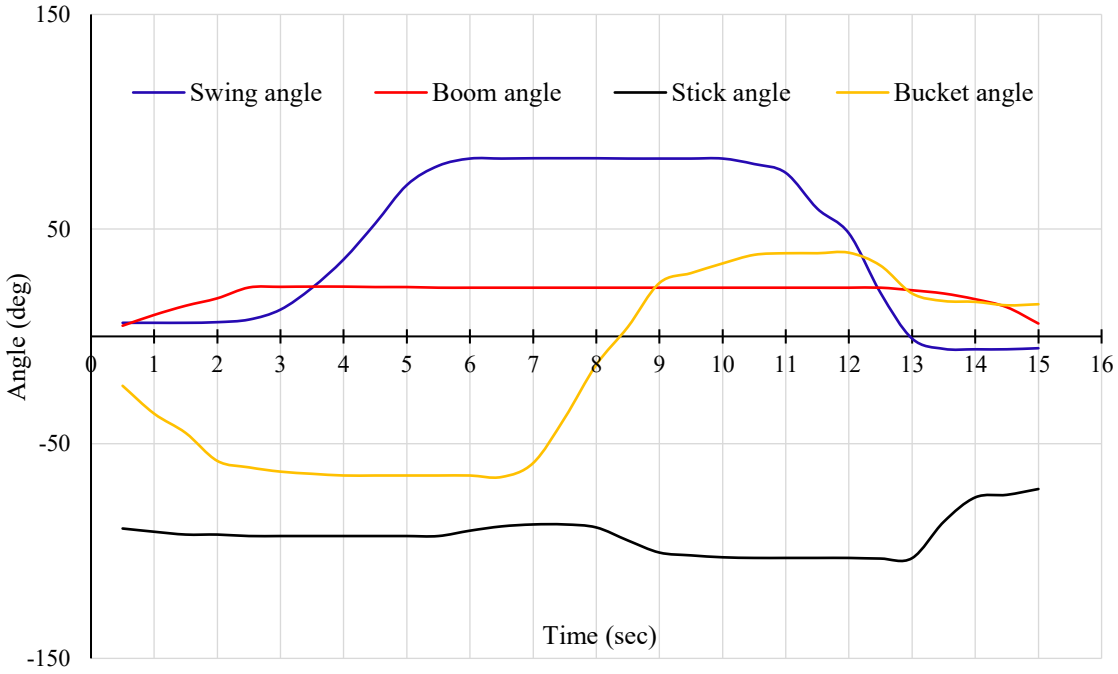

Figure 3.16. Trajectory of the excavator's movement

As an example, the error ellipses for bucket tip positioning at *99%* confidence level based on shaft angles with *0.1°* accuracy and actuator length with *0.02m* accuracy are derived along with the motion of the excavator depicted by the loading trajectory. Specific moments (A to D) are selected to represent different events. The postures of the excavator and the corresponding error ellipses for each moment based on shaft angles and actuator lengths are presented in Fig. 3.17 and Fig. 3.18 separately. By comparing the error ellipses at each moment, it is observed that the errors at each direction are evidently

different for the two methods (e.g. solo angular sensor based measurement; Actuator length measuring sensor's and one angle measuring sensor combination. For the same posture, spread of the error ellipse is different. For example, for posture A, actuator sensor based measurement visibly shows less spread that the angular sensor based measurement.

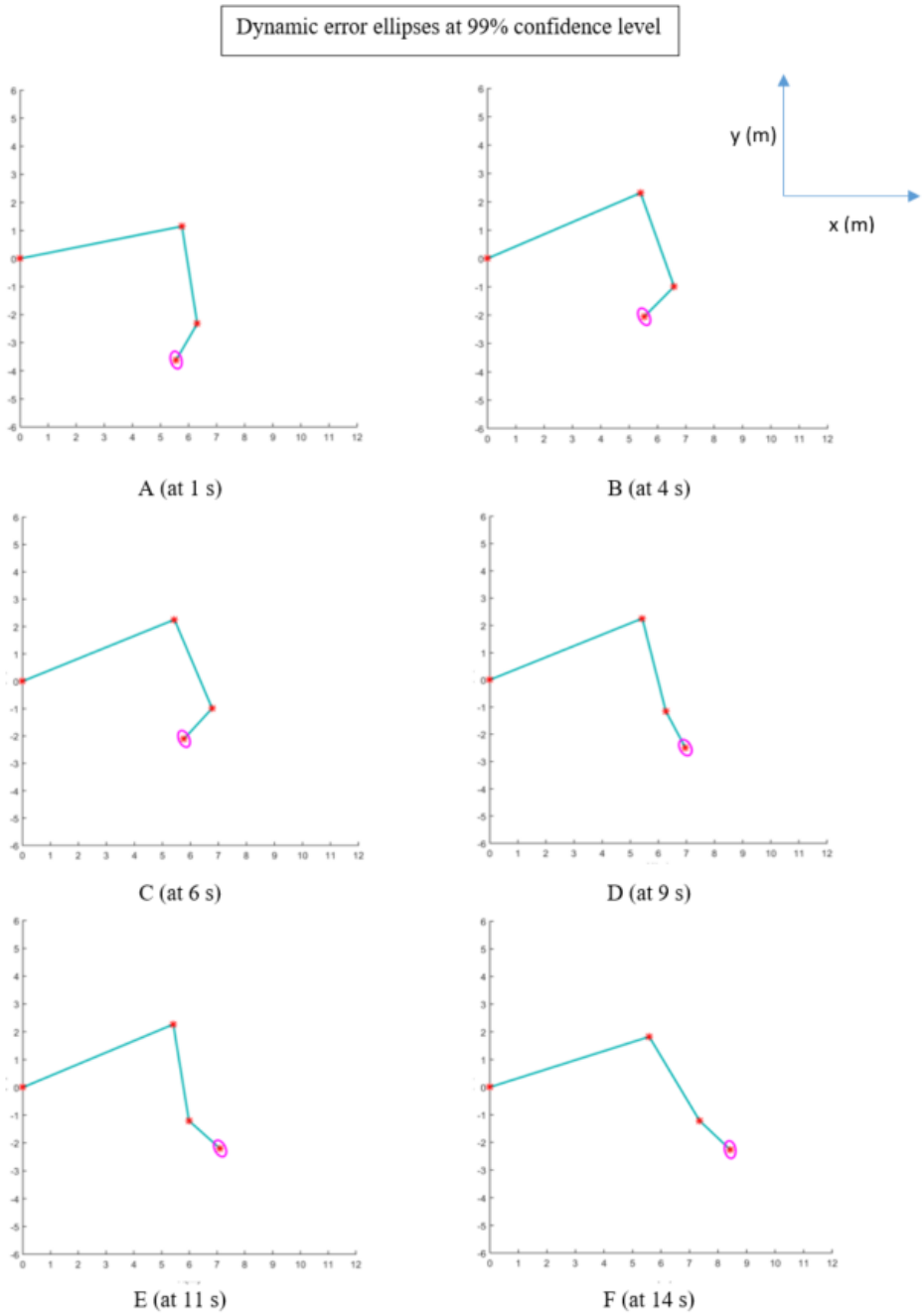

Figure 3.17 Excavator posture and error ellipse based on shaft angles.

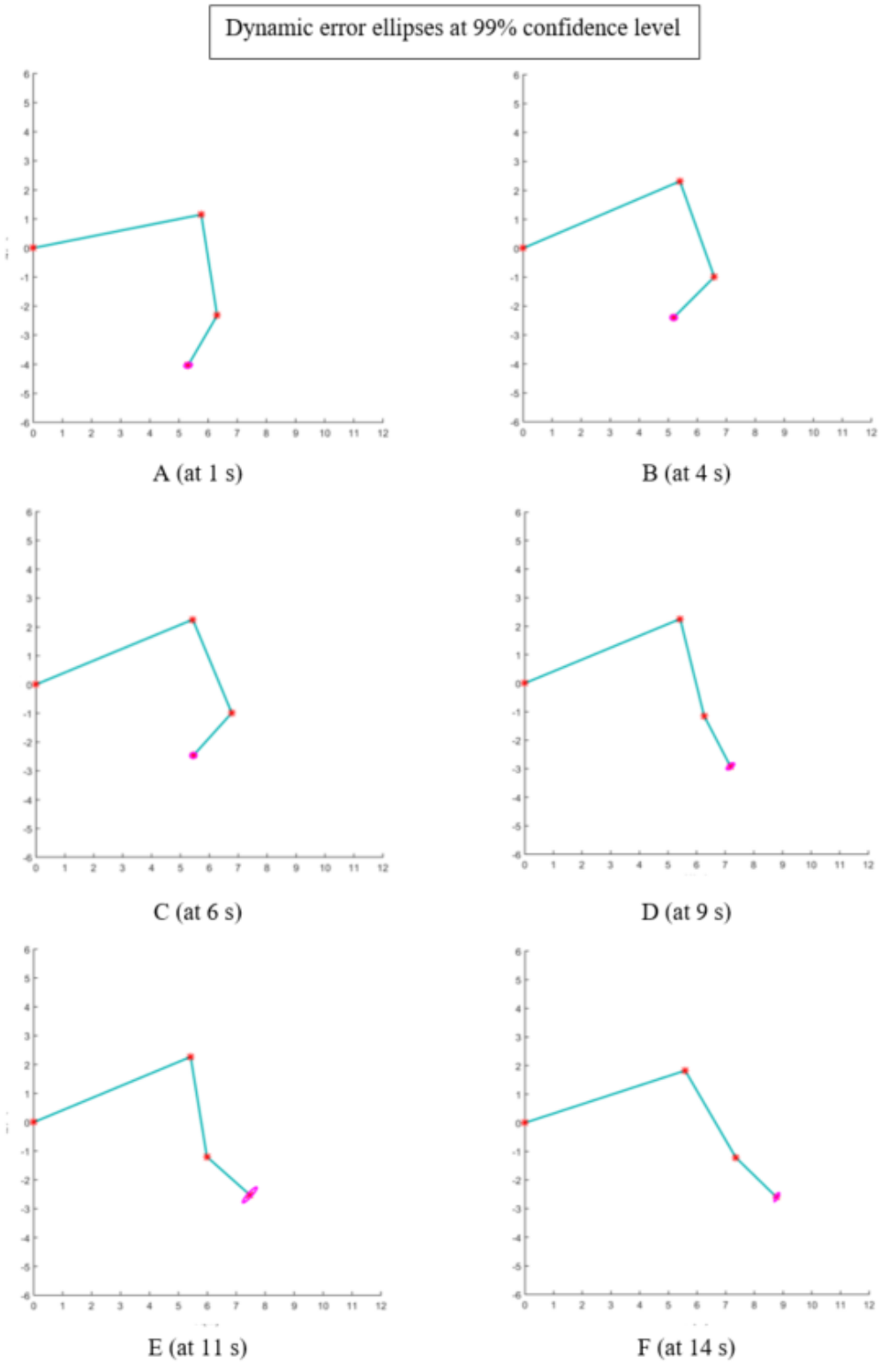

Figure 3.18 Excavator posture and error ellipse based on actuator lengths.

Again, in 3D case, as an example, the error ellipses for the bucket tip positioning at 99% confidence level can be fixed based on tilt angle measuring sensors on the four joints of the excavator. The sensor precision considered in this simulation is set at 0.1^{o} –which is the standard deviation of measurement error (the same for all four sensors) along with the motion of the excavator depicted by the same loading trajectory (Fig. 3.16). For the excavator trajectory, the maximum errors at 99% confidence limit are presented in Fig. 3.20. By comparing the error ellipses on different time points with different postures of the excavator, it is observed that the errors at each direction differ significantly over time.

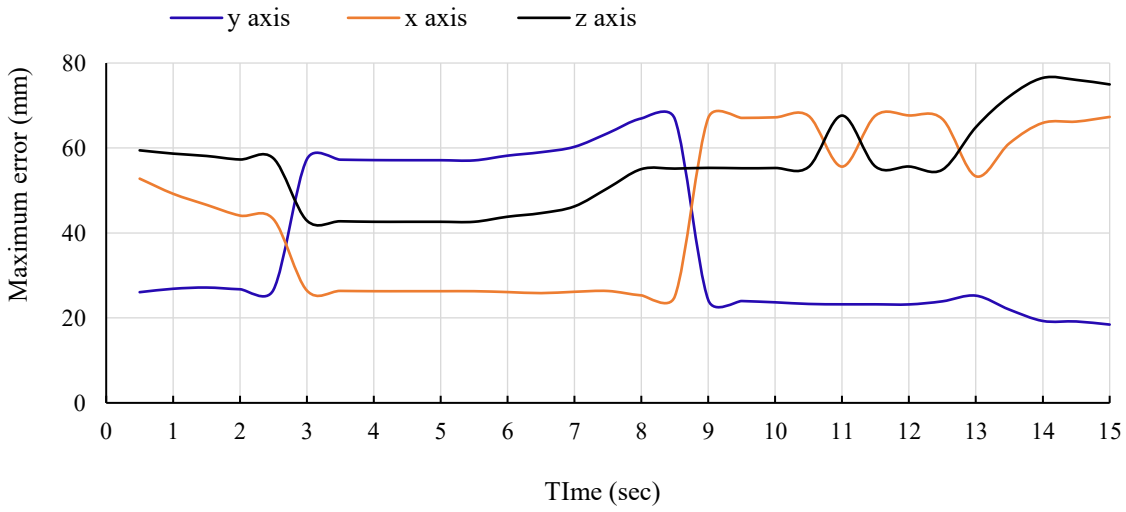

Figure 3.19 The spread of error along with different directions on 99.99% confidence level.

3.6 Sensor Selection Guide

The technique stated above can facilitate a construction planner to select job-specific, application-needs driven sensor types for tracking the excavator. It is commonly held that the cost of the sensor increases with the precision level of the sensors. A graph is generated based on implementing the method of error quantification as presented above. From Fig. 3.19, given the analyzed trajectory data of the excavator, it is evident that the directional errors along x and z axes reach the maximum at 15 sec and for y axis, the maximum error peaks at 8.5 sec. The poses of these particular moments are used for generating the error graph (Fig. 3.20) given sensors with varying precision levels (in

terms of standard deviation and considering the same type of sensor used on all joints). To read this error graph (Fig. 3.20), start with choosing the required measurement accuracy from Y axis; then the required minimum precision level for angle measuring sensors can be fixed in terms of standard deviation on the corresponding X axis data. For example, if the user needs to maintain 200 mm accuracy on the obtained position of the excavator's bucket tip, the minimum precision level of the reading of angle measuring sensors is 0.28^{o} in terms of standard deviation.

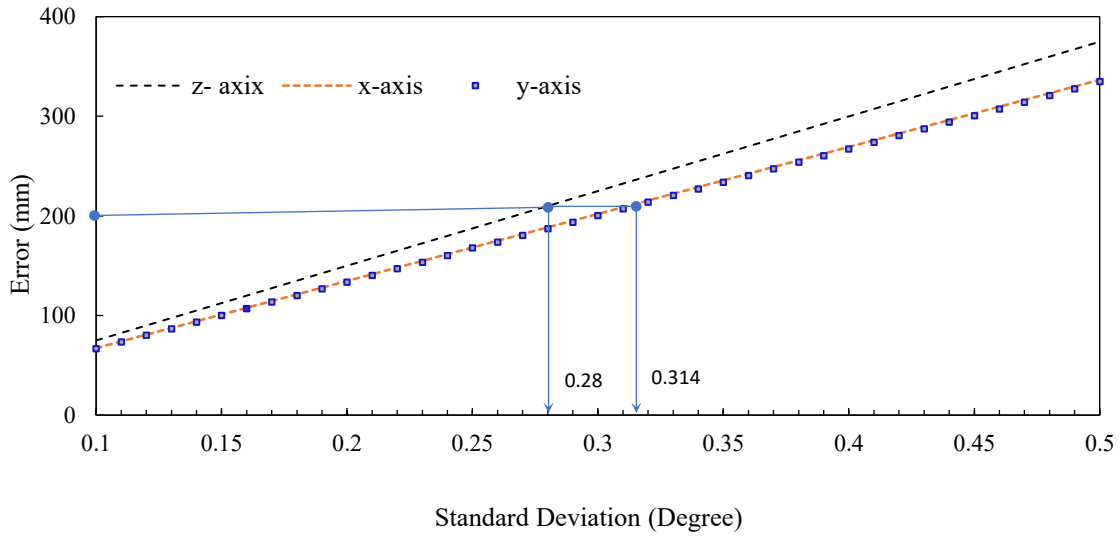

Figure 3.20. Impact of sensor's precision on position uncertainty of the bucket tip position.

Chapter 4

Excavator as a Survey Robot

4.1 General

Backhoe excavators are the most versatile construction equipment commonly employed in excavation, grading, pipeline installation, loading dump trucks, etc. An autonomous machine would eliminate many human errors and avoid productivity losses (Rowe, 1999), while proper planning makes a job site safe from machine-related accidents (Talmaki and Kamat, 2014). Autonomous machines can also be deployed to access the areas which are hazardous, toxic to humans. Besides making the workspace safe, lower operational costs can be materialized by reducing the number of guiding staff on site (e.g., spotters). In recent years, the concept of autonomous earth-moving machines has invoked intense interest among manufacturers and contractors in light of the substantial productivity improvement technological advances would bring about in the construction, mining, and quarrying industries. This chapter unveils the possibility of using the backhoe excavator as a survey robot while equipped with the angle measuring sensors to track its bucket tip from the fixed position of its base is described. A self-positioning mechanism with the help of three know reference for such excavator is going to be described in detail on the remaining sections of this chapter Also, the potential uses of such survey robot are briefed at the end.

4.2 Basic Idea of the Survey Robot

The previous chapter of this thesis describes the kinematics of the backhoe excavator in depth. Through explaining the kinematics, it actually illustrates the mechanism to track the pose of the excavator using angle or length measuring sensors. While determining the pose of the excavator the primary objective was to track the position of the bucket tip, P_B with respect to a fixed position of its base, O_L (Fig. 4.1). This fixed point situated at the base of the excavator is termed as the excavator's local reference origin, O_L. Excavator's body can move any direction in three-dimensional space with respect to this origin

considering it as the center of rotation. Since the excavator can track its bucket tip with respect to its local origin, any point it touches the coordinate of that point can be known in refer to the local reference frame attached to the local origin.

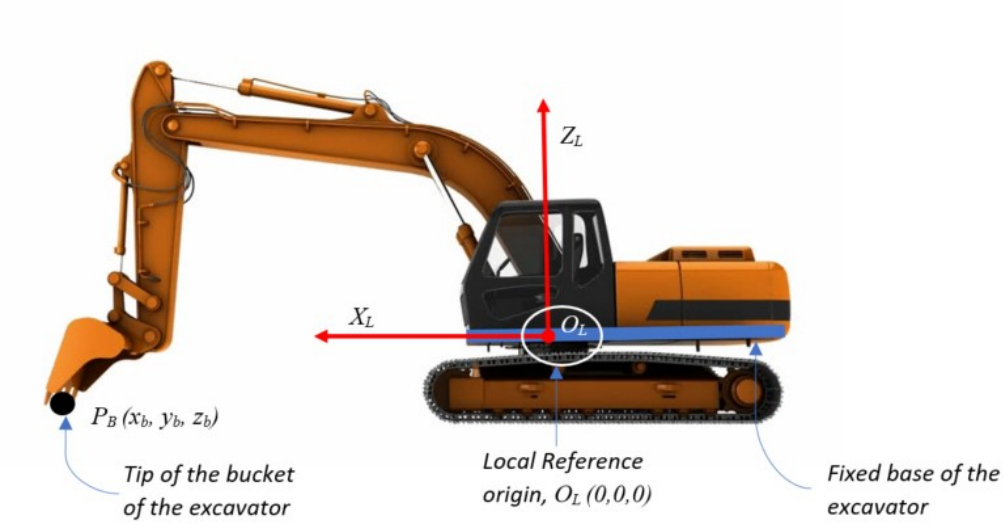

Figure 4.1. Positioning excavator's bucket tip in the local reference frame.

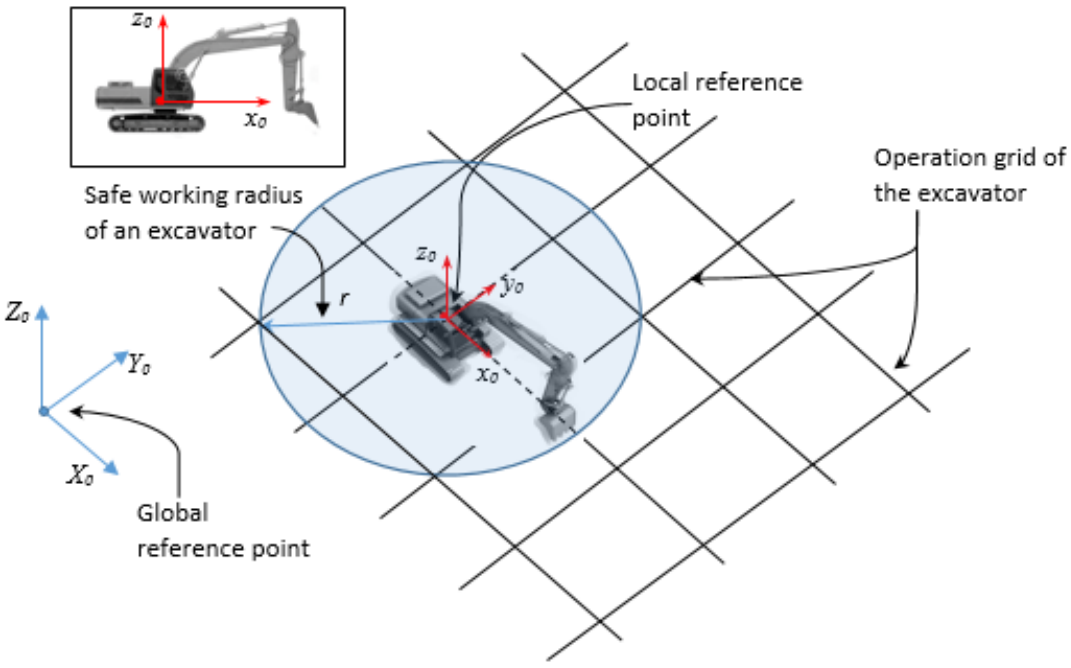

Figure 4.2. Two different reference frames of the excavator.

In reality, always tracking with reference to the local reference frame does not serve the purposefully. Excavator itself is a dynamic machine. Due to that, position of its base will not maintain the same position and orientation all the time. So, there is a need to develop a mechanism to track its base position and orientation with respect to a fixed reference frame. This reference frame can be termed as the global reference frame (Fig. 4.2). There are some ongoing researches on tracking the excavator's pose with using different sensors (Vahdatikhaki, 2015). In previous, Chapter 3 describes the necessity of measuring the uncertainty of the sensor measurements. So even the technology is available to track the position and orientation of the base in real time but there is always need for calibration of the sensors data. Remainder sections of this chapter is going describe a three-point positioning mechanism for the excavator itself. It is not only applicable to fix the position and orientation of the local reference of the excavator (excavator's base) in refer to the global reference with using three known reference coordinates, but also provide a systematic procedure to calibrate the sensors data when equipped with different position tracking sensors.

4.3 Extracting the Kinematics

A self-guided excavator is capable of tracking its position and poses with respect to any predefined master (global) reference during the time of its operation. Taking advantage of the sensor technology, it is very much possible to transform an ordinary excavator into a smart one (self-guided). Hasan and Lu (2017) pointed out the fact that, not always these excavator sensor technology needs to be very expensive to serve the purpose. Instead, it is possible to select a combination of sensors matching specific job requirements.

As addressed in the previous sections, a robot manipulator is composed of links and intermediate joints. Relative movement of one link to another can be obtained through tracking the frame movement at links. According to the DH convention each homogeneous transformation matrix A_i is represented as a product of four basic transformations and can be expressed by Eq. 3.44. Here, A_i is a homogeneous transformation matrix declared to express the position and orientation of frame $o_i x_i y_i z_i$ with respect to $o_{i-1} x_{i-1}\ y_{i-1}\ z_{i-1,}$ which varies as the configuration of the robotic arm is changed.

$$A_i^{i-1} = Rot_z(\theta_i)Trans_z(d_i)Trans_x(\alpha_i)Rot_x(\alpha_i)$$

Here the four inputs θ_i, a_i, d_i, α_i are the parameters associated with link L_i and joint J_i of any robotic arm. The four parameters a_i, α_i, d_i, and θ_i in above equation are generally referred to as *link length, link twist, link offset*, and *joint angle*, respectively.

Plugging the values from Table 3.1 in the above equation, the kinematic transformation of different links of an excavator model can be derived, with the total transformation matrix of the bucket tip using Eq. 3.43 as follows

$$T_4^0 = A_1A_2A_3A_4$$

$$where, \qquad T_4^0 = t(\theta_1, \theta_2, \theta_3, \theta_4); as\ a_1, a_2, a_3\ and\ a_4\ are\ constant$$

Now, the position of bucket tip, P_4 (x_4, y_4, z_4) can be fixed in terms of the reference frame as per Eq. 4.1,

$$P_4 = \begin{bmatrix} x_4 \\ y_4 \\ z_4 \\ 1 \end{bmatrix} = T_4^0 \begin{bmatrix} x_0 \\ y_0 \\ z_0 \\ 1 \end{bmatrix} = \begin{bmatrix} t_x(\theta_1, \theta_2, \theta_3, \theta_4) \\ t_y(\theta_1, \theta_2, \theta_3, \theta_4) \\ t_z(\theta_1, \theta_2, \theta_3, \theta_4) \end{bmatrix} \tag{4.1}$$

$$P_4 = P_B = T_4^0 \begin{bmatrix} x_0 \\ y_0 \\ z_0 \\ 1 \end{bmatrix} = T_4^0 O_L \tag{4.2}$$

Detail calculations steps are presented in the previous chapter.

4.4 Positioning the Excavator

Fixing the position of a dynamic equipment in the construction field in the real time is a challenge when it has the six degrees of freedom of movement as because of working in the three-dimensional (3D) space. Till present various technologies are being tested for efficient tracking of such equipment. Most of those are sensor dependent and some are based on real-time imaging. Considering the number and cost of the sensor devices involved for tracking and positioning, the practical implementation of such technologies is not yet being popular in practice. Even though the imaging addressed to be more cost-effective but still it has its limitation about performing on the less luminous environment. Such sort of constraints still keeping this is alive for researchers. In this research, a

simplified positioning mechanism for backhoe excavator has been proposed which involves only in total four angle or tilt measuring sensors to track the position and orientation. Proposed positioning methodology has two-dimensional application. The first one is, the positioning mechanism itself and the second one is, the calibrating the machine/mechanism used for tracking purpose. Hasan and Lu (2017) already showed that how sensors uncertainty can affect the final precision of measurement with a demonstration on a backhoe excavator case. In such case, the very same mechanism can be used for calibrating those sensors data and drive for precise measurement.

4.4.1 Positioning with Three References

Excavator like heavy machinery works at a certain position stationery and move after completing the task. This simple fact actually inspires this research to develop the positioning system architecture for the excavator. The underlying concept of the of fixing and tracking an excavator like the machine is to present the entire field of operation in terms of a single reference frame. Which can be termed as the global reference frame. On the other side, an excavator has its own references and with its arm wherever it touches can be known in terms of its own reference. It can be called as the local excavator reference frame. The idea is to find a mechanism to relate this local reference frame of the excavator with the global reference frame, what's how the excavator can be tracked in the field site.

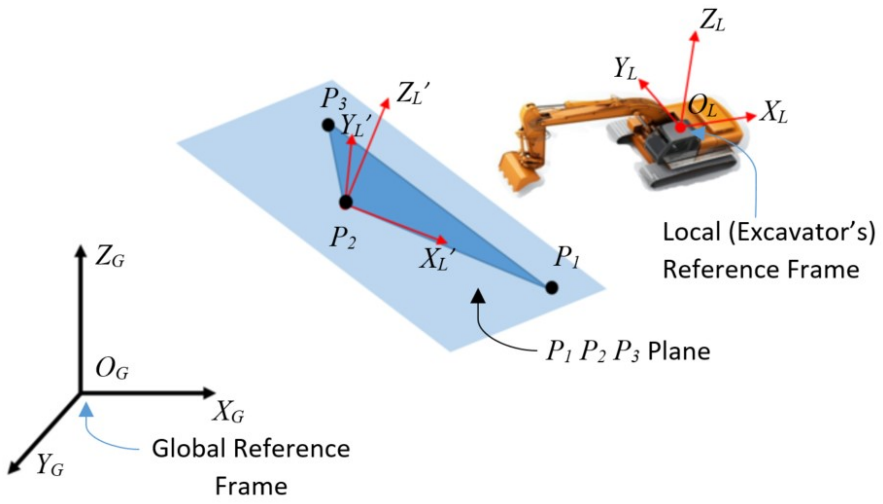

Figure 4.3. Transformation of the reference frame.

To refer local frame in terms of the global, here we used three common reference points. In this paper which is termed as the references. Coordinate of these reference points are known in terms of both local and global reference frame. These common references are needed to be fixed in such way that they cannot be linear that to allow forming a plane. In the Fig. 4.3, 0_G and 0_G are the origins of two reference frame called global and local reference frame respectively. P_1, P_2, P_3 are the reference points with known coordinates concerning both of the coordinate frames. Here two stages of the frame transformation have been proposed to deduce the find the final homogeneous transformation matrix. First, the local frame is being translated from O_L to the point P_2 and the same frame is being rotated to align the $\overrightarrow{X_L}$ along $\overrightarrow{P_2P_1}$ and where at the same time plane X_LY_L gets aligned with $P_1P_2P_3$ plane. Eq. 4.7 is being used for transformation and before that Eq. 4.3 to Eq. 4.5 are used to deduce the Roll-pitch-yaw angles.

The angle between a line and a plane is equal to the complementary acute angle that forms between the direction vector of the line and the normal vector of the plane. If in space given the direction vector of line L (Fig. 4.4) : $\vec{s} = \{l; m; n\}$ and the equation of the plane is $Ax + By + Cz + D = 0$, then the normal vector of the plane should be $\vec{q} = \{A; B; C\}$ and the angle between a line and a plane is equal to the complementary acute angle that forms between the direction vector of the line and the normal vector of the plane. Hence, the angle between this line and plane can be found using the formula below,

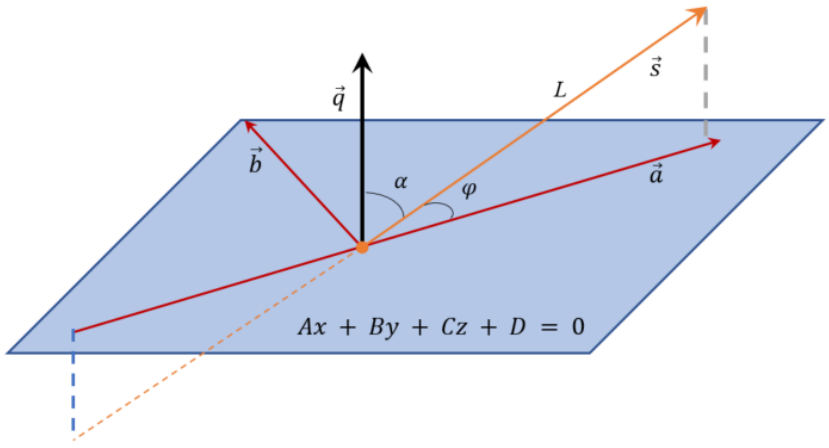

Figure 4.4. Finding the angle between a plane and a line vector.

$$sin\,\varphi = \frac{|\vec{q}.\vec{s}|}{|\vec{s}|.|\vec{q}|}$$

or,

$$\varphi = \arcsin\frac{|l.A + m.B + n.C|}{\sqrt{A^2 + B^2 + C^2}.\sqrt{l^2+m^2 + c^2}} \qquad (4.3)$$

Again, the angle between any two vectors $\vec{a}$ and $\vec{b}$ can be found using the following formula,

$$cos\,\varphi' = \frac{(\vec{a}.\vec{b})}{|\vec{a}|.|\vec{b}|}$$

or,

$$\varphi' = arccos\frac{(\vec{a}.\vec{b})}{|\vec{a}|.|\vec{b}|} \qquad (4.4)$$

Also, the angle between two planes is equal to the acute angle determined by the normal vectors of the planes. If $Ax + By + Cz + D = 0$ and $A'x + B'y + C'z + D' = 0$ are the equation of two planes and $\overrightarrow{n_1}$ and $\overrightarrow{n_2}$ are two normal vectors of the planes accordingly, the angle between two planes can be found using the following equations,

$$\varphi'' = arccos\frac{|\overrightarrow{n_1}.\overrightarrow{n_2}|}{|\overrightarrow{n_1}|.|\overrightarrow{n_2}|} \qquad (4.5)$$

Where, $\overrightarrow{n_1} = (A, B, C)$ and $\overrightarrow{n_2} = (A', B', C')$

Eq. 4.4 will help to find out the rotation angle for the plane to be aligned with line facing the same direction as well. Table 4.1 presents the sign convention and angle of rotation for the plan's axis (x-z plane will rotate about z axix). Here, the first objective is to align x axis will be aligned with the line vector $\overrightarrow{P_2P_1}$. So, rotation of plane x-z about z axis has to be determined first. Also, rotation angle between x-z plane and $\overrightarrow{P_2P_1}$ can be found using φ_1 can be found using Eq. 4.3.

To align the $\overrightarrow{x}$ axis with $\overrightarrow{P_2P_1}$, the next step is to find out the rotation angle (φ_2) between x-y plane and line vector $\overrightarrow{P_2P_1}$, which can be found again using Eq. 4.3. Here φ_2 should always be less than 90°. Table 4.2 presents the sign convention for the rotation angle φ_2.

When the $\overrightarrow{x}$ axis with $\overrightarrow{P_2P_1}$, need to find one more rotation angle φ_3 to completely align the x-y plane with the $P_1P_2P_3$ plane. Rotation angle φ_3 is the rotation of y axis about x axis and can be found by finding the angle between x-y plane and $P_1P_2P_3$ plane with Eq. 4.5. Sign convention for the rotation angle is shown in Table 4.3.

Table 4.1 Sign convention and rotation angle for x axis, about z axis.

Rotation about	Rotating axis	Position, P_2 with respect to P_1	Vector angle between $\overrightarrow{x}$ and $\overrightarrow{P_2P_1}$	Rotation direction	Rotational angle, φ_1
Z axis	X axis	$y_{p2} - y_{p1} \geq 0$	$\varphi' \geq 90°$	clock wise (-)	$180 - \varphi$
			$\varphi' < 90°$	clock wise (-)	φ
		$y_{p2} - y_{p1} < 0$	$\varphi' \geq 90°$	Anti-clock wise (+)	$180 - \varphi$
			$\varphi' < 90°$	Anti-clock wise (+)	φ

Table 4.2 Sign convention and rotation angle for x axis, about y axis.

Rotation about	Rotating axis	Position, P_2 with respect to P_1	Rotation direction of φ_2
Y axis	X axis	$z_{p2} - z_{p1} \geq 0$	clock wise (-)
		$z_{p2} - z_{p1} < 0$	Anti-clock wise (+)

Table 4.3 Sign convention and rotation angle for y axis, about x axis.

Rotation about	Rotating axis	Position, P_2 with respect to P_3	Rotation direction of φ_3
X axis	y axis	$z_{p2} - z_{p1} \geq 0$	clock wise (-)
		$z_{p2} - z_{p1} < 0$	Anti-clock wise (+)

Now, when all the rotation angle is known, complete rotation matrix for the frame transformation can derived from the following equations:

$$R = R_z(\varphi_1)R_y(\varphi_2)R_x(\varphi_3) \tag{4.6}$$

Here, $\varphi_1, \varphi_2 \; and \; \varphi_3$ are the roll, pitch and yaw angles respectively and

$$R_z(\varphi_1) = \begin{bmatrix} cos\varphi_1 & -sin\varphi_1 & 0 \\ sin\varphi_1 & cos\varphi_1 & 0 \\ 0 & 0 & 1 \end{bmatrix}$$

$$R_y(\varphi_2) = \begin{bmatrix} cos\varphi_2 & 0 & sin\varphi_2 \\ 0 & 1 & 0 \\ -sin\varphi_2 & 0 & cos\varphi_2 \end{bmatrix}$$

$$R_x(\varphi_3) = \begin{bmatrix} 1 & 0 & 0 \\ 0 & cos\varphi_3 & -sin\varphi_3 \\ 0 & sin\varphi_3 & cos\varphi_3 \end{bmatrix}$$

When the rotation matrix is known, the transformation matrix should be,

$$\begin{pmatrix} X'_L \\ Y'_L \\ Z'_L \\ 1 \end{pmatrix} = \begin{pmatrix} {}^{L'}R_L & t \\ 0_{1\times3} & 1 \end{pmatrix} \begin{pmatrix} X_L \\ Y_L \\ Z_L \\ 1 \end{pmatrix} = {}^{L'}T_L \begin{pmatrix} X_L \\ Y_L \\ Z_L \\ 1 \end{pmatrix}$$

or,

$$\begin{pmatrix} X'_L \\ Y'_L \\ Z'_L \\ 1 \end{pmatrix} = {}^{L'}T_L \begin{pmatrix} O_L \\ 1 \end{pmatrix} \tag{4.7}$$

where $t = (x, y, z)$ $[t = P_{2,L}\ for\ the\ first\ transformation\ case]$ is the translation of the frame and the orientation is ${}^{L'}R_L$. Also, ${}^{L'}T_L$ is referred to as a homogeneous transformation matrix, and O_L is the origin of the excavator's local frame.

In the second stage like the same way as described above the local framed can be transformed from P_2 to O_G coinciding with the global reference frame. Suppose in this case the homogeneous transformation matrix becomes ${}^{G}T_{L'}$ then the entire transformation matrix can be written as the following (Eq. 4.8)

$$\begin{pmatrix} X_G \\ Y_G \\ Z_G \\ 1 \end{pmatrix} = \left({}^{G}T_{L'}\right)\left({}^{L'}T_L\right) \begin{pmatrix} X_L \\ Y_L \\ Z_L \\ 1 \end{pmatrix}$$

or,

$$\begin{pmatrix} X_G \\ Y_G \\ Z_G \\ 1 \end{pmatrix} = \left({}^{G}T_{L}\right) \begin{pmatrix} O_L \\ 1 \end{pmatrix} \qquad (4.8)$$

Since Eq. 4.8 is the complete frame transformation matrix, now any point, $P_{4.L}$ (Eq. 4.2) is tracked with the excavator's bucket can be referred from the global reference frame with using following equation (Eq. 4.9)

$$P_{4.G} = \begin{pmatrix} X_G \\ Y_G \\ Z_G \\ 1 \end{pmatrix} = \left({}^{G}T_{L}\right) P_{4.L} \qquad (4.9)$$

4.5 Potential Applications of the Survey Robot

Backhoe excavators have wide and multidimensional use in construction projects. It can work at the same time as an excavator, loader and grader. Efficient operation of a backhoe excavator demands operator's experience and expertise. In order to avoid rework due to incorrect slope formation or collision with invisible underground facilities in the

field, careful handling and positioning of the excavator's bucket are mandatory. In case of deep excavation (trench like), it does not become possible for the operator to see the bucket tip and this kind of situation demand other helping hand to guide the operator. Frequent interruption is required in a project where this machine must ensure the proper slope alongside the excavation depth. Again, all above the operator's skill is the prime factor what actually drive the productivity of the work.

To increase the productivity of the backhoe excavator operation researchers are interested to track the bucket tip and excavator position in real time using various sensor-based measurement. The analytical procedure described in this article to track the position of the bucket tip and visualizing the uncertainty region can be a useful tool to solve the problem stated above and thus increase the productivity of the excavator operation.

4.5.1 Trench Like Excavation

A typical figure of trench excavation is illustrated in Fig. 4.5.

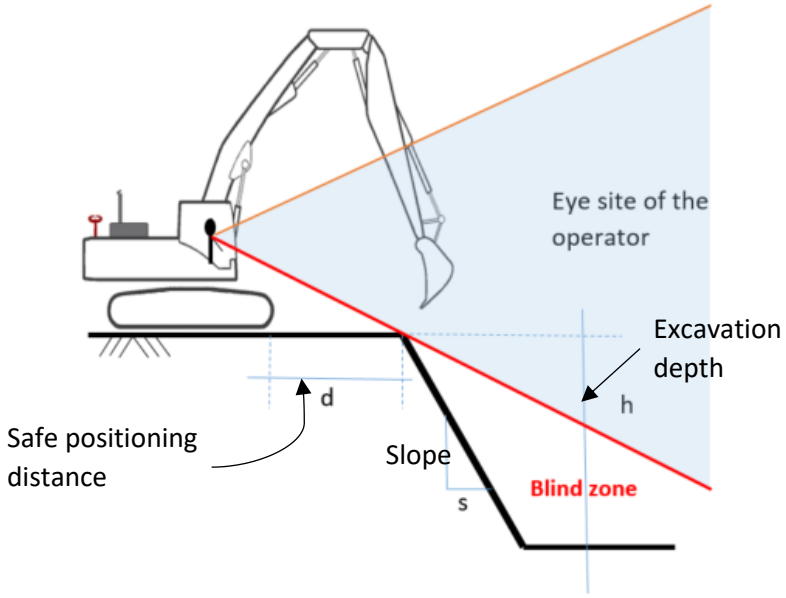

Figure 4.5. Excavator's blind zone.

Excavator always should maintain a safe position *d* from the line of excavation depending on the soil condition which influences the line of sight of the excavator operator. The line of sight is also dependent on the depth of the excavation depth, *h*. To operate on the excavator into the blind zone needs external assistance from outside.

Which slows down/interrupts the progress of the operation thus the productivity declines. An automated real-time bucket tip position tracking system element the need of outside assistance and increase the confidence of operator and eliminates the possibility of error.

4.5.2 Underground Utility line

It is the common practice in the mid of excavation work, if any underground lying utility line is confirmed, manual excavation proceeds or even if a mechanical excavator is used the progress becomes very slow to confirm the safety of the utility line. Precaution is mandatory because even sometimes an expert operator of a mechanical excavator may fail to peruse the safe depth of operation. An introduction of bucket tip tracker can make the work safe and faster and also can eliminate the need of manual excavation up to a safe distance (in Fig. 4.6, *h* is the safe distance of excavator operation) and save time and cost.

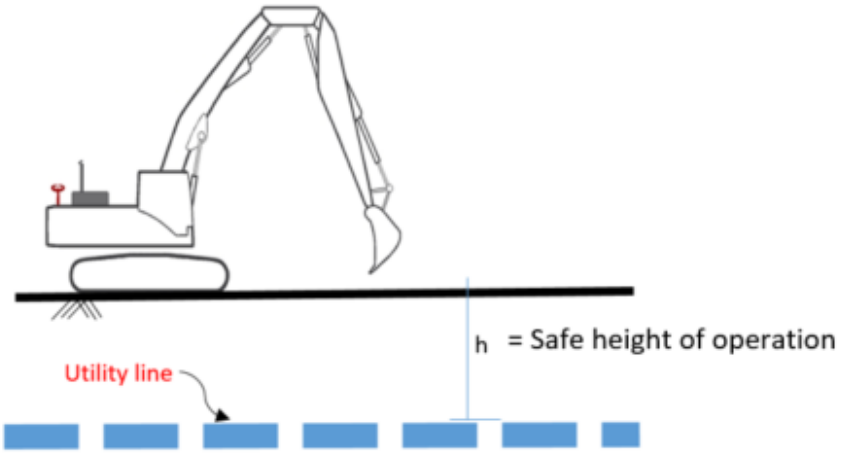

Figure 4.6. Excavator safe distance of working while working with the utility line.

An excavator with bucket tip tracking mechanism can be utilized to work safely on top of an underground utility line. Following pseudo code given in Table 4.4 should follow to visualize the entire work environment. First, it is necessary to identify the utility line in respect of the global coordinate system. To do so some key coordinate of the utility line has to be defined. It can be done at the time of preparing the site layout map by digging on some critical point. It is recommended that to confirm the total layout of the utility line prior to start the excavation work. A single line can be considered for a consistent

slope of the line. Where the line changes slope, that point can be considered for the start of the second line. While an excavator works representing the utility line key coordinates into concerning the local coordinate system is convenient for calculation. At the time of operation, excavator only have to consider the lines which are present in-between the excavator's safe working radius. A schematic drawing is given in Fig. 4.7.

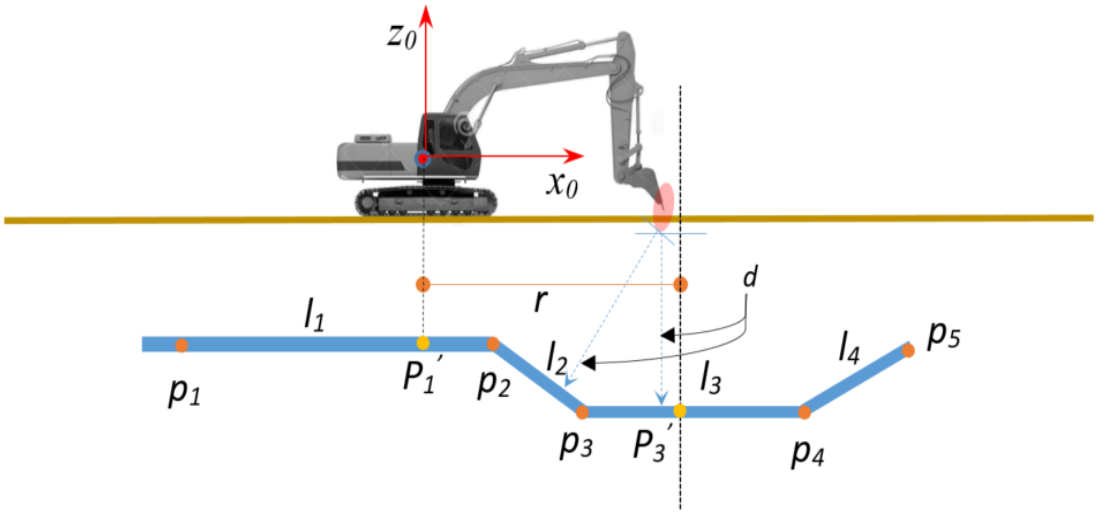

Figure 4.7 Excavator operation with the concern of underground utility line.

Table 4.4. Pseudo code for working with buried utility line for the excavator.

Algorithm 1	
Step 1	Initialize the global reference frame in terms of the excavator's local frame.
Step 2	Get the coordinate of the utility line as the input reference with respect to the global reference frame.
Step 3	Identify the working radius, *r* of the excavator (Fig. 4.7)
Step 4	Identify the key coordinates of utility line present in between safe working radius (P_1', P_2, P_3, P_3')
Step 5	Structure the equations of the lines.
Step 6	Start working and track the distance between the line and bucket tip and when its tool close set the warning sign.
Step 7	If work is done in a position, check the total work. If the work is complete then end operation or move to next position and start again Step 4

4.5.3 Trajectory Planning for Excavator's Movement

The new approach of precise position tracking of the excavator's bucket tip can use to plan the operation trajectory (Fig. 4.8) of the excavator's arm to minimize the movement and cycle time based on the excavating capacity on a single cycle of operation (mainly depends on the bucket capacity). An automatic self-guided excavation proses can be developed based on this concept.

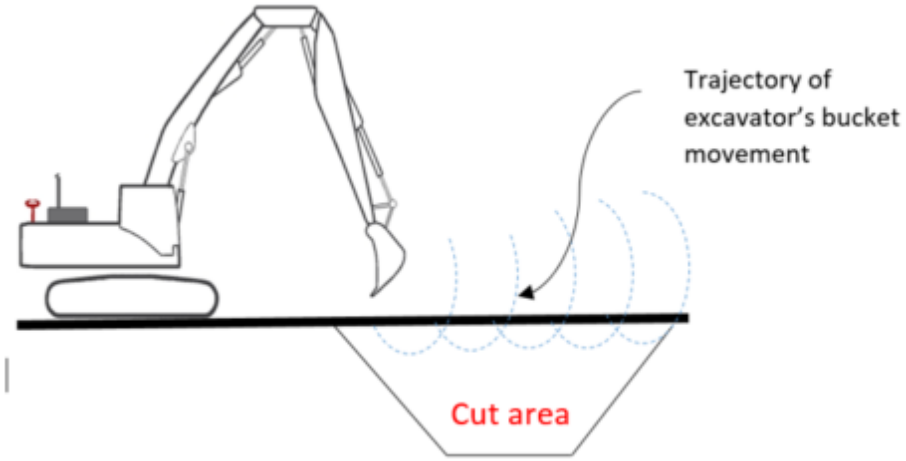

Figure 4.8. Trajectory Planning for Excavator's Movement.

4.5.4 Record Keeping and productivity study

Table 4.5. Pseudo code for the work progress measurement for excavation like task.

Algorithm 2	
Step 1	Initialize the global reference frame in terms of the excavator's local frame.
Step 2	Take the initial ground level $L_{i,I}(x_i, y_i, z_i)$ and designed target ground level $L_{j,T}(x_i, y_i, z_j)$ as the input.
Step 3	Start digging operation and at the same time track the bucket tip of the excavator $L_{k,B}(x_i, y_i, z_k)$
Step 4	Check $d_i = z_{k,B} - z_{j,T}$; If $d > 0$, continue digging.
Step 5	Store the progress, excavated depth $L_m(x_i, y_i, d_i)$ And store progress, $P_i(x_i, y_i, z_i - d_i)$ Extract the volume from the progress coordinate, P_i

Step 6	If $d = 0$ check the surface points (x_i, y_i) being covered. If all are covered then end process. or, move bucket into new position [new (x_i, y_i)] and return to Step 3 or, continue digging on the same position.

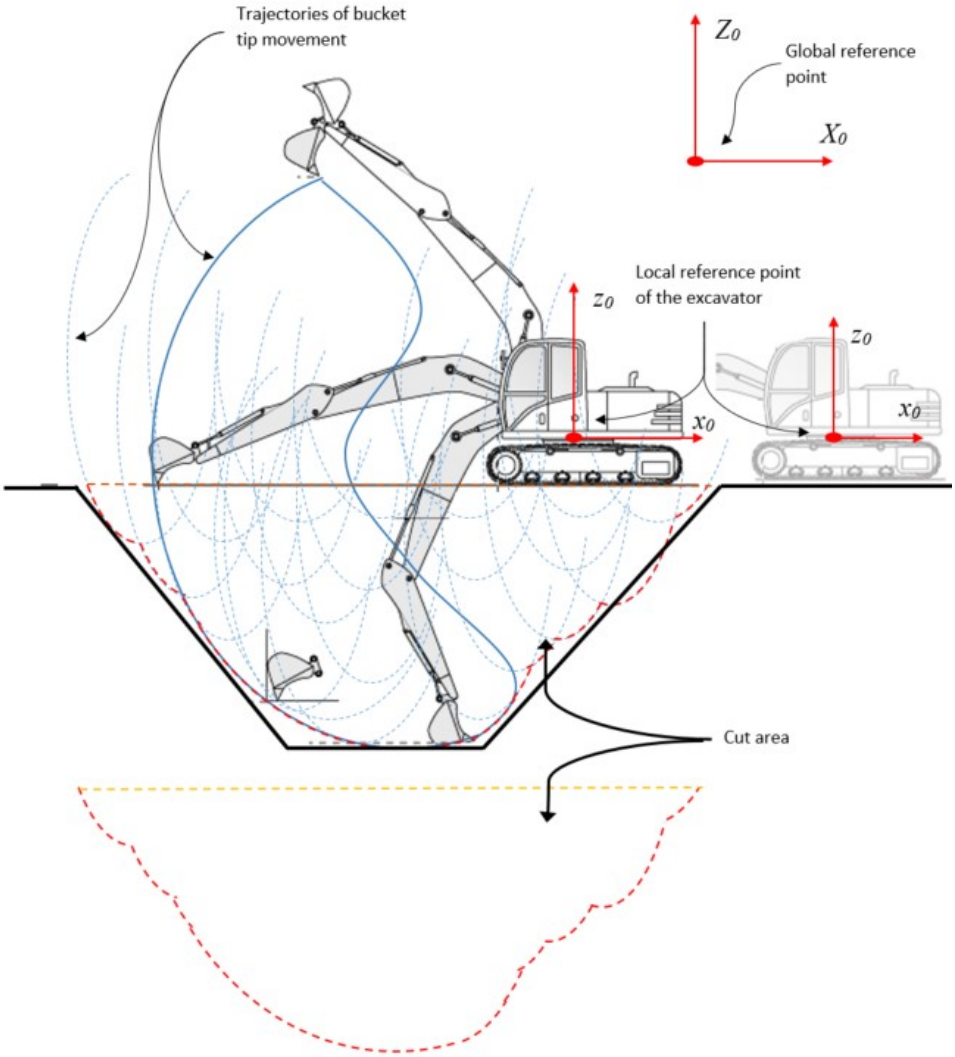

Figure 4.9 Visualization of an excavator's work progress.

When excavator's bucket position can be stored with respect to any fixes master reference frame, it can be used as the work progress measuring instrument while working

in any excavation site. The technique so far discussed can be customized as automatic record keeper with integrated with the time domain. This record can be vital to perform the productivity study too. Table 4.5 shows the pseudo code for the work progress measurement for excavation like task. An illustration of the process is also given in Fig. 4.9. Fig. 4.9 shows, for record keeping purpose, only the extreme (lowest) $z_{i,B}$ coordinate for any $x_{i,B}$, $y_{i,B}$ combination on the travel trajectory of the excavator bucket tip are the point of interest. Those points help to extract the excavated earth area when integrated with the pre-ground level coordinates.

4.6 Summary

There are many survey technologies available in market for real-time job site monitoring and work progress measurement, starting from chain/tape-based measurement to drone-based imaging or radio signal sensing. The automatic total station is also a popular survey machine to measure the site elevation for different job purposes. The main disadvantage using such technology is, it directly interferes the job progress. Drone-based photogrammetry or radio signal based sensing technology serves the purpose well in this case but can be too costly and always needs expert personnel in the background to operate and monitor. In contrast, as discussed above in this chapter excavator like as survey robot can be a good solution. Using such technology three prime goals can be achieved at the same time,

i. Gathering real-time site survey data without interrupting the job.
ii. Gathering the job progress information in real time.
iii. Ensuring site safety by keep tracking of its position.

Chapter 5

Earthmoving Job Plan

5.1 General

On a fictitious grading project, in the starting stage surveyor's data on the elevations of different locations is available. An excavator fitted with its arm's movement measuring sensors can be tracked in a virtual environment in a global coordinate system in the field. The origin (x = 0, y= 0, z= 0) of the field coordinate frame is known. To guide the operations of the excavator a clear site layout plan is mandatory which is representable in the 3D virtual environment. The key center points depicting excavator operations can also be predefined. Alternatively, the excavator can work on the go by positioning itself in the field coordinate frame. The position of the bucket tip of an excavator can always be fixed referring the local reference coordinate frame of the excavator. In order to define the position of the excavator referring the field coordinate frame, the local reference point on the excavator is tracked down. So, the exactor's arm movement is tracked down with reference to the local reference point of the excavator itself, and thus the position of the excavator can be tracked concerning the field coordinate frame through transformation. Fig. 5.1(a) explains the movement of the excavator given a simple site layout plan where the site is positioned with respect to a global reference point, and an excavator is also visualized with respect to a local reference frame. On Fig 5.1(b) working radius fix mechanism of the excavator's working radius is shown. The working radius can be termed as the length (minimum) which is easily accessible by the excavator's arm in specific working condition.

5.2 Single Cell Job Plan

The objective of sensor equipped excavator is not only limited to track the position of the excavator's arm but also to improve the productivity of the earthmoving operation. To confirm that, a better-structured job plan is mandatory. Which actually will ensure the least number of maneuvering from place to place and lots of unnecessary back and forth

movement. In general, while planning massive earthmoving jobs for a grading project, the total area is used to be divided into some regular grids for the purpose of grading design. Cut and fill volumes are measured from the survey data and then balanced in between cells of the grids. Heavy machinery like excavator and truck fleets are deployed thereafter.

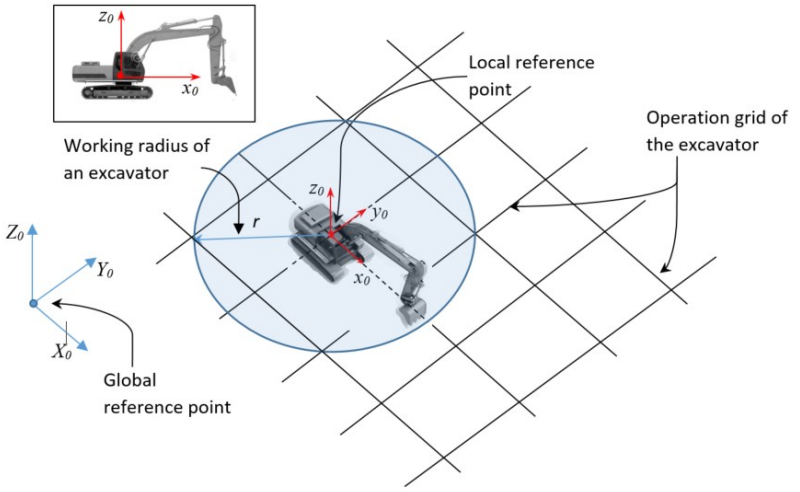

(a)

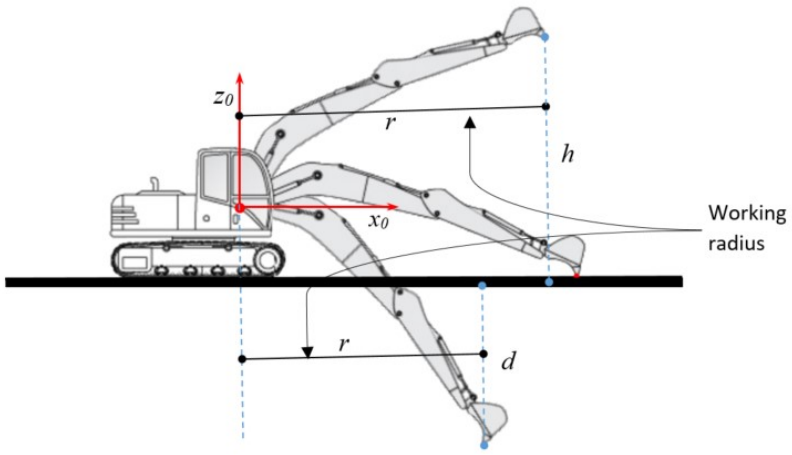

(b)

Figure 5.1. Positioning of the excavator; (a) Selecting the working grid in terms of accessible working radius; (b) working radius definition.

Planning the jobs for the excavator involves three steps. These steps are described in the following sections one by one.

5.2.1 Defining the Working Space for the Excavator

Workspace of an excavator can be selected based on the maximum allowable working radius of the excavator's arm. Since, allowable operating radius, r depends on the elevation of the digging area, h_i and type of the excavator (arm length, l_{arm}) use (Eq. 5.1), should be preselected.

$$r = f\,(l_{arm}, \max|h_i|) \tag{5.1}$$

When the working radius is fixed, the workspace, *Ws* can be defined too. Eq. 5.4 gives the final workspace for an excavator operation.

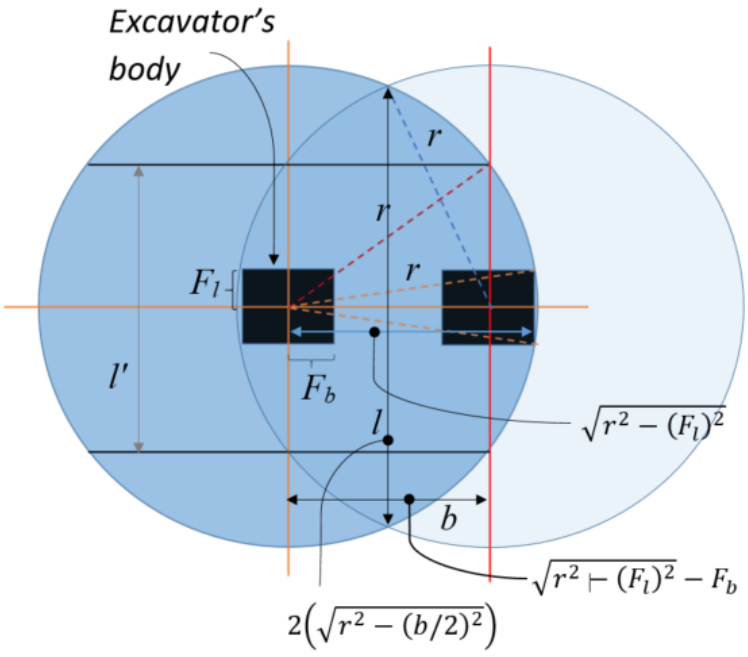

Figure 5.2. Defining the workspace of an excavator.

From Fig. 5.2,

$$b = \sqrt{r^2-(F_l)^2} - F_b \tag{5.2}$$

$$l = 2\left(\sqrt{r^2-(b/2)^2}\right) \tag{5.3}$$

and,

$$W_s = l \times b \tag{5.4}$$

Here, l and b are the length and breadth of the excavator's workspace respectively, $2F_b$ and $2F_l$ are the occupancy width and length for the excavator itself respectively (Fig. 5.2). These are also can be called the grid spacing for excavator maneuvering.

5.2.2 Counting the Number of Moves for the Excavator

If Lc and Bc are the length and breadth of a single rectangular grid the number of moves, n for an excavator to complete its job can be counted using the following equations (Eq. 5.5 to Eq. 5.7). Fig. 5.3 explained how the excavator will define its workspace progressively.

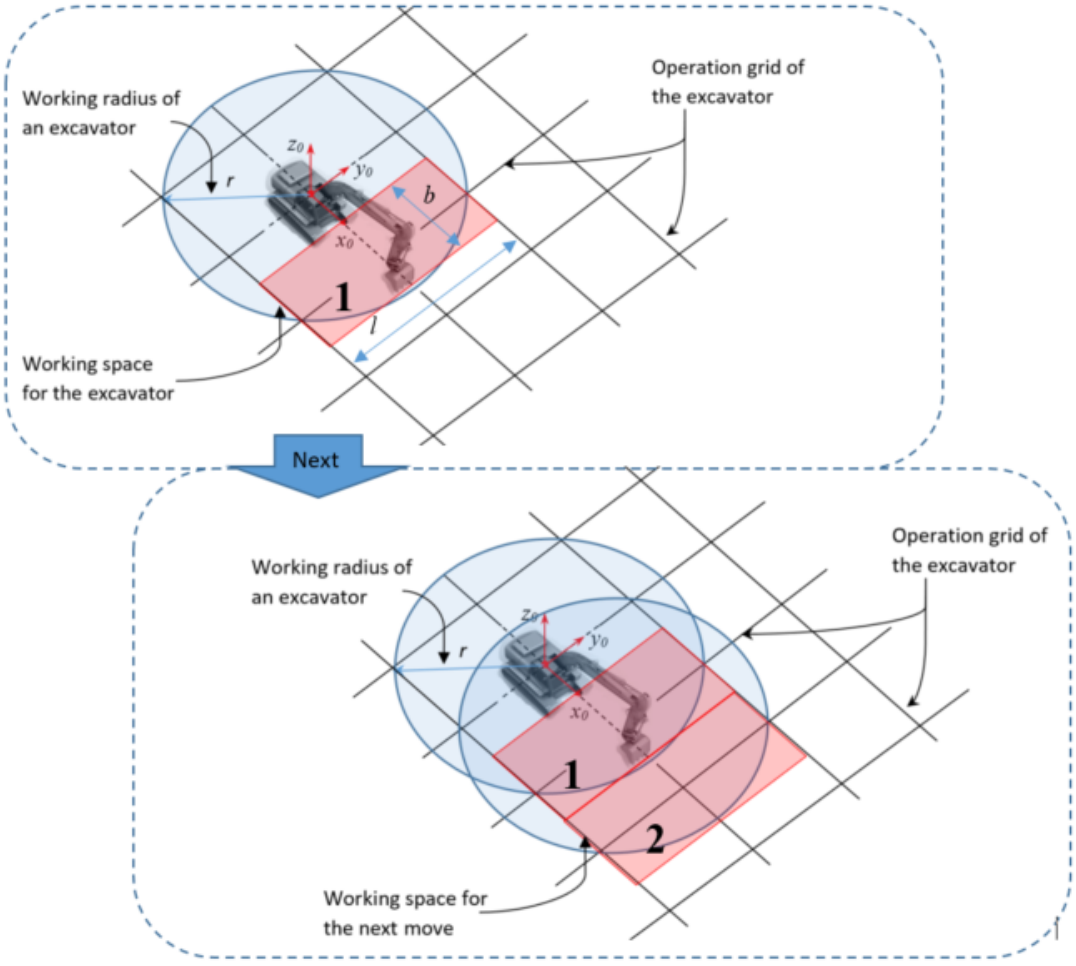

Figure 5.3. Defining the progressive workspace of the excavator.

$$n_1 = \left(\frac{Lc}{b}\right) \tag{5.5}$$

$$n_2 = \left(\frac{Bc}{l}\right) \tag{5.6}$$

$$n = n_1 \times n_2 \tag{5.7}$$

5.2.3 Setting the References

It is recommended to set up the origin of the global reference frame outside the area of operation thus to keep the x and y coordinate values positive for any point present at the top of the surface. Before starting the excavation job, at least three reference points need to be set up by the surveyor which are close enough to access (touch) by an excavator with its arm from a single standing position. These are called the primary references. This should be the place from where the excavator from where the excavator will start its first move. So, this reference should be as much close as possible from first defined workspace of the excavator inside the operation cell. One this should keep in mind that these reference points cannot be collinear.

The idea is, the excavator will complete its job in a single workspace by standing constantly in a single position and then move onto the next one. The excavator has the sensors to track its bucket tip with respect to its local reference (Fig 5.1a). When it touched some know references with its arm, can be able to transform its own coordinate frame in terms of the global reference frame. Then anything it touches can be tracked in terms of the global reference frame. So, after finishing the work on one space when moved on to the new position, again it will have to calibrate the frame references to match with the global system. To do that, the excavator has to define new auxiliary references after completing a job on the first workspace. It can be done by staffing (surveyor) or by making scratches on the ground (by the excavator itself) following the same principle of reference set up like primary references. Least required number of auxiliary references, *Ap* can even be counted beforehand by using Eq. 5.8. A schematic diagram showing the primary and auxiliary references is shown in Fig. 5.4.

$$Ap = 2n + n_1 \tag{5.8}$$

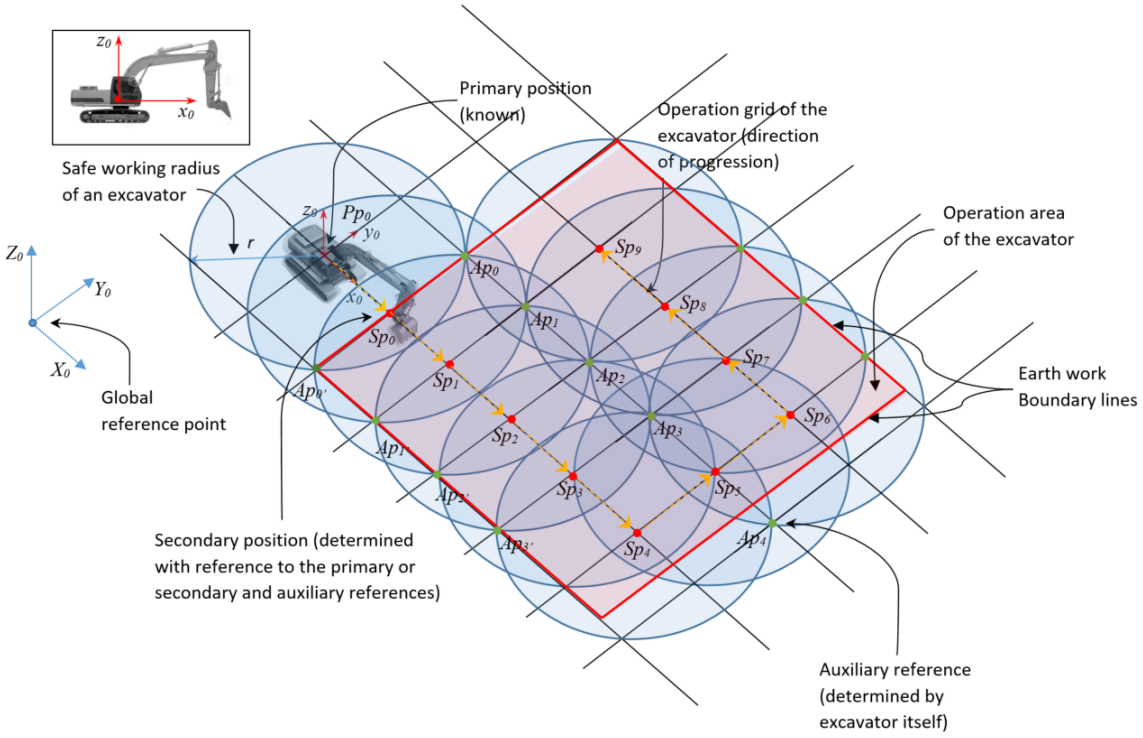

Figure 5.4. Different types of references for calibrating excavator's position.

5.3 Example Case

To better clarify the workspace structure, we took an example case where a CAT 336D excavator, working on a cut area of 100m x 100m dimension. For such excavator, the width, *W*, and length, *L* (Fig. 5.5) are 3.3 m and 5.0 m respectively.

Figure 5.5. Defining body factor for the excavator.

Thus, the body factors will be,

$$F_l = \frac{W}{2} \times FS = \frac{3.3}{2} \times 1.1 = 1.82\ m$$

And

$$F_b = \frac{L}{2} \times FS = \frac{5}{2} \times 1.1 = 3.03\ m$$

Here, 10 % shape factor (FS) is induced for entire workspace related calculations as a factor of safety. If the maximum workspace radius for the mass boom excavator is $r_{max} = 9.2\ m$ and the minimum workspace radius would be $r_{min} = F_b = 3.03\ m$. Then using Eq. 5.3 and 5.4, we can find,

$$b = \sqrt{r^2 - (F_l)^2} - F_b = \sqrt{(9.2)^2 - (1.82)^2} - 3.03 = 6.00\ m$$

And $$l = 2\left(\sqrt{r^2 - (b/2)^2}\right) = l = 2\left(\sqrt{(9.2)^2 - (6/2)^2}\right) = 17.4\ m$$

The workspace area will be, $W_s = 17.4 \times 6 = 104.5\ m^2$

According to Eq. 5.1, the number of workspaces required to complete the excavation task in the whole area will be,

$$n = n_1 \times n_2 = \left(\frac{100}{6}\right) \times \left(\frac{100}{17.4}\right) = 17 \times 6 = 102$$

Besides three fixed primary references, total number of auxiliary references will be needed to establish

$$Ar = 2n + n_1 = 2 \times 102 + 17 = 221$$

So, grid spacing for excavator operation will be, $\frac{l}{2} = \frac{17}{2} = 8.5\ m$ in the transverse direction and $b = 6.0\ m$ in the longitudinal direction.

5.4 Maneuvering Plan

The conceptual illustration of a work package is shown at the top of Fig. 5.6. Further, the detailed work breakdown of the excavator's operation is given as the arrow diagram on the bottom of the same figure. The comprehensive jobs can be defined as follows,

Job 1. Set the safe operating radius r for the excavator (Fig. 5.1b)

Job 2. Plan the excavator's movement route (which is the shortest path to travel to complete whole excavation, Fig. 5.6a)

Job 3. Set the excavator's Primary position and orientation in terms of global reference frame position

Job 4. Complete excavating operation (detail is given in the following section)

Job 5. Set the Auxiliary references for the next move (marking on the ground, Fig. 5.6b)

Job 6. Turn the excavator arm to the back (this keeps track of its movement while moving towards the next position of operation Fig. 5.6c)

Job 7. Move towards the next position of operation (Fig. 5.6d)

Job 8. Set the new (secondary) position of the excavator with reference to the auxiliary references (primary/ secondary reference points of the previous movement can be counted as an auxiliary reference point)

Job 8.1 Turn and touch the auxiliary references.

Job 8.2 Setting up the secondary reference for the position of the excavator referencing the global reference frame.

(a)

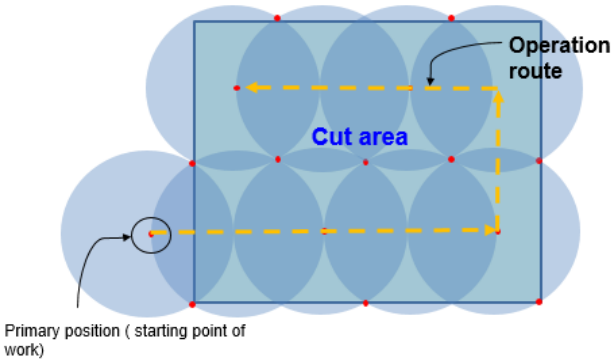

(b)

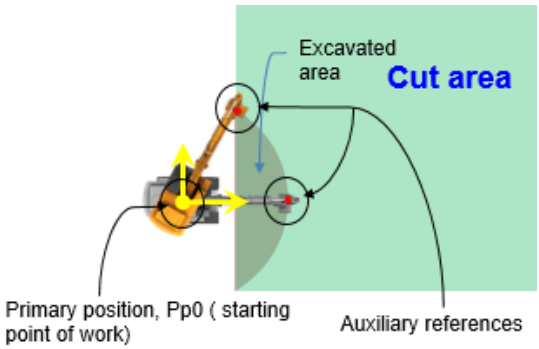

(c)

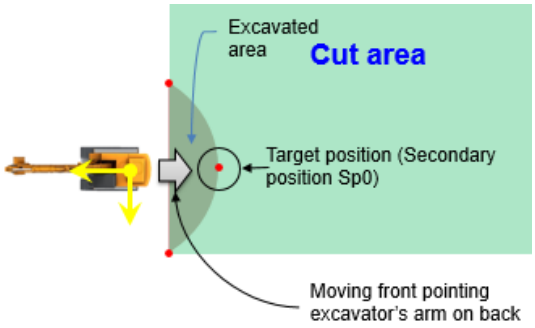

(d)

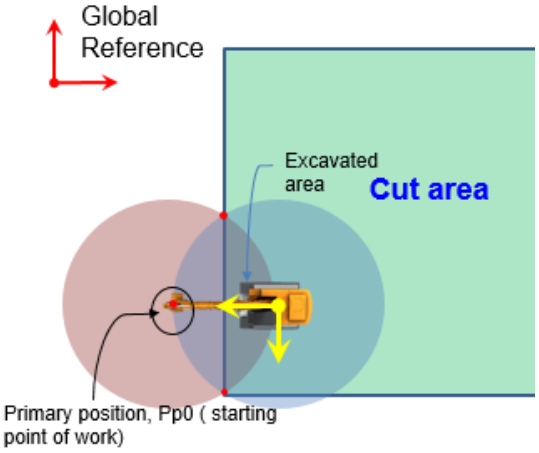

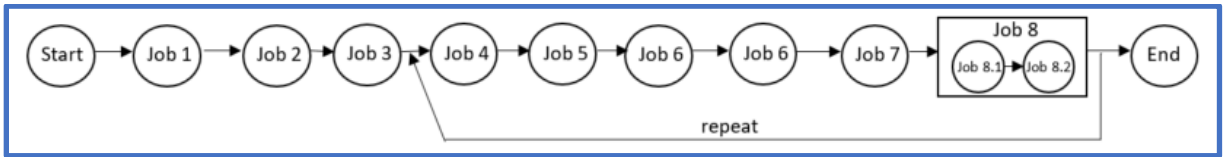

Figure 5.6. Operation package of a self-guided excavator.

5.5 Excavation Operation

The most prominent advantage of using a sensor-equipped excavator is its control over the excavation operation.

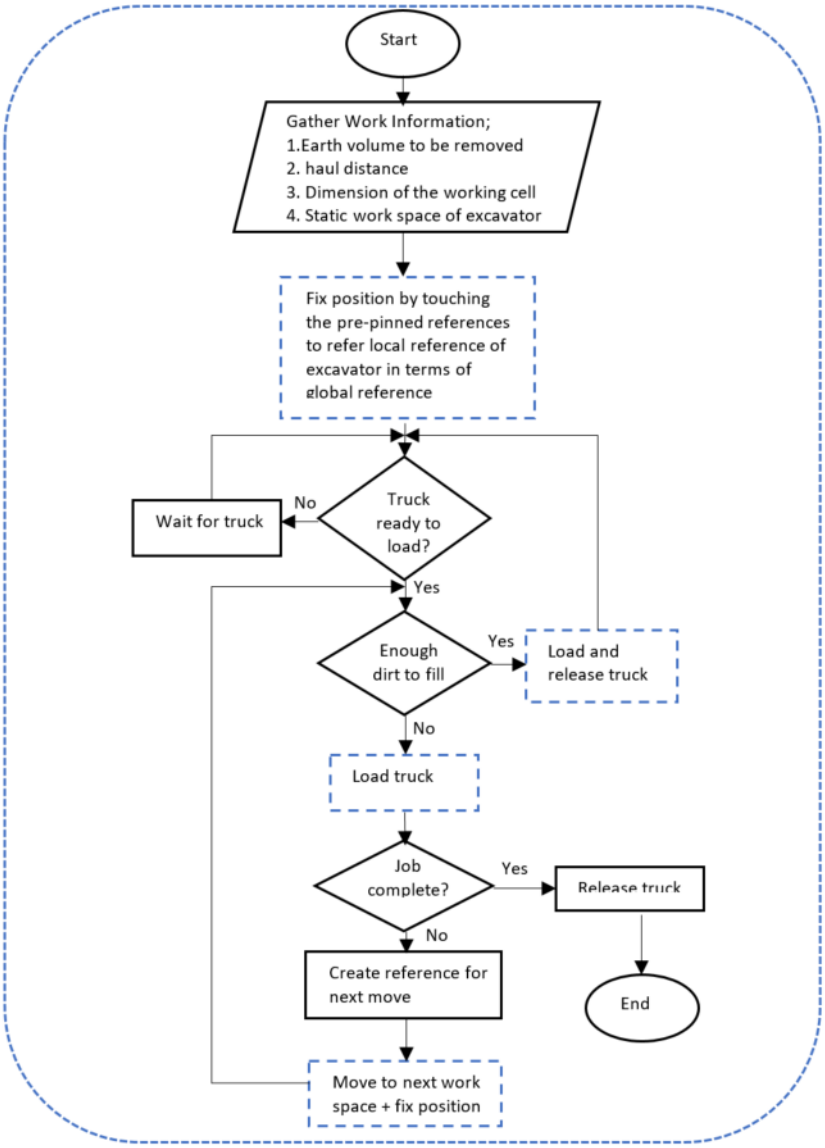

Figure 5.7. Operation algorithm of a self-guided excavator.

For a general excavator, excavation efficiency and accuracy mostly depend on the operator's skill and navigation capacity of the guiding crew. Whereas, this excavator can complete the total excavation task with precision, at the same time eliminates the need for extra manpower for guiding the excavation operation. Thus, it enhances the operation

efficiency and ensures economy. The operation algorithm for the entire excavation process is shown in Fig 5.7. Also, the algorithm for checking the progress of the work ensuring the grading requirement is presented as pseudo code in Table 5.1.

Table 5.1. Work progress measurement algorithm.

Algorithm 3	
Step 1	Initialize the global reference frame in terms of the excavator's local frame.
Step 2	Take the initial ground level $L_{i,I}(x_i, y_i, z_i)$ and designed target ground level $L_{j,T}(x_i, y_i, z_j)$ as the input.
Step 3	Start digging operation and at the same time track the bucket tip of the excavator $L_{k,B}(x_i, y_i, z_k)$
Step 4	Check $d_i = z_{k,B} - z_{j,T}$; If $d > 0$, continue digging (Fig 5.8).
Step 5	Store the progress, excavated depth $L_m(x_i, y_i, d_i)$
Step 6	If $d = 0$ check the surface points (x_i, y_i) being covered. If all are covered then end process. or, move bucket into new position [new (x_i, y_i)] and return to Step 3 or, continue digging on the same position.

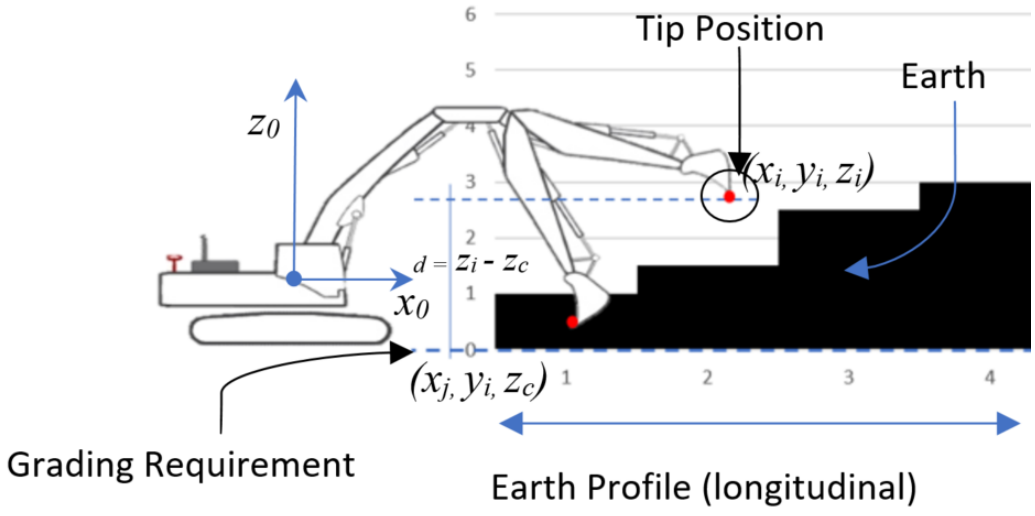

Figure 5.8. Checking the grading of the earth while digging.

5.6 Similar job Application

The framework described is applicable for any trench like construction process too. A conceptual procedure of the trench construction is shown in the Fig. 5.9. The steps involved in construction operation are simple as before. The first step should be initializing the position of the excavator in terms of the global reference where the trench's existing and design grades are provided with respect to the same reference frame too. The second step should start digging operation while it must check the target grade and bucket tip position simultaneously. After completing the digging by standing in a fixed position, it has to set auxiliary references for the next move. Next, change the position and fix the position with respect to the prefixed auxiliary reference and progress the work as like as the same way before.

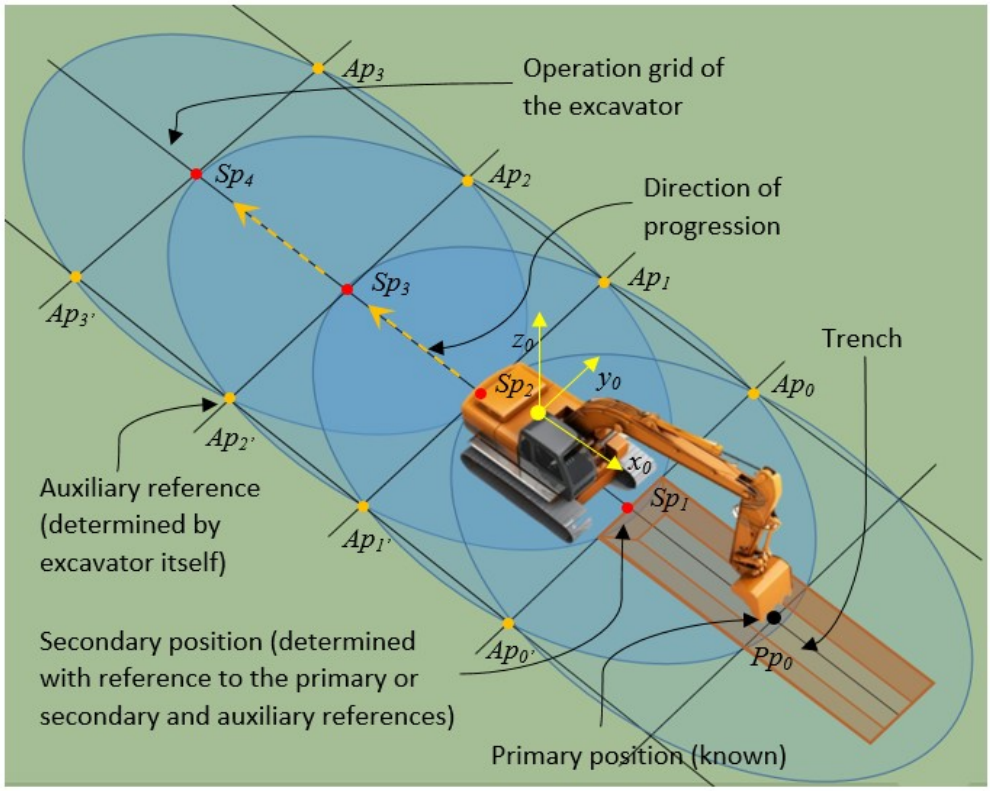

Figure 5.9. Trench construction with the self-guided excavator.

Chapter 6

Conclusions & Suggestions

6.1 General

A massive earthwork project is very cost sensitive to proper planning. An ill-planned project can cost a lot of money and time. Project economy and efficiency can be increased in two ways, namely: excellent job planning and increasing the productivity of the on-field crew operation. This research makes contributions in both directions. First, it discusses the methodology about, how efficiently sensors technology can be used to turn an ordinary excavator into a smart (self-guided) one and then presents the structured working plan for materializing the concept and introduces comprehensive operation planning framework for bulk excavation work. This framework not only improves the field productivity by eliminating rework volume but also increases crew utilization rate and at the same time, excludes the need for field survey crew during construction.

This research is focused on sensor-based excavator positioning methods and the theory for identifying the error boundary derived from sensor dependent measurements of the excavator's pose/position. The positioning error on the excavator has been computed analytically and visualized in a straightforward fashion. A discussion is made how the proposed methodology can be efficiently used in the field operation by turning an excavator into a survey robot which can track its own position through computing based on "sensing" the ground in real time. This research contributes to structuring the operation sequence of a self-guided excavator. Detailed step by step algorithms for planning the work of a self-guided excavator is presented in the following sections. The excavator is termed as the self-guided one because of its capability of fixing its positioning by itself regarding any reference system. A three-reference point based positioning system for such excavator is also described in detail. Although this methodology is built on top of the working procedure of tilt and angle measuring sensors

equipped excavator, a similar framework can be readily adapted for other autonomous excavator operation cases.

6.2 Conclusions

Based on the study of “Analytical Framework for Field Positioning and Work Planning for a Backhoe Excavator” problem as discussed in the previous chapters, following conclusions can be drawn:

- This study highlights the necessity of error quantification on the sensor data regardless of the particular sensors being used in order to automate the positioning of a backhoe excavator and determine its kinematic state.
- A chart is also produced to show the propagated position uncertainty, which can be readily used to enhance the operator's efficiency in site operations, while at the same time eliminating the need for any extra guiding staff on site.
- A sensor selection guideline based on job-specific needs is also given based on a particular excavator example. Though the derived chart is limited to use for the tilt angle measuring sensors, this concept can be applied as the guidance to produce equipment-specific selection charts given different types of sensors.
- A three-point (three references) positioning mechanism (fixing the position and orientation of the excavator-base with respect to the global/master reference frame) for the excavator which can track its bucket tip from own local reference is discussed in detail.
- A detailed operation planning framework for a self-guided excavator is presented in this study. This framework not only improves the field productivity by eliminating rework volume but also increases crew utilization rate and at the same time, eliminates the need for field survey crew.

6.3 Recommendations

The contribution of this study is limited to excavator' s pose estimation methodology by using only angle or length measuring sensors. Thus, the sensor selection guide is developed based on the angle measuring sensors only. Again, the framework generated in

this case is just being tested in the virtual environment but not yet in a real test bed. Considering the limitations of this study some scope for future research is laid out as follows:

- The analytical methodology developed here is the perfect match for any angle and length measuring sensors, but similar methodology can be used for other types of sensors too. Since this study does not consider such options, future research contribution can be made to structure such methodology relying on different kinds of sensors.
- The error propagation theory is only applied to quantify the position error of the excavator bucket tip from sensors attached to the excavator's arm. At the same time, a methodology is explained where such excavator can fix its position itself from three references and gradually can progress via setting up its own auxiliary references. Since the same sensors are used for localizing the position of the excavator on the next move, the sensor error will propagate in each round on the tip position and eventually spread of the position uncertainty will increase. Such phenomenon is not addressed in this study. Future research contribution can be made to consider such aspects to account it in for the bucket tip's position uncertainty.
- The entire framework described in this literature is only tested in the virtual environment. A future research effort is recommended to physically check this framework in the actual field.

References

Alderton, M. (2015). The Robots Are Coming! Driverless Dozers and the Dawn of Autonomous Vehicle Technology in Construction. Autodesk.com, Retrieved from: https://www.autodesk.com/redshift/autonomous-vehicle-technology-in-construction (12 August 2017)

Ardiny, H., Witwicki, S., & Mondada, F. (2015). Are Autonomous Mobile Robots Able to Take Over Construction? A Review. International Journal of Robotics, 4(3), 10–21.

Azar, E. R., Agnew, G., & Parker, A. (2015). Effectiveness of automated machine guidence technology in productivity improvement: case study. Proceedings of 5th International/11th Construction Specialty Conference, (269), 1 – 10.

Azar, E. R., Feng, C., & Kamat, V. R. (2015). Feasibility of in-plane articulation monitoring of excavator arm using planar marker tracking. Journal of Information Technology in Construction, 20(July 2014), 213–229.

Balaguer, C., & Abderrahim, M. (2008). Trends in robotics and automation in construction. Robotics and Automation in Construction, 1–22. https://doi.org/10.5772/5865

Balaguer, C., Giménez, A., Pastor, J. M., Padrón, V. M., & Abderrahim, M. (2000). Climbing autonomous robot for inspection applications in 3D complex environments. Robotica, 18(3), 287–297. https://doi.org/10.1017/S0263574799002258

Bernold, L. (1993). Motion and Path Control for Robotic Excavation. Journal of Aerospace Engineering, 6(1), 1 –18.

Bock, T. (2015). The future of construction automation: Technological disruption and the upcoming ubiquity of robotics. Automation in Construction, 59, 113–121. https://doi.org/10.1016/j.autcon.2015.07.022

Bonchis, A., Hillier, N., Ryde, J., Duff, E., & Pradalier, C. (2011). Experiments in autonomous earth moving. IFAC Proceedings Volumes (IFAC-PapersOnline), 18(PART 1), 11588–11593. https://doi.org/10.3182/20110828-6-IT-1002.00536

Bosché, F. (2010). Automated recognition of 3D CAD model objects in laser scans and calculation of as-built dimensions for dimensional compliance control in construction. Advanced Engineering Informatics, 24(1), 107–118. https://doi.org/10.1016/j.aei.2009.08.006

CAT 325F L (2017), www.cat.com. Retrieved from: http://s7d2.scene7.com/is/image/Caterpillar/CM20160928-34878-01096?$cc-g$ (02 August 2017).

Caterpillar. (2017) Taking telematics one byte at a time. www.cat.com. Retrieved from: https://www.cat.com/en_US/articles/support/telematics.html (12 August 2017)

Chi, S., & Caldas, C. H. (2012). Design of a preliminary error impact analysis model for spatial safety assessment of earthmoving operations. Automation in Construction, 22, 212–222. https://doi.org/10.1016/j.autcon.2011.06.019

Cho, H. H., Kim, B. J., An, S. H., & Kang, K. I. (2007). Analysis of a steel frame fabrication process for the automation of building construction. International Conference on Control, Automation and Systems, 1213–1216. https://doi.org/10.1109/ICCAS.2007.4406519

Cho, Y., Haas, C., Sreenivasan, S., and Liapi, K. (2004). Position Error Modeling for Automated Construction Manipulators. J. Constr. Eng. Manage., 130(1), 50 – 58.

Chua, D. K. H., and Li, G. M. (2002). RiSim: Resource-interacted simulation modeling in construction. Journal of Construction Engineering and Management, 128(3), 195–202.

Corke, P. (2011). Robotics, vision and control: fundamental algorithms in MATLAB®. Vol. 73. Springer Science & Business Media. Robotics Research (pp. 329–340). https://doi.org/10.1007/978-3-540-73958-6_2

Dadhich, S., Bodin, U., & Andersson, U. (2015). Key challenges in automation of earth-moving machines. Automation in Construction, 68, 212–222. https://doi.org/10.1016/j.autcon.2016.05.009

De-Cursi, Eduardo Souza Sampaio, R. (2015). Uncertainty Quantification and Stochastic Modeling with Matlab. (P. Breitkopf, Ed.) (1st ed.). Elsevier (S&T). Retrieved from https://www.elsevier.com/books/uncertainty-quantification-and-stochastic-modeling-with-matlab/souza-de-cursi/978-1-78548-005-8

Deb, S. (1990). Automation and Robotics Based Technologies for Road Construction, Maintenance and Operations. Journal of Transportation Engineering, 116(3), 261–271. https://doi.org/10.1061/(ASCE)0733-947X(1990)116

Delisio, A., & Zhao, J. (2014). A new model for TBM performance prediction in blocky rock conditions. Tunnelling and Underground Space Technology, 43, 440–452. https://doi.org/10.1016/j.tust.2014.06.004

Earthwave Technologies. (2017). Wireless fleet management for the construction industry. Web Address: http://www.earthwavetech.com/ (12 August 2017).

Feng, C., Dong, S., Lundeen, K. M., Xiao, Y., & Kamat, V. R. (2015). Vision-Based Articulated Machine Pose Estimation for Excavation Monitoring and Guidance. Proceedings of the 32nd International Symposium on Automation and Robotics in Construction (ISARC).

Feng, C., Xiao, Y., Willette, A., McGee, W., & Kamat, V. R. (2015). Vision guided autonomous robotic assembly and as-built scanning on unstructured construction sites. Automation in Construction, 59, 128–138. https://doi.org/10.1016/j.autcon.2015.06.002

forconstructionpros.com (2015). Excavators Get Smart. Retrieved from: https://www.forconstructionpros.com/equipment/earthmoving/excavators/article/12027620/excavators-get-smarter-to-enhance-earthmoving-efficiency (12 August 2017)

Ford, M. (2009). The Lights in the Tunnel: Automation, Accelerating Technology and the Economy of the Future. US: Acculant Publishing. Retrieved from www.TheLightsintheTunnel.com

Gambao, E. and Balaguer, C. (2002). Robotics and Automation in Construction [Guest Editors], IEEE Robotics & Automation Magazine (April 2002). https://doi.org/10.1109/MRA.2002.993150

Ghanem, R., Owhadi, H., & Higdon, D. (2017). Handbook of uncertainty quantification. Handbook of Uncertainty Quantification. https://doi.org/10.1007/978-3-319-12385-1

Golparvar-Fard, M., Peña-Mora, F., & Savarese, S. (2015). Automated Progress Monitoring Using Unordered Daily Construction Photographs and IFC-Based Building Information Models. Journal of Computing in Civil Engineering, 29(1), 4014025. https://doi.org/10.1061/(ASCE)CP.1943-5487.0000205

Hager, I., Golonka, A., & Putanowicz, R. (2016). 3D Printing of Buildings and Building Components as the Future of Sustainable Construction? Procedia Engineering, 151, 292–299. https://doi.org/10.1016/j.proeng.2016.07.357

Ham, Y. B., Kwon, S. W., Noh, J. H., Han, J. G., & Kim, K. T. (2006). Development of road stripe removing equipment using high-pressure water jet. Automation in Construction, 15(5), 578–588. https://doi.org/10.1016/j.autcon.2005.06.017

Hasan, M. and Lu, M. (2017). Error Quantification and Visualization in Using Sensors to Position Backhoe Excavator. Proceedings of International Workshop on Computing for Civil Engineering (IWCCE), 25 – 27 June 2017, 8 pages.

Hemami, A., & Hassani, F. (2009). An overview of autonomous loading of bulk material. 26th International Symposium on Automation, (Isarc), 405–411. Retrieved from http://www.iaarc.org/publications/fulltext/An_Overview_of_Autonomous_Loading_of_Bulk_Material.pdf

Hwang, S., & Liu, L. (2007). Modeling Excavation Process Using Dynamic Modeling Approach. Computing in Civil Engineering (2007), 159–167. https://doi.org/doi:10.1061/40937(261)20

Kamat, V. and Martinez, J. (2005). "Dynamic 3D Visualization of Articulated Construction Equipment." J. Comput. Civ. Eng., 19(4), 356 – 368.

Kamat, V. R., Martinez, J. C., Fischer, M., Golparvar-Fard, M., Peña-Mora, F., & Savarese, S. (2011). Research in Visualization Techniques for Field Construction. Journal of Construction Engineering and Management, 137(10), 853–862. https://doi.org/10.1061/(ASCE)CO.1943-7862.0000262

Kashani, A. H., Owen, W. S., Himmelman, N., Lawrence, P. D., & Hall, R. A. (2010). Laser scanner-based end-effector tracking and joint variable extraction for heavy machinery. International Journal of Robotics Research, 29(10), 1338–1352. https://doi.org/10.1177/0278364909359316

Kim, D., Kim, J., Lee, K., Park, C., Song, J., & Kang, D. (2009). Excavator tele-operation system using a human arm. Automation in Construction, 18(2), 173–182. https://doi.org/10.1016/j.autcon.2008.07.002

Lee, J. H., Yoo, H. S., Kim, Y. S., Lee, J. B., & Cho, M. Y. (2006). The development of a machine vision-assisted, teleoperated pavement crack sealer. Automation in Construction, 15(5), 616–626. https://doi.org/10.1016/j.autcon.2005.06.018

Lee, S. H., Kang, M. S., Shin, D. S., & Han, C. S. (2012). Estimation with applications to dynamic status of an excavator without renovation. Gerontechnology, 11(2). https://doi.org/10.4017/gt.2012.11.02.417.00

Li, C. C., Oloufa, A. A., & Thomas, H. R. (1996). A GIS-based system for tracking pavement compaction. Automation in Construction, 5(1), 51–59. https://doi.org/10.1016/0926-5805(95)00019-4

Li, S., Cai, H., & Kamat, V. R. (2015). Uncertainty-aware geospatial system for mapping and visualizing underground utilities. Auto. Con., 53, 105 –119.

Liang, X., Lu, M., & Asce, M. (2010). 3D Visualization for Tunnel Boring Machine Steering and Alignment Control in Microtunneling Ph . D . Candidate, Dept . of Civil and Structural Engineering, Hong Polytechnic Univ ., Hong Kong SAR , China ; PH (852) 2766-6080 ; FAX Associate Professor , 1–10.

Liu, C. and Lu, M. (2014). Evaluation of Temporary Haul Road Networks Design for Mass Earthworks Projects. Journal of Construction Engineering and Management,141(3). https://doi.org/10.1061/(ASCE)CO.1943-7862.0000940

Liu, D. K., Dissayanake, G., Manamperi, P. B., Brooks, P. a., Fang, G., Paul, G., Ren, T. R. (2008). A Robotic System for Steel Bridge Maintenance: Research Challenges and System Design. 2008 Australasian Conference on Robotics and Automation. Retrieved from http://www.scopus.com/inward/record.url?eid=2-s2.0-84862909210&partnerID=tZOtx3y1

Lorenc, S. J., Handlon, B. E., & Bernold, L. E. (2000). Development of a robotic bridge maintenance system. Automation in Construction, 9(3), 251–258. https://doi.org/10.1016/S0926-5805(99)00040-0

Louis, J., & Dunston, P. S. (2017). Methodology for Real-Time Monitoring of Construction Operations Using Finite State Machines and Discrete-Event Operation Models. Journal of Construction Engineering and Management, 143(3), 4016106. https://doi.org/10.1061/(ASCE)CO.1943-7862.0001243

Lu, M. and Liang, X. (2012).“Real-Time 3D Positioning and Visualization of Articulated Construction Equipment: Case of Backhoe Excavators.”J. Comput. Civ. Eng., 12, 196-203. https://doi.org/10.1061/9780784412343.0025

Lundeen, K. M., Dong, S., Fredricks, N., Akula, M., & Kamat, V. R. (2015). Electromechanical development of a low cost end effector pose estimation system for articulated excavators. 32nd International Symposium on Automation and Robotics in Construction and Mining: Connected to the Future, Proceedings.

Lundeen, K. M., Dong, S., Fredricks, N., Akula, M., Seo, J., & Kamat, V. R. (2016). Optical marker-based end effector pose estimation for articulated excavators. Automation in Construction, 65, 51–64. https://doi.org/10.1016/j.autcon.2016.02.003

Maeda, G. J. (2013). Learning and reacting with inaccurate prediction: Applications to autonomous excavation. PhD Thesis, University of Sydney, Graduate School of Engineering and IT, School of Aerospace, Mechanical and Mechatronic Engineering. http://hdl.handle.net/2123/9460

Maeda, J. (1994). Development and Application of the SMART System. Elsevier Science, 6, 457–464.

Maeda, J., & Miyatake, Y. (1997). Improvement of a Computer Integrated and Automated Construction System for High-rise Building and its Application for RC (Rail City) Yokohama Building. The 14th International Association for Automation and Robatics in Construction, 139–146.

Mao, S., Shen, X., & Lu, M. (2015). Virtual Laser Target Board for Alignment Control and Machine Guidance in Tunnel-Boring Operations. Journal of Intelligent and Robotic Systems: Theory and Applications, 79(3–4), 385–400. https://doi.org/10.1007/s10846-014-0113-y

Mao, S.; Li, D. & Lu, M. (2015). "Analytical Comparison of Distance based and Angle Based Kinematic Models for Positioning Backhoe Excavators." 15th International Conference on Construction Applications of Virtual Reality (CONVR 2015), 5 – 7 October. (9 pages).

Mascarenas, D., Flynn, E., Farrar, C., Park, G., & Todd, M. (2009). A mobile host approach for wireless powering and interrogation of structural health monitoring sensor networks. IEEE Sensors Journal, 9(12), 1719–1726. https://doi.org/10.1109/JSEN.2009.2030706

Mirjan, A., Federico, A., Raffaello, D., Fabio, G., & Matthias, K. (2016). Robotic Fabrication in Architecture, Art and Design 2016. https://doi.org/10.1007/978-3-319-26378-6

Momin, S. J., Patil, J. R., & Nale, R. R. (2015). Enhancement of Road Construction Sector using Automation. International Research Journal of Engineering and Technology, 2395–56.

Montgomery, D. C. and Runger, G. C. (2003). Applied Statistics and Probability for Engineers, John Wiley & Sons, Inc.

Moselhi, O., & Alshibani, A. (2009). Optimization of Earthmoving Operations in Heavy Civil Engineering Projects. Journal of Construction Engineering and Management, 135(10), 948–954.

Myung, H., Lee, S., & Lee, B. (2011). Paired structured light for structural health monitoring Robot System. Structural Health Monitoring, 10(1), 49–64. https://doi.org/10.1177/1475921710365413

Navon, R., & Sacks, R. (2007). Assessing research issues in Automated Project Performance Control (APPC). Automation in Construction, 16(4), 474–484. https://doi.org/10.1016/j.autcon.2006.08.001

Navon, R., Goldschmidt, E., & Shpatnisky, Y. (2004). A concept proving prototype of automated earthmoving control. Automation in Construction, 13(2), 225–239.

Oh, J. K., Jang, G., Oh, S., Lee, J. H., Yi, B. J., Moon, Y. S., Choi, Y. (2009). Bridge inspection robot system with machine vision. Automation in Construction, 18(7), 929–941. https://doi.org/10.1016/j.autcon.2009.04.003

Oloufa, A. A. (2002). Quality control of asphalt compaction using GPS-based system architecture. IEEE Robotics and Automation Magazine, 9(1), 29–35. https://doi.org/10.1109/100.993152

Pmsolid.com, Putmizer document: TS 876-10 GB (2017). Machines, Equipment and Systems for Tunnel Construction. Retrieved from: http://www.pmsolid.com/psp/data/TS_876_GB.pdf (12 August 2017)

Peyret, F., Jurasz, J., Carrel, a, Zekri, E., & Gorham, B. (2000). The Computer Integrated Road Construction project. Automation in Construction, 9, 447–461. https://doi.org/10.1016/S0926-5805(00)00057-1

Razavi, S. N., & Moselhi, O. (2012). GPS-less indoor construction location sensing. Automation in Construction, 28, 128–136. https://doi.org/10.1016/j.autcon.2012.05.015

Rojas, E. M., & Aramvareekul, P. (2003). Is construction labor productivity really declining? Journal of Construction Engineering and Management, 129(1), 41–46. https://doi.org/10.1061/(ASCE)0733-9364(2003)129:1(41)

Rowe, P. S. (1999). "Adaptive Motion Planning for Autonomous Mass Excavation." Doctoral dissertation, tech. report CMU-RI-TR-99-09, The Robotics Institute of Carnegie Mellon University, Pittsburgh, Pennsylvania, January 28.

Sakin, M., & Kiroglu, Y. C. (2017). 3D Printing of Buildings: Construction of the Sustainable Houses of the Future by BIM. Energy Procedia, 134, 702–711. https://doi.org/10.1016/j.egypro.2017.09.562

Shen, X., Lu, M., & Chen, W. (2011). Tunnel-Boring Machine Positioning during Microtunneling Operations through Integrating Automated Data Collection with Real-Time Computing. Journal of Construction Engineering and Management, 137(1), 72–85. https://doi.org/10.1061/(ASCE)CO.1943-7862.0000250

Shi, J. J. (2000) Object-oriented technology for enhancing activity-based modeling functionality. Proceedings of 2000 Winter Simulation Conference, IEEE, Piscataway, NJ, 1938–1944.

Singh, S. (1997). State of the Art in Automation of Earthmoving. Journal of Aerospace Engineering, 10(4), 179–188. https://doi.org/10.1061/(ASCE)0893-1321(1997)10:4(179)

Soleimanifar, M., Shen, X., Lu, M., & Nikolaidis, I. (2014). Applying received signal strength based methods for indoor positioning and tracking in construction applications. Canadian Journal of Civil Engineering, 41(8), 703–716. https://doi.org/10.1139/cjce-2013-0433

Spong, M. W., Hutchinson, S., & Vidyasagar, M. (2004). Robot dynamics and control. Automatica, 28(3), 655–656. https://doi.org/10.1016/0005-1098(92)90197-N

Stentz, A., Bares, J., Singh, S., & Rowe, P. (1999). A Robotic Excavator for Autonomous Truck Loading. Proceedings of the IEEE/RSJ International Conference on Intelligent Robotic Systems. (9 pages)

Su, X., Li, S., Yuan, C., Cai, H., & Kamat, V. R. (2014). Enhanced Boundary Condition–Based Approach for Construction Location Sensing Using RFID and RTK GPS. Journal of Construction Engineering and Management, 140(10), 4014048. https://doi.org/10.1061/(ASCE)CO.1943-7862.0000889

Sukkarieh, S., Nebot, E. M., & Durrant-Whyte, H. F. (1999). A high integrity IMU/GPS navigation loop for autonomous land vehicle applications. IEEE Transactions on Robotics and Automation, 15(3), 572–578. https://doi.org/10.1109/70.768189

Talmaki, S. and Kamat, V. (2014). "Real-Time Hybrid Virtuality for Prevention of Excavation Related Utility Strikes." J. Comput. Civ. Eng., 28(3), 1 – 16.

Tatum, C. B., Vorster, M., & Klingler, M. (2006). Innovations in Earthmoving Equipment: New Forms and Their Evolution. Journal of Construction Engineering and Management, 132(9), 987–997. https://doi.org/10.1061/(ASCE)0733-9364(2006)132:9(987)

Teicholz, P. (2013). Labor-productivity declines in the construction indus- try: Causes and remedies (another look). Retrieved from: http://www.aecbytes.com/viewpoint/2013/issue_67.html (12 August 2017)

Turkan, Y., Bosche, F., Haas, C. T., & Haas, R. (2012). Automated progress tracking using 4D schedule and 3D sensing technologies. Automation in Construction, 22, 414–421. https://doi.org/10.1016/j.autcon.2011.10.003

Vähä, P., Heikkilä, T., Kilpeläinen, P., Järviluoma, M., & Gambao, E. (2013). Automation in Construction Extending automation of building construction — Survey on potential sensor technologies and robotic applications." Auto. Con., 36, 168–178.

Vahdatikhaki, F., Hammad, A., & Siddiqui, H. (2015). Optimization-based excavator pose estimation using real-time location systems. Automation in Construction, 56, 76–92.

Vereen, S. C., Asce, M., Rasdorf, W., Asce, F., & Hummer, J. E. (2016). Development and Comparative Analysis of Construction Industry Labor Productivity Metrics. Journal of Construction Engineering and Management, 142(7), 1–9. https://doi.org/10.1061/(ASCE)CO.1943-7862.0001112.

Vrijhoef, R., & Koskela, L. (2005). A critical review of construction as a project-based industry: identifying paths towards a project-independent approach to construction. Proceedings of the CIB Joint Symposium, 'Combining Forces – Advancing Facilities Management and Construction through Innovation, 13–24.

WenZhongShi. (2014). Principles of Modeling Uncertainties in Spatial Data and Spatial Analysis. Katalog BPS (Vol. XXXIII, pp. 81–87). https://doi.org/10.1007/s13398-014-0173-7.2

Winck, R. C., Elton, M., & Book, W. J. (2014). Automation in Construction A practical interface for coordinated position control of an excavator arm. Automation in Construction, 51, 46–58. https://doi.org/10.1016/j.autcon.2014.12.012

Yoo, W. S., Lee, H. J., Kim, D. I., Kang, K. I., & Cho, H. (2012). Genetic algorithm-based steel erection planning model for a construction automation system. Automation in Construction, 24, 30–39. https://doi.org/10.1016/j.autcon.2012.02.007

Yoon, J., & Manurung, A. (2010). Automation in Construction Development of an intuitive user interface for a hydraulic backhoe. Automation in Construction, 19(6), 779–790. https://doi.org/10.1016/j.autcon.2010.04.002

Yoon, J., Kim, J., Seo, J., & Suh, S. (2014). "Spatial factors affecting the loading efficiency of excavators." Auto. Con., 48, 97–106.

Yuan, C., Li, S., and Cai, H. (2016). "Vision-Based Excavator Detection and Tracking Using Hybrid Kinematic Shapes and Key Nodes." J. Comput. Civ. Eng., 04016038 (16 pages).

Zhang, M., Cao, T., & Zhao, X. (2017). Applying sensor-based technology to improve construction safety management. Sensors (Switzerland), 17(8). https://doi.org/10.3390/s17081841

Appendix A

Example Solution for Different Equations

Error Quantification

Use of Eq. 3.5

A car's speedometer has an absolute error of +0.09 km/hr and the while measuring the mass of the car the weight measuring sensor has an absolute error +0.5 kg.

Measured reading,

$$speed, v = 54\ km/hr = 15\ m/s$$

$$mass, m = 1.65\ ton = 1497\ kg$$

The error while calculating the kinetic energy would be,

So,

$$dv = 0.09\frac{km}{hr} = 0.025\frac{m}{s}$$

$$dm = 0.5\ kg$$

Kinetic energy, $K = \frac{1}{2}mv^2$;

So from Eq. 3.5

$$dK = \begin{bmatrix}\frac{\partial K}{\partial m} & \frac{\partial K}{\partial v}\end{bmatrix}\begin{bmatrix}dm \\ dv\end{bmatrix}$$

$$dK = \frac{\partial K}{\partial m}dm + \frac{\partial K}{\partial v}dv = \frac{1}{2}v^2 dm + mvdv$$

$$= 0.5(15)^2(0.5) + (1497)(15)(0.025)$$

$$= 617.625\ J$$

Use of Eq. 3.20

Suppose x_1 and x_2 are two field measurements and the quantity z is calculated from x_1 and x_2 in two indeterminate quantities,

$$y_1 = 3x_1 + x_2 + 2$$

$$y_2 = x_1 + 2x_2 + 3$$

$$z = y_1 + y_2 = 4x_1 + 3x_2 + 5$$

Now if error in measurement,

$$\sigma_{x_1} = \pm 5\ cm;\ \sigma_{x_1} = \pm 3\ cm$$

The final error in measurement (from Eq. 3.20)

$$\sigma_z{}^2 = C_z = \begin{bmatrix} \frac{\partial z}{\partial x_1} & \frac{\partial z}{\partial x_2} \end{bmatrix} \begin{bmatrix} \sigma_{x_1}^2 & \sigma_{x_1 x_2} \\ \sigma_{x_1 x_2} & \sigma_{x_1}^2 \end{bmatrix} \begin{bmatrix} \frac{\partial z}{\partial x_1} \\ \frac{\partial z}{\partial x_2} \end{bmatrix}$$

$$= [4 \quad 3] \begin{bmatrix} 25 & 0 \\ 0 & 9 \end{bmatrix} \begin{bmatrix} 4 \\ 3 \end{bmatrix};\ \sigma_{x_1 x_2} = 0\ as\ x_1\ and\ x_1\ are\ uncorrelated$$

$$= [4 \quad 3] \begin{bmatrix} 25 \times 4 + 0 \times 3 \\ 0 \times 4 + 9 \times 3 \end{bmatrix}$$

$$= [4 \quad 3] \begin{bmatrix} 100 \\ 27 \end{bmatrix}$$

$$= 4 \times 100 + 3 \times 27$$

$$= 481$$

So,

$$\sigma_z = \pm 21.9\ cm$$

Use of Eq. 3.34 to 3.37

The random error of a position is expressed by a bivariate normal distribution with parameters

$$\mu_x = \mu_y = 0, \qquad \sigma_x = \ 0.22\ m, \sigma_y = 0.14\ m\ and\ \rho = 0.80$$

The standard error ellipse would be

$$\sigma_{xy} = \ \rho\sigma_x\sigma_y = (0.80)(0.22)(0.14) = 0.0246\ m^2$$

From Eq. 3.34 and 3.35

$$\sigma_{x'}^2 = \frac{\sigma_x^2 + \sigma_y^2}{2} + \sqrt{\left(\frac{\sigma_x^2 - \sigma_y^2}{2}\right)^2 + \sigma_{xy}^2}$$

$$= \frac{(0.22)^2 + (0.14)^2}{2} + \sqrt{\left(\frac{(0.22)^2 - (0.14)^2}{2}\right)^2 + (0.0246)^2}$$

$$= 0.0340 + 0.0285 = 0.0625\ m^2$$

$$\sigma_{y'}^2 = 0.0340 - 0.0285 = 0.0055\ m^2$$

From Eq. 3.37

$$tan2\theta = \frac{2(0.0246)}{(0.22)^2 - (0.14)^2}$$

$$\theta = 29.8^o$$

Error Visualization

Use of Eq. 3.38

Evaluate the semimajor and semiminor axes of the ellipse within which it is 90 % probable that the error in position will lie.

$$P[U \leq c^2\ ] = 0.90$$

From Eq. 3.40

$$1 - e^{\frac{-c^2}{2}} = 0.90$$

$$\ln(0.10) = \ln\left[e^{-\frac{c^2}{2}}\right]$$

or,

$$c = 2.146$$

The semimajor and semiminor axes are (Eq. 3.38):

$$c\sigma_{x'} = 2.146\sqrt{0.0625} = 0.54\,m$$

$$c\sigma_{x'} = 2.146\sqrt{.0055} = 0.16\,m$$

Excavator Kinematics

Use of Eq. 3.43 and 3.45 (position coordinate calculation)

Find out the end position of a two-link planar arm (Spong et al, 2006)

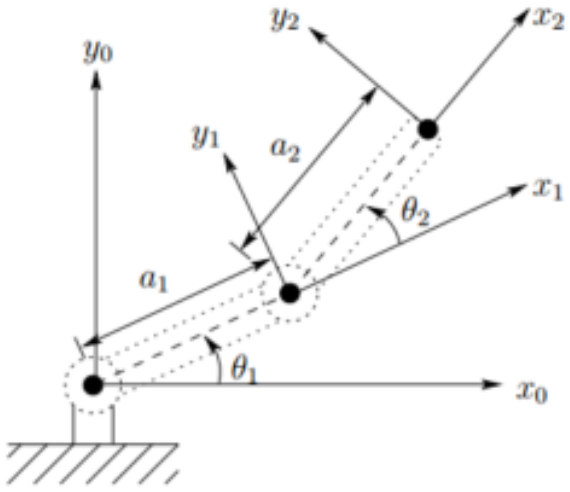

Figure A.1. Two-link planar arm (

Link	$\boldsymbol{a_i}$	$\boldsymbol{d_i}$	$\boldsymbol{\alpha_i}$	$\boldsymbol{\theta_i^*}$
L1	a_1	0	0°	θ_1
L2	a_2	0	0°	θ_2

From Eq. 4.1.5

$$A_1 = \begin{bmatrix} cos\theta_1 & -sin\theta_1 & 0 & a_1cos\theta_1 \\ sin\theta_1 & cos\theta_1 & 0 & a_1sin\theta_1 \\ 0 & 0 & 1 & 0 \\ 0 & 0 & 0 & 1 \end{bmatrix}$$

$$A_2 = \begin{bmatrix} cos\theta_2 & -sin\theta_2 & 0 & a_2cos\theta_2 \\ sin\theta_2 & cos\theta_2 & 0 & a_2sin\theta_2 \\ 0 & 0 & 1 & 0 \\ 0 & 0 & 0 & 1 \end{bmatrix}$$

From Eq.

$$T_2^0 = A_1A_2 = \begin{bmatrix} cos\theta_1 & -sin\theta_1 & 0 & a_1cos\theta_1 \\ sin\theta_1 & cos\theta_1 & 0 & a_1sin\theta_1 \\ 0 & 0 & 1 & 0 \\ 0 & 0 & 0 & 1 \end{bmatrix} \begin{bmatrix} cos\theta_2 & -sin\theta_2 & 0 & a_2cos\theta_2 \\ sin\theta_2 & cos\theta_2 & 0 & a_2sin\theta_2 \\ 0 & 0 & 1 & 0 \\ 0 & 0 & 0 & 1 \end{bmatrix}$$

$$= \begin{bmatrix} cos\theta_1cos\theta_2 & -sin\theta_1sin\theta_2 & 0 & a_1cos\theta_1 + a_2cos\theta_2 \\ -sin\theta_1sin\theta_2 & cos\theta_1cos\theta_2 & 0 & a_1sin\theta_1 + a_2sin\theta_2 \\ 0 & 0 & 1 & 0 \\ 0 & 0 & 0 & 1 \end{bmatrix}$$

From Eq. 4.1.3

$$\begin{bmatrix} x_2 \\ y_2 \\ z_2 \\ 1 \end{bmatrix} = T_2^0 \begin{bmatrix} x_0 \\ y_0 \\ z_0 \\ 1 \end{bmatrix}$$

$$\begin{bmatrix} x_2 \\ y_2 \\ z_2 \\ 1 \end{bmatrix} = \begin{bmatrix} cos\theta_1cos\theta_2 & -sin\theta_1sin\theta_2 & 0 & a_1cos\theta_1 + a_2cos\theta_1cos\theta_2 \\ -sin\theta_1sin\theta_2 & cos\theta_1cos\theta_2 & 0 & a_1sin\theta_1 + a_2sin\theta_1sin\theta_2 \\ 0 & 0 & 1 & 0 \\ 0 & 0 & 0 & 1 \end{bmatrix} \begin{bmatrix} 0 \\ 0 \\ 0 \\ 1 \end{bmatrix}$$

$$\begin{bmatrix} x_2 \\ y_2 \end{bmatrix} = \begin{bmatrix} a_1cos\theta_1 + a_2cos\theta_1cos\theta_2 \\ a_1sin\theta_1 + a_2sin\theta_1sin\theta_2 \end{bmatrix}$$

Appendix B

Computer Codes (MATLAB)

Tracking the position of the bucket tip with respect to the local frame of the excavator

```
% a1 = 0; d1 = 0; al1 = 0; th1 = 0; %intializing


% test case
% DH_input = [45, 0, 1, 0; 45, 0, 1, 0];

%correction
% DH_input = [th1, d1, a1, al1;   % link 1
%     th1, d1, a1, al1;           % link 2
%     th1, d1, a1, al1;           % link 3
%     th1, d1, a1, al1;           % link 4
%     th1, d1, a1, al1];          % link 5


function pos_bckt = l_pos_bckt (DH_input)


r = size (DH_input,1);          % number of row of the DH_input matrix
( number of links)

T_mat=1;

for i = 1:r
    th =  DH_input(i,1);
    d =   DH_input(i,2);
    a =   DH_input(i,3);
    al=   DH_input(i,4);

    T_mat = T_mat * A_mat(th,d,a,al);
end

% pose of the bucket tip

l_origine = [0, 0, 0, 1];      %local origine
pos_bckt = T_mat * l_origine';
pos_bckt = pos_bckt(1:end-1);   %pose of the buckettip wrt local frame
end
```

homogeneous transformation matrix that expresses the position and orientation of ojxjyizj with respect to oixiyizi: Computing T matrix

```
function y = t_mat(th,d,a,al)

th = conv_deg_rad(th);
al = conv_deg_rad(al);

rotz_th = [cos(th), - sin(th), 0, 0; - sin(th), cos(th), 0, 0; 0, 0, 1,
0; 0, 0, 0, 1]; % rotation of axis z
tranz_d = [1, 0, 0, 0; 0, 1, 0, 0; 0, 0, 1, d; 0, 0, 0, 1];
% translation of axix z
tranx_a = [1, 0, 0, a; 0, 1, 0, 0; 0, 0, 1, 0; 0, 0, 0, 1];
% translation of axis x
rotx_al = [1, 0, 0, 0; cos(al), - sin(al), 0, 0; sin(al), cos(al), 0,
0; 0, 0, 0, 1];   % rotation of axis x
y = rotz_th * tranz_d * tranx_a * rotx_al;
end
```

homogeneous transformation matrix that expresses the position and orientation of ojxjyizj with respect to oixiyizi: Computing A matrix

```
function y = A_mat(th,d,a,al)

th = conv_deg_rad(th);
al = conv_deg_rad(al);

rotz_th = [cos(th), - sin(th), 0, 0; sin(th), cos(th), 0, 0; 0, 0, 1,
0; 0, 0, 0, 1];   % rotation about axis z
tranz_d = [1, 0, 0, 0; 0, 1, 0, 0; 0, 0, 1, d; 0, 0, 0, 1];
% translation along axix z
tranx_a = [1, 0, 0, a; 0, 1, 0, 0; 0, 0, 1, 0; 0, 0, 0, 1];
% translation along axis x
rotx_al = [1, 0, 0, 0; 0, cos(al), - sin(al), 0; 0, sin(al), cos(al),
0; 0, 0, 0, 1];   % rotation about axis x
y = rotz_th * tranz_d * tranx_a * rotx_al;
end
```

computing the Jacobian Matrix

```
function jac_mat = J_mat (DH_input,v)

f = l_pos_bckt(DH_input);                % extracting the function

jac_mat = jacobian(f,v );                % Jacobian calculation

end
```

Error matrix

```
function e = E_mat(J, sd)
r = size (sd,2);              % number of column of the sd matrix (
number of sensors)
sd_mat = zeros(r,r);          % creating r x r zero matrix
for i = 1:r
    sd_mat (i,i)= (sd(1,i))^2;
end
e = J*sd_mat*J';            % covariance error matrix
end
```

Computing Error Ellipse and Getting the visual

```
function h=error_ellipse(varargin)
% ERROR_ELLIPSE - plot an error ellipse, or ellipsoid, defining
confidence region
%    ERROR_ELLIPSE(C22) - Given a 2x2 covariance matrix, plot the
%    associated error ellipse, at the origin. It returns a graphics
handle
%    of the ellipse that was drawn.
%
%    ERROR_ELLIPSE(C33) - Given a 3x3 covariance matrix, plot the
%    associated error ellipsoid, at the origin, as well as its
projections
%    onto the three axes. Returns a vector of 4 graphics handles, for
the
%    three ellipses (in the X-Y, Y-Z, and Z-X planes, respectively) and
for
%    the ellipsoid.
%
%    ERROR_ELLIPSE(C,MU) - Plot the ellipse, or ellipsoid, centered at
MU,
%    a vector whose length should match that of C (which is 2x2 or
3x3).
%
%    ERROR_ELLIPSE(...,'Property1',Value1,'Name2',Value2,...) sets the
%    values of specified properties, including:
%      'C' - Alternate method of specifying the covariance matrix
%      'mu' - Alternate method of specifying the ellipse (-oid) center
%      'conf' - A value betwen 0 and 1 specifying the confidence
interval.
%        the default is 0.5 which is the 50% error ellipse.
%      'scale' - Allow the plot the be scaled to difference units.
%      'style' - A plotting style used to format ellipses.
%      'clip' - specifies a clipping radius. Portions of the ellipse, -
oid,
%        outside the radius will not be shown.
%
%    NOTES: C must be positive definite for this function to work
properly.

default_properties = struct(...
  'C', [], ... % The covaraince matrix (required)
  'mu', [], ... % Center of ellipse (optional)
```

```
  'conf', 0.9999, ... % Percent confidence/100
  'scale', 1, ... % Scale factor, e.g. 1e-3 to plot m as km
  'style', '', ...  % Plot style
  'clip', inf); % Clipping radius

if length(varargin) >= 1 & isnumeric(varargin{1})
  default_properties.C = varargin{1};
  varargin(1) = [];
end

if length(varargin) >= 1 & isnumeric(varargin{1})
  default_properties.mu = varargin{1};
  varargin(1) = [];
end

if length(varargin) >= 1 & isnumeric(varargin{1})
  default_properties.conf = varargin{1};
  varargin(1) = [];
end

if length(varargin) >= 1 & isnumeric(varargin{1})
  default_properties.scale = varargin{1};
  varargin(1) = [];
end

if length(varargin) >= 1 & ~ischar(varargin{1})
  error('Invalid parameter/value pair arguments.')
end

prop = getopt(default_properties, varargin{:});
C = prop.C;

if isempty(prop.mu)
  mu = zeros(length(C),1);
else
  mu = prop.mu;
end

conf = prop.conf;
scale = prop.scale;
style = prop.style;

if conf <= 0 | conf >= 1
  error('conf parameter must be in range 0 to 1, exclusive')
end

[r,c] = size(C);
if r ~= c | (r ~= 2 & r ~= 3)
  error(['Don''t know what to do with ',num2str(r),'x',num2str(c),'
matrix'])
end

x0=mu(1);
y0=mu(2);

% Compute quantile for the desired percentile
```

```
k = sqrt(qchisq(conf,r)); % r is the number of dimensions (degrees of
freedom)

hold_state = get(gca,'nextplot');

if r==3 & c==3
  z0=mu(3);

  % Make the matrix has positive eigenvalues - else it's not a valid
covariance matrix!
  if any(eig(C) <=0)
    error('The covariance matrix must be positive definite (it has non-
positive eigenvalues)')
  end

  % C is 3x3; extract the 2x2 matricies, and plot the associated error
  % ellipses. They are drawn in space, around the ellipsoid; it may be
  % preferable to draw them on the axes.
  Cxy = C(1:2,1:2);
  Cyz = C(2:3,2:3);
  Czx = C([3 1],[3 1]);

  [x,y,z] = getpoints(Cxy,prop.clip);
  h1=plot3(x0+k*x,y0+k*y,z0+k*z,prop.style);hold on
  [y,z,x] = getpoints(Cyz,prop.clip);
  h2=plot3(x0+k*x,y0+k*y,z0+k*z,prop.style);hold on
  [z,x,y] = getpoints(Czx,prop.clip);
  h3=plot3(x0+k*x,y0+k*y,z0+k*z,prop.style);hold on


  [eigvec,eigval] = eig(C);

  [X,Y,Z] = ellipsoid(0,0,0,1,1,1);
  XYZ = [X(:),Y(:),Z(:)]*sqrt(eigval)*eigvec';

  X(:) = scale*(k*XYZ(:,1)+x0);
  Y(:) = scale*(k*XYZ(:,2)+y0);
  Z(:) = scale*(k*XYZ(:,3)+z0);
  h4=surf(X,Y,Z);
  colormap gray
  alpha(0.3)
  camlight
  if nargout
    h=[h1 h2 h3 h4];
  end
elseif r==2 & c==2
  % Make the matrix has positive eigenvalues - else it's not a valid
covariance matrix!
  if any(eig(C) <=0)
    error('The covariance matrix must be positive definite (it has non-
positive eigenvalues)')
  end

  [x,y,z] = getpoints(C,prop.clip);
  h1=plot(scale*(x0+k*x),scale*(y0+k*y),prop.style);
  set(h1,'zdata',z+1)
  if nargout
```

```
    h=h1;
  end
else
  error('C (covaraince matrix) must be specified as a 2x2 or 3x3
matrix)')
end
%axis equal

set(gca,'nextplot',hold_state);

%---------------------------------------------------------------
% getpoints - Generate x and y points that define an ellipse, given a
2x2
%   covariance matrix, C. z, if requested, is all zeros with same shape
as
%   x and y.
function [x,y,z] = getpoints(C,clipping_radius)

n=100; % Number of points around ellipse
p=0:pi/n:2*pi; % angles around a circle

[eigvec,eigval] = eig(C); % Compute eigen-stuff
xy = [cos(p'),sin(p')] * sqrt(eigval) * eigvec'; % Transformation
x = xy(:,1);
y = xy(:,2);
z = zeros(size(x));

% Clip data to a bounding radius
if nargin >= 2
  r = sqrt(sum(xy.^2,2)); % Euclidian distance (distance from center)
  x(r > clipping_radius) = nan;
  y(r > clipping_radius) = nan;
  z(r > clipping_radius) = nan;
end

%---------------------------------------------------------------
function x=qchisq(P,n)
% QCHISQ(P,N) - quantile of the chi-square distribution.
if nargin<2
  n=1;
end

s0 = P==0;
s1 = P==1;
s = P>0 & P<1;
x = 0.5*ones(size(P));
x(s0) = -inf;
x(s1) = inf;
x(~(s0|s1|s))=nan;

for ii=1:14
  dx = -(pchisq(x(s),n)-P(s))./dchisq(x(s),n);
  x(s) = x(s)+dx;
  if all(abs(dx) < 1e-6)
    break;
  end
end
```

```
%-----------------------------------------------------------------
function F=pchisq(x,n)
% PCHISQ(X,N) - Probability function of the chi-square distribution.
if nargin<2
  n=1;
end
F=zeros(size(x));

if rem(n,2) == 0
  s = x>0;
  k = 0;
  for jj = 0:n/2-1;
    k = k + (x(s)/2).^jj/factorial(jj);
  end
  F(s) = 1-exp(-x(s)/2).*k;
else
  for ii=1:numel(x)
    if x(ii) > 0
      F(ii) = quadl(@dchisq,0,x(ii),1e-6,0,n);
    else
      F(ii) = 0;
    end
  end
end

%-----------------------------------------------------------------
function f=dchisq(x,n)
% DCHISQ(X,N) - Density function of the chi-square distribution.
if nargin<2
  n=1;
end
f=zeros(size(x));
s = x>=0;
f(s) = x(s).^(n/2-1).*exp(-x(s)/2)./(2^(n/2)*gamma(n/2));

%-----------------------------------------------------------------
function properties = getopt(properties,varargin)
%GETOPT - Process paired optional arguments as
'prop1',val1,'prop2',val2,...
%
%   getopt(properties,varargin) returns a modified properties
structure,
%   given an initial properties structure, and a list of paired
arguments.
%   Each argumnet pair should be of the form property_name,val where
%   property_name is the name of one of the field in properties, and
val is
%   the value to be assigned to that structure field.
%
%   No validation of the values is performed.
%
% EXAMPLE:
%   properties =
struct('zoom',1.0,'aspect',1.0,'gamma',1.0,'file',[],'bg',[]);
%   properties = getopt(properties,'aspect',0.76,'file','mydata.dat')
% would return:
```

```
%   properties =
%         zoom: 1
%       aspect: 0.7600
%        gamma: 1
%         file: 'mydata.dat'
%           bg: []
%
% Typical usage in a function:
%   properties = getopt(properties,varargin{:})

% Process the properties (optional input arguments)
prop_names = fieldnames(properties);
TargetField = [];
for ii=1:length(varargin)
  arg = varargin{ii};
  if isempty(TargetField)
    if ~ischar(arg)
      error('Propery names must be character strings');
    end
    f = find(strcmp(prop_names, arg));
    if length(f) == 0
      error('%s ',['invalid property ''',arg,'''; must be one
of:'],prop_names{:});
    end
    TargetField = arg;
  else
    % properties.(TargetField) = arg; % Ver 6.5 and later only
    properties = setfield(properties, TargetField, arg); % Ver 6.1
friendly
    TargetField = '';
  end
end
if ~isempty(TargetField)
  error('Property names and values must be specified in pairs.');
end
```

Error ellipse dimension calculation

```
syms la1 ld1 lal1 lth1 la2 ld2 lal2 lth2 la3 ld3 lal3 lth3 la4 ld4 lal4
lth4 la5 ld5 lal5 lth5 sd1 sd2 sd3 sd4 sd5


% Defined DH Parameter Symbols
DH_parameter =  [lth1, ld1, la1, lal1;
                 lth2, ld2, la2, lal2;
                 lth3, ld3, la3, lal3;
                 lth4, ld4, la4, lal4;
                 lth5, ld5, la5, lal5];

% Link definition

l = 4;                                          % link numbers
```

```
DH_input = DH_parameter(1:l, :);
DH_actual = [90, 0, 2, 90; 30, 0, 5.55, 0;
               -90, 0, 2.5, 0; -60, 0, 1.2, 0];


% DH_input = [lth1, ld1, la1, lal1; lth2, ld2,la2,lal2 ];
v = [lth1,lth2,lth3,lth4];
J=J_mat(DH_input,v);
size(J);                                    % size of the Jacobian
matrix


J = subs(J,DH_input,DH_actual);             % substituting the values
of the jacobian matrix
eval (J);                                   % evaluationg the jacobian
matrix for true values


% testing different precission  level
range = [0.1: 0.01: .5];
n =  size(range,2);
error_x = zeros(1,n);
error_y = zeros(1,n);
error_z = zeros(1,n);

for i = 1
    sigma = 0.1;                                %standard deviation
of the sensors
    sd = [sigma,sigma, sigma, sigma];
    elpse = E_mat(J, sd);

    elpse = eval (elpse);                               % changed it
error
    e = elpse                                   % error
    e = eig (e)
    e = sqrt(e)
    error_x(1,i) = 4.598*1000*e(1,1);
    error_y(1,i) = 4.598*1000*e(2,1);
    error_z(1,i) = 4.598*1000*e(3,1);
    f = error_ellipse (elpse);
    %plot (f)
end

%ploting the graph
% plot(range, error_x,'g', range, error_y,'b--', range, error_z, 'c.')
%
% title('Error Graph 99.99% confidence level')
% xlabel('Standard Deviation')
% ylabel('Error(mm)')
% legend('X','y','z')
%
```

Max error plot for different dimension

```
% get the input data
data=dlmread('excavatordata.txt');
time = data (:,1);
swingangle = data(:,2);
boomangle = data (:, 3);
stickangle = data (:,4);
bucketangle = data (:,5);



% % Link definition
%
% l = 4;                                          % link numbers
% DH_input = DH_parameter(1:l, :);
%
%
%
% DH_actual = [90, 0, 2, 90; 30, 0, 5.55, 0;
%               -90, 0, 2.5, 0; -60, 0, 1.2, 0];
%
%
%
% % tip position
% test = l_pos_bckt (DH_input);
% test = subs(test,DH_input,DH_actual);
% eval(test);
%
%
% % DH_input = [lth1, ld1, la1, lal1; lth2, ld2,la2,lal2 ];
% v = [lth1,lth2,lth3,lth4];
% J=J_mat(DH_input,v);
% size(J);                                        % size of the Jacobian
matrix


m = size (time,1);
time = time';
error_x = zeros(1,m);
error_y = zeros(1,m);
error_z = zeros(1,m);


for K = 1:m

    s = swingangle(K,1);
    b = boomangle(K,1);
    stk = stickangle (K,1);
    bkt = bucketangle (K,1);
```

```
syms la1 ld1 lal1 lth1 la2 ld2 lal2 lth2 la3 ld3 lal3 lth3 la4 ld4 lal4
lth4 la5 ld5 lal5 lth5 sd1 sd2 sd3 sd4 sd5

    DH_parameter =  [lth1, ld1, la1, lal1;
                     lth2, ld2, la2, lal2;
                     lth3, ld3, la3, lal3;
                     lth4, ld4, la4, lal4;
                     lth5, ld5, la5, lal5];
    l = 4;                                          % link numbers
    DH_input = DH_parameter(1:l, :);



    DH_actual = [s, 0, 2, 90; b, 0, 5.55, 0;    % DH parameters for the
backhow excavator
                 stk, 0, 2.5, 0; bkt, 0, 1.2, 0];
    v = [lth1,lth2,lth3,lth4];
    J=J_mat(DH_input,v);


    J = subs(J,DH_input,DH_actual);             % substituting the
values of the jacobian matrix
    sigma = 0.1;                                % declaring the value
of sigma
    sd = [sigma,sigma, sigma, sigma];
    e = E_mat(J, sd);

    %e = eval (e);                               % error
    e = eig (e);
    e = sqrt(e);

    error_x(1,K) = 4.598*1000*e(1,1);
    error_y(1,K) = 4.598*1000*e(2,1);
    error_z(1,K) = 4.598*1000*e(3,1);
end
% ploting the graph
plot(time, error_x,'g', time, error_y,'b', time, error_z, 'c')

title('Error Graph 99.99% confidence level')
xlabel('time')
ylabel('Error(mm)')
legend('X','y','z')
```